

2.1 Introduction: Land–climate interactions

This chapter assesses the literature on two-way interactions between climate and land, with focus on scientific findings published since AR5 and some aspects of the land–climate interactions that were not assessed in previous IPCC reports. Previous IPCC assessments recognised that climate affects land cover and land surface processes, which in turn affect climate. However, previous assessments mostly focused on the contribution of land to global climate change via its role in emitting and absorbing greenhouse gases (GHGs) and short-lived climate forcers (SLCFs), or via implications of changes in surface reflective properties (i.e., albedo) for solar radiation absorbed by the surface. This chapter examines scientific advances in understanding the interactive changes of climate and land, including impacts of climate change, variability and extremes on managed and unmanaged lands. It assesses climate forcing of land changes from direct (e.g., land use change and land management) and indirect (e.g., increasing atmospheric CO₂ concentration and nitrogen deposition) effects at local, regional and global scales.

2.1.1 Recap of previous IPCC and other relevant reports as baselines

The evidence that land cover matters for the climate system have long been known, especially from early paleoclimate modelling studies and impacts of human-induced deforestation at the margin of deserts (de Noblet et al. 1996; Kageyama et al. 2004). The understanding of how land use activities impact climate has been put forward by the pioneering work of Charney (1975) who examined the role of overgrazing-induced desertification on the Sahelian climate.

Since then there have been many modelling studies that reported impacts of idealised or simplified land cover changes on weather patterns (e.g., Pielke et al. 2011). The number of studies dealing with such issues has increased significantly over the past 10 years, with more studies that address realistic past or projected land changes. However, very few studies have addressed the impacts of land cover changes on climate as very few land surface models embedded within climate models (whether global or regional), include a representation of land management. Observation-based evidence of land-induced climate impacts emerged even more recently (e.g., Alkama and Cescatti 2016; Bright et al. 2017; Lee et al. 2011; Li et al. 2015; Duveiller et al. 2018; Forzieri et al. 2017) and the literature is therefore limited.

In previous IPCC reports, the interactions between climate change and land were covered separately by three working groups. AR5 WGI assessed the role of land use change in radiative forcing, land-based GHGs source and sink, and water cycle changes that focused on changes of evapotranspiration, snow and ice, runoff and humidity. AR5 WGII examined impacts of climate change on land, including terrestrial and freshwater ecosystems, managed ecosystems, and cities and settlements. AR5 WGIII assessed land-based climate change mitigation goals and pathways related to the agriculture, forestry and other land use (AFOLU). Here, this chapter assesses land–climate interactions from all three working groups. It also

builds on previous special reports such as the Special Report on Global Warming of 1.5°C (SR15). It links to the IPCC Guidelines on National Greenhouse Gas Inventories in the land sector. Importantly, this chapter assesses knowledge that has never been reported in any of those previous reports. Finally, the chapter also tries to reconcile the possible inconsistencies across the various IPCC reports.

Land-based water cycle changes

AR5 reported an increase in global evapotranspiration from the early 1980s to 2000s, but a constraint on further increases from low soil moisture availability. Rising CO₂ concentration limits stomatal opening and thus also reduces transpiration, a component of evapotranspiration. Increasing aerosol levels, declining surface wind speeds and declining levels of solar radiation reaching the ground are additional regional causes of the decrease in evapotranspiration.

Land area precipitation change

Averaged over the mid-latitude land areas of the northern hemisphere, precipitation has increased since 1901 (*medium confidence* before 1951 and *high confidence* thereafter). For other latitudes, area-averaged long-term positive or negative trends have *low confidence*. There are *likely* more land regions where the number of heavy precipitation events has increased than where it has decreased. Extreme precipitation events over most of the mid-latitude land masses and over wet tropical regions will very likely become more intense and more frequent (IPCC 2013a).

Land-based GHGs

AR5 reported that annual net CO₂ emissions from anthropogenic land use change were 0.9 [0.1–1.7] GtC yr⁻¹ on average during 2002–2011 (*medium confidence*). From 1750–2011, CO₂ emissions from fossil fuel combustion have released an estimated 375 [345–405] GtC to the atmosphere, while deforestation and other land use change have released an estimated 180 [100–260] GtC. Of these cumulative anthropogenic CO₂ emissions, 240 [230–250] GtC have accumulated in the atmosphere, 155 [125–185] GtC have been taken up by the ocean and 160 [70–250] GtC have accumulated in terrestrial ecosystems (i.e., the cumulative residual land sink) (Ciais et al. 2013a). Updated assessment and knowledge gaps are covered in Section 2.3.

Future terrestrial carbon source/sink

AR5 projected with *high confidence* that tropical ecosystems will uptake less carbon and with *medium confidence* that at high latitudes, land carbon sink will increase in a warmer climate. Thawing permafrost in the high latitudes is potentially a large carbon source in warmer climate conditions, however the magnitude of CO₂ and CH₄ emissions due to permafrost thawing is still uncertain. The SR15 further indicates that constraining warming to 1.5°C would prevent the melting of an estimated permafrost area of 2 million km² over the next centuries compared to 2°C. Updates to these assessments are found in Section 2.3.

Chapter 2

Land–climate interactions

Land use change altered albedo

AR5 stated with *high confidence* that anthropogenic land use change has increased the land surface albedo, which has led to a RF of $-0.15 \pm 0.10 \text{ W m}^{-2}$. However, it also underlined that the sources of the large spread across independent estimates were caused by differences in assumptions for the albedo of natural and managed surfaces and for the fraction of land use change before 1750. Generally, our understanding of albedo changes from land use change has been enhanced from AR4 to AR5, with a narrower range of estimates and a higher confidence level. The radiative forcing from changes in albedo induced by land use changes was estimated in AR5 at -0.15 W m^{-2} (-0.25 to about -0.05), with *medium confidence* in AR5 (Myhre et al. 2013). This was an improvement over AR4 in which it was estimated at -0.2 W m^{-2} (-0.4 to about 0), with *low to medium confidence* (Forster et al. 2007). Section 2.5 shows that albedo is not the only source of biophysical land-based climate forcing to be considered.

Hydrological feedback to climate

Land use changes also affect surface temperatures through non-radiative processes, and particularly through the hydrological cycle. These processes are less well known and are difficult to quantify but tend to offset the impact of albedo changes. As a consequence, there is low agreement on the sign of the net change in global mean temperature as a result of land use change (Hartmann et al. 2013a). An updated assessment on these points is covered in Sections 2.5 and 2.2.

Climate-related extremes on land

AR5 reported that impacts from recent climate-related extremes reveal significant vulnerability and exposure of some ecosystems to current climate variability. Impacts of such climate-related extremes include alteration of ecosystems, disruption of food production and water supply, damage to infrastructure and settlements, morbidity and mortality, and consequences for mental health and human well-being (Burkett et al. 2014). The SR15 further indicates that limiting global warming to 1.5°C limits the risks of increases in heavy precipitation events in several regions (*high confidence*). In urban areas, climate change is projected to increase risks for people, assets, economies and ecosystems (*very high confidence*). These risks are amplified for those lacking essential infrastructure and services or living in exposed areas. An updated assessment and a knowledge gap for this chapter are covered in Section 2.2 and Cross-Chapter Box 4.

Land-based climate change adaptation and mitigation

AR5 reported that adaptation and mitigation choices in the near-term will affect the risks related to climate change throughout the 21st century (Burkett et al. 2014). AFOLU are responsible for about $10\text{--}12 \text{ GtCO}_2\text{eq yr}^{-1}$ anthropogenic greenhouse gas emissions, mainly from deforestation and agricultural production. Global CO_2 emissions from forestry and other land use have declined since AR4, largely due to increased afforestation. The SR15 further indicates that afforestation and bioenergy with carbon capture and storage

(BECCS) are important land-based carbon dioxide removal (CDR) options. It also states that land use and land-use change emerge as a critical feature of virtually all mitigation pathways that seek to limit global warming to 1.5°C . The Climate Change 2014 Synthesis Report concluded that co-benefits and adverse side effects of mitigation could affect achievement of other objectives, such as those related to human health, food security, biodiversity, local environmental quality, energy access, livelihoods and equitable sustainable development. Updated assessment and knowledge gaps are covered in Section 2.6 and Chapter 7.

Overall, sustainable land management is largely constrained by climate change and extremes, but also puts bounds on the capacity of land to effectively adapt to climate change and mitigate its impacts. Scientific knowledge has advanced on how to optimise our adaptation and mitigation efforts while coordinating sustainable land management across sectors and stakeholders. Details are assessed in subsequent sections.

2.1.2 Introduction to the chapter structure

This chapter assesses the consequences of changes in land cover and functioning, resulting from both land use and climate change, to global and regional climates. The chapter starts with an assessment of the historical and projected responses of land processes to climate change and extremes (Section 2.2). Subsequently, the chapter assesses historical and future changes in terrestrial GHG fluxes (Section 2.3) as well as non-GHG fluxes and precursors of SLCFs (Section 2.4). Section 2.5 focuses on how historical and future changes in land use and land cover influence climate change/variability through biophysical and biogeochemical forcing and feedbacks, how specific land management affects climate, and how, in turn, climate-induced land changes feed back to climate. Section 2.6 assesses the consequences of land-based adaptation and mitigation options for the climate system in GHG and non-GHG exchanges. Sections 2.3 and 2.6 address implications of the Paris Agreement for land–climate interactions, and the scientific evidence base for ongoing negotiations around the Paris rulebook, the global stocktake and credibility in measuring, reporting and verifying the climate impacts of anthropogenic activities on land. This chapter also examines how land use and management practices may affect climate change through biophysical feedbacks and radiative forcing (Section 2.5), and assesses policy-relevant projected land use changes and sustainable land management for mitigation and adaptation (Section 2.6). Finally, the chapter concludes with a brief assessment of advances in the understanding of the ecological and biogeochemical processes underlying land–climate interactions (Section 2.7).

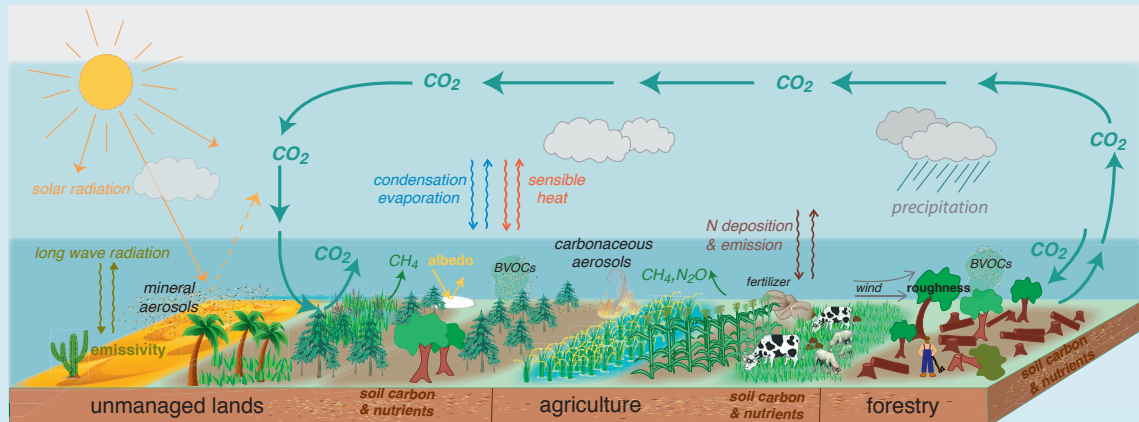
The chapter includes three chapter boxes providing general overview of (i) processes underlying land–climate interactions (Box 2.1), (ii) methodological approaches for estimating anthropogenic land carbon fluxes from national to global scales (Box 2.2), and (iii) CO_2 fertilisation and enhanced terrestrial uptake of carbon (Box 2.3). In addition, this chapter includes two cross-chapter boxes on climate change and fire (Cross-Chapter Box 3), and on urbanisation and climate change (Cross-Chapter Box 4).

In summary, the chapter assesses scientific understanding related to (i) how a changing climate affects terrestrial ecosystems, including those on managed lands, (ii) how land affects climate through biophysical and biogeochemical feedbacks, and (iii) how land use or

cover change and land management play an important and complex role in the climate system. This chapter also pays special attention to advances in understanding cross-scale interactions, emerging issues, heterogeneity and teleconnections.

Box 2.1 | Processes underlying land–climate interactions

Land continuously interacts with the atmosphere through exchanges of, for instance, GHGs (e.g., CO₂, CH₄, N₂O), water, energy or precursors of short lived-climate forcers (e.g., biogenic volatile organic compounds, dust, black carbon). The terrestrial biosphere also interacts with oceans through processes such as the influx of freshwater, nutrients, carbon and particles. These interactions affect where and when rain falls and thus irrigation needs for crops, frequency and intensity of heatwaves, and air quality. They are modified by global and regional climate change, decadal, inter-annual and seasonal climatic variations, and weather extremes, as well as human actions on land (e.g., crop and forest management, afforestation and deforestation). This in turn affects atmospheric composition, surface temperature, hydrological cycle and thus local, regional and global climate. This box introduces some of the fundamental land processes governing biophysical and biogeochemical effects and feedbacks to the climate (Box 2.1, Figure 1).



Box 2.1, Figure 1 | The structure and functioning of managed and unmanaged ecosystems that affect local, regional and global climate. Land surface characteristics such as albedo and emissivity determine the amount of solar and long-wave radiation absorbed by land and reflected or emitted to the atmosphere. Surface roughness influences turbulent exchanges of momentum, energy, water and biogeochemical tracers. Land ecosystems modulate the atmospheric composition through emissions and removals of many GHGs and precursors of SLCFs, including biogenic volatile organic compounds (BVOCs) and mineral dust. Atmospheric aerosols formed from these precursors affect regional climate by altering the amounts of precipitation and radiation reaching land surfaces through their role in clouds physics.

'Biophysical interactions' are exchanges of water and energy between the land and the atmosphere (Section 2.5). Land warms up from absorbing solar and long-wave radiation; it cools down through transfers of sensible heat (via conduction and convection) and latent heat (energy associated with water evapotranspiration) to the atmosphere and through long-wave radiation emission from the land surface (Box 2.1, Figure 1). These interactions between the land and the atmosphere depend on land surface characteristics, including reflectivity of shortwave radiation (albedo), emissivity of long wave radiation by vegetation and soils, surface roughness and soil water access by vegetation, which depends on both soil characteristics and amounts of roots. Over seasonal, inter-annual and decadal timescales, these characteristics vary among different land cover and land-use types and are affected by both natural processes and land management (Anderson et al. 2011). A dense vegetation with high leaf area index, like forests, may absorb more energy than nearby herbaceous vegetation partly due to differences in surface albedo (especially when snow is on the ground). However, denser vegetation also sends more energy back to the atmosphere in the form of evapotranspiration (Bonan, 2008; Burakowski et al., 2018; Ellison et al., 2017) (Section 2.5.2) and this contributes to changes in atmospheric water vapour content, and subsequently to changes in rainfall.

Particularly in extra-tropical regions, these characteristics exhibit strong seasonal patterns with the development and senescence of the vegetation (e.g., leaf colour change and drop). For example, in deciduous forests, seasonal growth increases albedo by 20–50% from the spring minima to growing season maxima, followed by rapid decrease during leaf fall, whereas in grasslands, spring greening causes albedo decreases and only increases with vegetation browning (Hollinger et al. 2010). The seasonal patterns of sensible and latent heat fluxes are also driven by the cycle of leaf development and senescence in temperate deciduous forests: sensible heat fluxes peak in spring and autumn and latent heat fluxes peak in mid-summer (Moore et al. 1996; Richardson et al. 2013).

Box 2.1 (continued)

Exchanges of GHGs between the land and the atmosphere are referred to as ‘biogeochemical interactions’ (Section 2.3), which are driven mainly by the balance between photosynthesis and respiration by plants, and by the decomposition of soil organic matter by microbes. The conversion of atmospheric carbon dioxide into organic compounds by plant photosynthesis, known as terrestrial net primary productivity, is the source of plant growth, food for human and other organisms, and soil organic carbon. Due to strong seasonal patterns of growth, northern hemisphere terrestrial ecosystems are largely responsible for the seasonal variations in global atmospheric CO₂ concentrations. In addition to CO₂, soils emit methane (CH₄) and nitrous oxide (N₂O) (Section 2.3). Soil temperature and moisture strongly affect microbial activities and resulting fluxes of these three GHGs.

Much like fossil fuel emissions, GHG emissions from anthropogenic land cover change and land management are ‘forcers’ on the climate system. Other land-based changes to climate are described as ‘feedbacks’ to the climate system – a process by which climate change influences some property of land, which in turn diminishes (negative feedback) or amplifies (positive feedback) climate change. Examples of feedbacks include the changes in the strength of land carbon sinks or sources, soil moisture and plant phenology (Section 2.5.3).

Incorporating these land–climate processes into climate projections allows for increased understanding of the land’s response to climate change (Section 2.2), and to better quantify the potential of land-based response options for climate change mitigation (Section 2.6). However, to date Earth system models (ESMs) incorporate some combined biophysical and biogeochemical processes only to limited extent and many relevant processes about how plants and soils interactively respond to climate changes are still to be included (Section 2.7). And even within this class of models, the spread in ESM projections is large, in part because of their varying ability to represent land–climate processes (Hoffman et al. 2014). Significant progress in understanding of these processes has nevertheless been made since AR5.

2.2 The effect of climate variability and change on land

2.2.1 Overview of climate impacts on land

2.2.1.1 Climate drivers of land form and function

Energy is redistributed from the warm equator to the colder poles through large-scale atmospheric and oceanic processes driving the Earth’s weather and climate (Oort and Peixoto 1983; Carissimo et al. 1985; Yang et al. 2015a). Subsequently, a number of global climate zones have been classified ranging from large-scale primary climate zones (tropical, sub-tropical, temperate, sub-polar, polar) to much higher-resolution, regional climate zones (e.g., the Köppen-Geiger classification, Kottek et al. 2006). Biomes are adapted to regional climates (Figure 2.1) and may shift as climate, land surface characteristics (e.g., geomorphology, hydrology), CO₂ fertilisation and fire interact. These biomes and the processes therein are subject to modes of natural variability in the ocean-atmosphere system that result in regionally wetter/drier or hotter/cooler periods having temporal scales from weeks to months (e.g., Southern Annular Mode), months to seasons (e.g., Madden-Julian Oscillation), years (e.g., El Niño Southern Oscillation) and decades (e.g., Pacific Decadal Oscillation). Furthermore, climate and weather extremes (such as drought, heatwaves, very heavy rainfall, strong winds), whose frequency, intensity and duration are often a function of large-scale modes of variability, impact ecosystems at various space and timescales.

It is *very likely* that changes to natural climate variability as a result of global warming has and will continue to impact terrestrial ecosystems

with subsequent impacts on land processes (Hulme et al. 1999; Parmesan and Yohe 2003; Di Lorenzo et al. 2008; Kløve et al. 2014; Berg et al. 2015; Lemordant et al. 2016; Pecl et al. 2017). This chapter assesses climate variability and change, particularly extreme weather and climate, in the context of desertification, land degradation, food security and terrestrial ecosystems more generally. This section does specifically assess the impacts of climate variability and climate change on desertification, land degradation and food security as these impacts are assessed respectively in Chapters 3, 4 and 5. This chapter begins with an assessment of observed warming on land.

2.2.1.2 Changes in global land surface air temperature

Based on analysis of several global and regional land surface air temperature (LSAT) datasets, AR5 concluded that the global LSAT had increased over the instrumental period of record, with the warming rate approximately double that reported over the oceans since 1979 and that ‘it is certain that globally averaged LSAT has risen since the late 19th century and that this warming has been particularly marked since the 1970s’. Warming found in the global land datasets is also in a broad agreement with station observations (Hartmann et al. 2013a).

Since AR5, LSAT datasets have been improved and extended. The National Center for Environmental Information, which is a part of the US National Oceanic and Atmospheric Administration (NOAA), developed a new, fourth version of the Global Historical Climatology Network monthly dataset (GHCN, v4). The dataset provides an expanded set of station temperature records with more than 25,000 total monthly temperature stations compared to 7200 in versions v2 and v3 (Menne et al. 2018). Goddard Institute for Space Studies, which is a part of

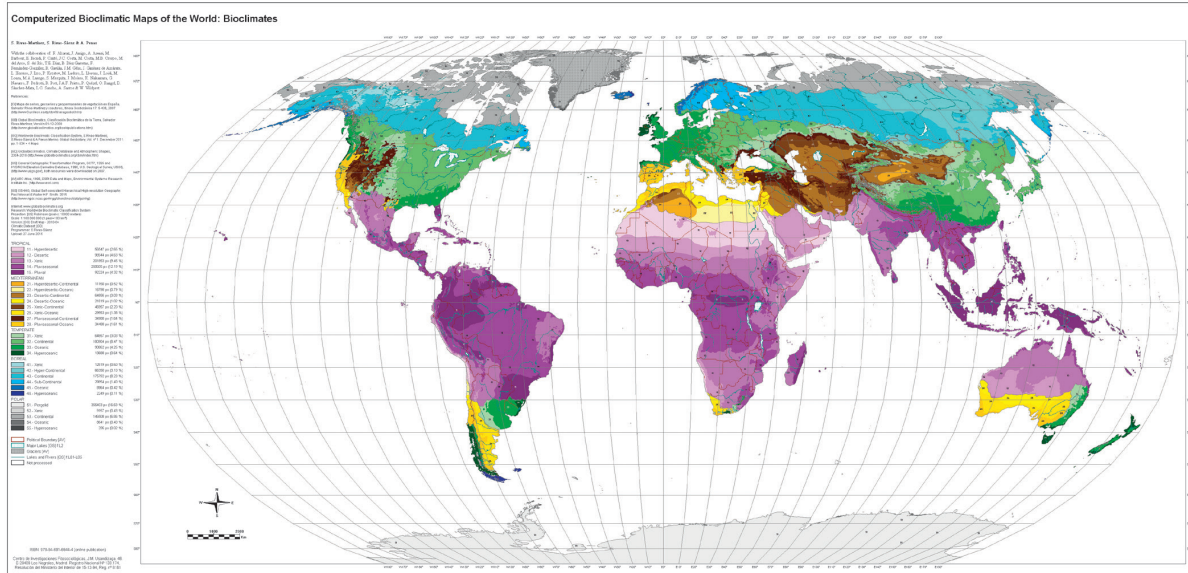


Figure 2.1 | Worldwide Bioclimatic Classification System, 1996–2018. Source: Rivas-Martinez et al. (2011). Online at www.globalbioclimatics.org.

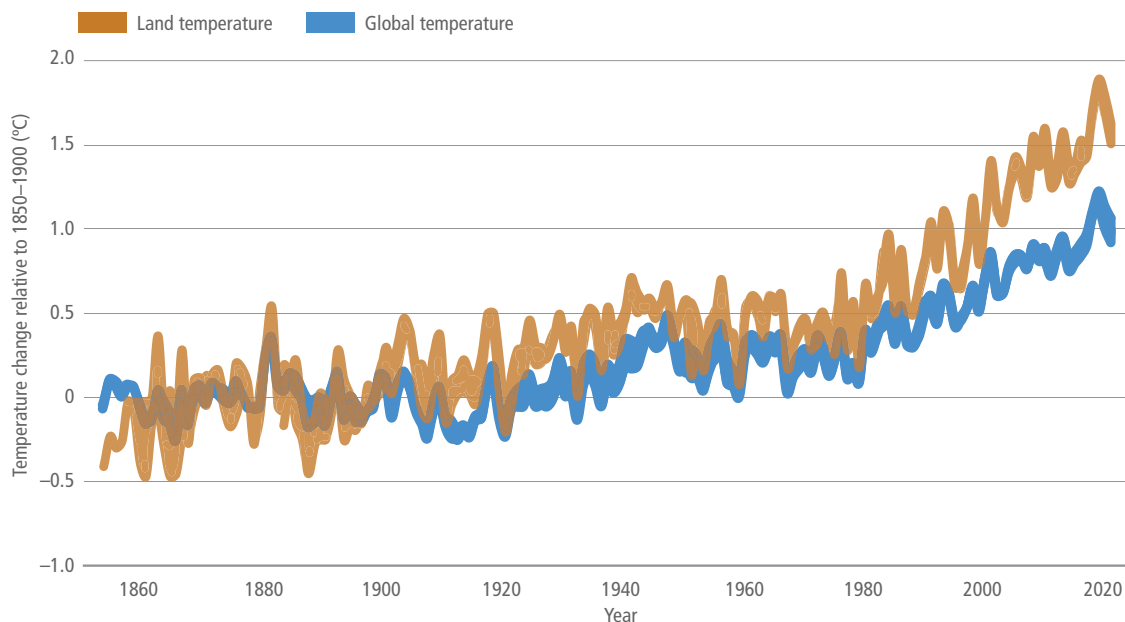


Figure 2.2 | Evolution of land surface air temperature (LSAT) and global mean surface temperature (GMST) over the period of instrumental observations. The brown line shows annual mean LSAT in the BEST, CRUTEM4.6, GHCNv4 and GISTEMP datasets, expressed as departures from global average LSAT in 1850–1900, with the brown line thickness indicating inter-dataset range. The blue line shows annual mean GMST in the HadCRUT4, NOAAGlobal Temp, GISTEMP and Cowtan&Way datasets (monthly values of which were reported in the Special Report on Global Warming of 1.5°C; Allen et al. 2018).

the US National Aeronautics and Space Administration, (NASA/GISS), provides estimate of land and ocean temperature anomalies (GISTEMP). The GISTEMP land temperature anomalies are based upon primarily NOAA/GHCN version 3 dataset (Lawrimore et al. 2011) and account for urban effects through nightlight adjustments (Hansen et al. 2010). The Climatic Research Unit (CRU) of the University of East Anglia, UK (CRUTEM) dataset, now version CRUTEM4.6,

incorporates additional stations (Jones et al. 2012). Finally, the Berkeley Earth Surface Temperature (BEST) dataset provides LSAT from 1750 to present based on almost 46,000 time series and has the longest temporal coverage of the four datasets (Rohde et al. 2013). This dataset was derived with methods distinct from those used for development of the NOAA GHCNm, NASA/GISS GISTEMP and the University of East Anglia CRUTEM datasets.

Table 2.1 | Increases in land surface air temperature (LSAT) from preindustrial period and the late 19th century to present day.

Time period	Dataset of LSAT increase (°C)			
	BEST	CRUTEM4.6	GHCNv, v4	GISTEMP
From 1850–1900 to 2006–2015	1.53 1.38–1.68 (95% confidence)	1.32*		
From 1850–1900 to 1999–2018	1.52 1.39–1.66 (95% confidence)	1.31	NA	NA
From 1881–1900 to 1999–2018	1.51 1.40–1.63 (95% confidence)	1.31	1.37	1.45

* CRUTEM4.6 LSAT increase is computed from 1856–1900 average.

2

According to the available observations in the four datasets, the globally averaged LSAT increased by 1.44°C from the preindustrial period (1850–1900) to the present day (1999–2018). The warming from the late 19th century (1881–1900) to the present day (1999–2018) was 1.41°C (1.31°C–1.51°C) (Table 2.1). The 1.31°C–1.51°C range represents the spread in median estimates from the four available land datasets and does not reflect uncertainty in data coverage or methods used. Based on the BEST dataset (the longest dataset with the most extensive land coverage) the total observed increase in LSAT between the average of the 1850–1900 period and the 2006–2015 period was 1.53°C, (1.38–1.68°C; 95% confidence), while the GMST increase for the same period was 0.87°C (0.75–0.99°C; 90% confidence) (IPCC, 2018: Summary for policymakers, Allen et al. 2018).

The extended and improved land datasets reaffirmed the AR5 conclusion that it is certain that globally averaged LSAT has risen since the preindustrial period and that this warming has been particularly marked since the 1970s (Figure 2.2).

Recent analyses of LSAT and sea surface temperature (SST) observations, as well as analyses of climate model simulations, have refined our understanding of underlying mechanisms responsible for a faster rate of warming over land than over oceans. Analyses of paleo records, historical observations, model simulations and underlying physical principles are all in agreement that the land is warming faster than the oceans as a result of differences in evaporation, land–climate feedbacks (Section 2.5) and changes in the aerosol forcing over land (*very high confidence*) (Braconnot et al. 2012; Joshi et al. 2013; Sejas et al. 2014; Byrne and O’Gorman 2013, 2015; Wallace and Joshi 2018; Allen et al. 2019). There is also *high confidence* that difference in land and ocean heat capacity is not the primary reason for faster land than ocean warming. For the recent period, the land-to-ocean warming ratio is in close agreement between different observational records (about 1.6) and the CMIP5 climate model simulations (the *likely* range of 1.54°C to 1.81°C). Earlier studies analysing slab ocean models (models in which it is assumed that the deep ocean has equilibrated) produced a higher land temperature increases than sea surface temperature (Manabe et al. 1991; Sutton et al. 2007).

It is certain that globally averaged LSAT has risen faster than GMST from the preindustrial period (1850–1900) to the present day (1999–2018). This is because the warming rate of the land compared to the ocean is substantially higher over the historical

period (by approximately 60%) and because the Earth’s surface is approximately one-third land and two-thirds ocean. This enhanced land warming impacts land processes with implications for desertification (Section 2.2.2 and Chapter 3), food security (Section 2.2.3 and Chapter 5), terrestrial ecosystems (Section 2.2.4), and GHG and non-GHG fluxes between the land and climate (Sections 2.3 and 2.4). Future changes in land characteristics through adaptation and mitigation processes and associated land–climate feedbacks can dampen warming in some regions and enhance warming in others (Section 2.5).

2.2.2 Climate-driven changes in aridity

Desertification is defined and discussed at length in Chapter 3 and is a function of both human activity and climate variability and change. There are uncertainties in distinguishing between historical climate-caused aridification and desertification and future projections of aridity as different measurement methods of aridity do not agree on historical or projected changes (Sections 3.1.1 and 3.2.1). However, warming trends over drylands are twice the global average (Lickley and Solomon 2018) and some temperate drylands are projected to convert to subtropical drylands as a result of an increased drought frequency causing reduced soil moisture availability in the growing season (Engelbrecht et al. 2015; Schlaepfer et al. 2017). We therefore assess with *medium confidence* that a warming climate will result in regional increases in the spatial extent of drylands under mid- and high emission scenarios and that these regions will warm faster than the global average warming rate.

2.2.3 The influence of climate change on food security

Food security and the various components thereof are addressed in depth in Chapter 5. Climate variables relevant to food security and food systems are predominantly temperature and precipitation-related, but also include integrated metrics that combine these and other variables (e.g., solar radiation, wind, humidity) and extreme weather and climate events including storm surge (Section 5.2.1). The impact of climate change through changes in these variables is projected to negatively impact all aspects of food security (food availability, access, utilisation and stability), leading to complex impacts on global food security (*high confidence*) (Chapter 5, Table 5.1).

Climate change will have regionally distributed impacts, even under aggressive mitigation scenarios (Howden et al. 2007; Rosenzweig et al. 2013; Challinor et al. 2014; Parry et al. 2005; Lobell and Tebaldi 2014; Wheeler and Von Braun 2013). For example, in the northern hemisphere the northward expansion of warmer temperatures in the middle and higher latitudes will lengthen the growing season (Gregory and Marshall 2012; Yang et al. 2015b) which may benefit crop productivity (Parry et al. 2004; Rosenzweig et al. 2014; Deryng et al. 2016). However, continued rising temperatures are expected to impact global wheat yields by about 4–6% reductions for every degree of temperature rise (Liu et al. 2016a; Asseng et al. 2015) and across both mid- and low latitude regions, rising temperatures are also expected to be a constraining factor for maize productivity by the end of the century (Bassu et al. 2014; Zhao et al. 2017). Although there has been a general reduction in frost occurrence during winter and spring, and a lengthening of the frost free season in response to growing concentrations of GHGs (Fischer and Knutti 2014; Wypych et al. 2017), there are regions where the frost season length has increased, for example, in southern Australia (Crimp et al. 2016). Despite the general reduced frost season length, late spring frosts may increase risk of damage to warming induced precocious vegetation growth and flowering (Meier et al. 2018). Observed and projected warmer minimum temperatures have, and will continue to, reduce the number of winter chill units required by temperate fruit and nut trees (Luedeling 2012). Crop yields are impacted negatively by increases of seasonal rainfall variability in the tropics, sub-tropics, water-limited and high elevation environments, while drought severity and growing season temperatures also have a negative impact on crop yield (Nelson et al. 2009; Schlenker and Lobell 2010; Müller et al. 2017; Parry et al. 2004; Wheeler and Von Braun 2013; Challinor et al. 2014).

Changes in extreme weather and climate (Section 2.2.5) have negative impacts on food security through regional reductions of crop yields. A recent study shows that 18–43% of the explained yield variance of four crops (maize, soybeans, rice and spring wheat) is attributable to extremes of temperature and rainfall, depending on the crop type (Vogel et al. 2019). Climate shocks, particularly severe drought impact low-income small-holder producers disproportionately (Vermeulen et al. 2012; Rivera Ferre 2014). Extremes also compromise critical food supply chain infrastructure, making transport of and access to harvested food more difficult (Brown et al. 2015; Fanzo et al. 2018). There is *high confidence* that the impacts of enhanced climate extremes, together with non-climate factors such as nutrient limitation, soil health and competitive plant species, generally outweighs the regionally positive impacts of warming (Lobell et al. 2011; Leakey et al. 2012; Porter et al. 2014; Gray et al. 2016; Pugh et al. 2016; Wheeler and Von Braun 2013; Beer 2018).

2.2.4 Climate-driven changes in terrestrial ecosystems

Previously, the IPCC AR5 reported high confidence that the Earth's biota composition and ecosystem processes have been strongly affected by past changes in global climate and that the magnitudes of projected changes for the 21st century under high warming scenarios (for example, RCP8.5) are higher than those under historic climate change (Settele et al. 2014). There is *high confidence* that as a

result of climate changes over recent decades many plant and animal species have experienced range size and location changes, altered abundances and shifts in seasonal activities (Urban 2015; Ernakovich et al. 2014; Elsen and Tingley 2015; Hatfield and Prueger 2015; Savage and Vellend 2015; Yin et al. 2016; Pecl et al. 2017; Gonsamo et al. 2017; Fadrique et al. 2018; Laurance et al. 2018). There is *high confidence* that climate zones have already shifted in many parts of the world, primarily as an increase of dry, arid climates accompanied by a decrease of polar climates (Chan and Wu 2015; Chen and Chen 2013; Spinoni et al. 2015b). Regional climate zones shifts have been observed over the Asian monsoon region (Son and Bae 2015), Europe (Jylhä et al. 2010), China (Yin et al. 2019), Pakistan (Adnan et al. 2017), the Alps (Rubel et al. 2017) and north-eastern Brazil, southern Argentina, the Sahel, Zambia and Zimbabwe, the Mediterranean area, Alaska, Canada and north-eastern Russia (Spinoni et al. 2015b).

There is *high confidence* that bioclimates zones will further shift as the climate warms (Williams et al. 2007; Rubel and Kottek 2010; Garcia et al. 2016; Mahony et al. 2017; Law et al. 2018). There is also *high confidence* that novel, unprecedented climates (climate conditions with no analogue in the observational record) will emerge, particularly in the tropics (Williams and Jackson 2007; Colwell et al. 2008a; Mora et al. 2013, 2014; Hawkins et al. 2014; Mahony et al. 2017; Maule et al. 2017). It is *very likely* that terrestrial ecosystems and land processes will be exposed to disturbances beyond the range of current natural variability as a result of global warming, even under low- to medium-range warming scenarios, and that these disturbances will alter the structure, composition and functioning of the system (Settele et al. 2014; Gauthier et al. 2015; Seddon et al. 2016).

In a warming climate, many species will be unable to track their climate niche as it moves, especially those in extensive flat landscapes with low dispersal capacity and in the tropics whose thermal optimum is already near current temperature (Diffenbaugh and Field 2013; Warszawski et al. 2013). Range expansion in higher latitudes and elevations as a result of warming often, but not exclusively, occurs in abandoned lands (Harsch et al. 2009; Landhäuser et al. 2010; Gottfried et al. 2012; Boisvert-Marsh et al. 2014; Bryn and Potthoff 2018; Rumpf et al. 2018; Buitenhof et al. 2018; Steinbauer et al. 2018). This expansion typically favours thermophilic species at the expense of cold adapted species as the climate becomes suitable for lower latitude/altitude species (Rumpf et al. 2018). In temperate drylands, however, range expansion can be countered by intense and frequent drought conditions which result in accelerated rates of taxonomic change and spatial heterogeneity in an ecotone (Tietjen et al. 2017).

Since the advent of satellite observation platforms, a global increase in vegetation photosynthetic activity (i.e., greening) as evidenced through remotely sensed indices such as leaf area index (LAI) and normalised difference vegetation index (NDVI). Three satellite-based leaf area index records (GIMMS3g, GLASS and GLOMAP) imply increased growing season LAI (greening) over 25–50% and browning over less than 4% of the global vegetated area, resulting in greening trend of $0.068 \pm 0.045 \text{ m}^2 \text{ m}^{-2} \text{ yr}^{-1}$ over 1982–2009 (Zhu et al. 2016). Greening has been observed in southern Amazonia, southern Australia, the Sahel and central Africa, India, eastern China and the northern extratropical latitudes (Myneni et al. 1997; de Jong et al.

2012; Los 2013; Piao et al. 2015; Mao et al. 2016; Zhu et al. 2016; Carlson et al. 2017; Forzieri et al. 2017; Pan et al. 2018; Chen et al. 2019). Greening has been attributed to direct factors, namely human land use management and indirect factors such as CO₂ fertilisation, climate change, and nitrogen deposition (Donohue et al. 2013; Keenan et al. 2016; Zhu et al. 2016). Indirect factors have been used to explain most greening trends primarily through CO₂ fertilisation in the tropics and through an extended growing season and increased growing season temperatures as a result of climate change in the high latitudes (Fensholt et al. 2012; Zhu et al. 2016). The extension of the growing season in high latitudes has occurred together with an earlier spring greenup (the time at which plants begin to produce leaves in northern mid- and high-latitude ecosystems) (Goetz et al. 2015; Xu et al. 2016a, 2018) with subsequent earlier spring carbon uptake (2.3 days per decade) and gross primary productivity (GPP) (Pulliainen et al. 2017). The role of direct factors of greening are being increasingly investigated and a recent study has attributed over a third of observed global greening between 2000 and 2017 to direct factors, namely afforestation and croplands, in China and India (Chen et al. 2019).

It should be noted that measured greening is a product of satellite-derived radiance data and, as such, does not provide information on ecosystem health indicators such as species composition and richness, homeostasis, absence of disease, vigour, system resilience and the different components of ecosystems (Jørgensen et al. 2016). For example, a regional greening attributable to croplands expansion or intensification might occur at the expense of ecosystem biodiversity.

Within the global greening trend are also detected regional decreases in vegetation photosynthetic activity (i.e., browning) in northern Eurasia, the southwestern USA, boreal forests in North America, inner Asia and the Congo Basin, largely as a result of intensified drought stress. Since the late 1990s rates and extents of browning have exceeded those of greening in some regions, the collective result of which has been a slowdown of the global greening rate (de Jong et al. 2012; Pan et al. 2018). Within these long-term trends, inter-annual variability of regional greening and browning is attributable to regional climate variability, responses to extremes such as drought, disease and insect infestation and large-scale tele-connective controls such as ENSO and the Atlantic Multi-decadal Organization (Verbyla 2008; Revadekar et al. 2012; Epstein et al. 2018; Zhao et al. 2018).

Projected increases in drought conditions in many regions suggest long-term global vegetation greening trends are at risk of reversal to browning in a warmer climate (de Jong et al. 2012; Pan et al. 2018; Pausas and Millán 2018). On the other hand, in higher latitudes vegetation productivity is projected to increase as a result of higher atmospheric CO₂ concentrations and longer growing periods as a result of warming (Ito et al. 2016) (Section 2.3 and Box 2.3). Additionally, climate-driven transitions of ecosystems, particularly range changes, can take years to decades for the equilibrium state to be realised and the rates of these ‘committed ecosystem changes’ (Jones et al. 2009) vary between low and high latitudes (Jones et al. 2010). Furthermore, as direct factors are poorly integrated into Earth

systems models (ESMs) uncertainties in projected trends of greening and browning are further compounded (Buitenhof et al. 2018; Chen et al. 2019). Therefore, there is *low confidence* in the projection of global greening and browning trends.

Increased atmospheric CO₂ concentrations have both direct and indirect effects on terrestrial ecosystems (Sections 2.2.2 and 2.2.3, and Box 2.3). The direct effect is primarily through increased vegetation photosynthetic activity as described above. Indirect effects include decreased evapotranspiration that may offset the projected impact of drought in some water-stressed plants through improved water use efficiency in temperate regions, suggesting that some rain-fed cropping systems and grasslands will benefit from elevated atmospheric CO₂ concentrations (Roy et al. 2016; Milly and Dunne 2016; Swann et al. 2016; Chang et al. 2017; Zhu et al. 2017). In tropical regions, increased flowering activity is associated primarily with increasing atmospheric CO₂, suggesting that a long-term increase in flowering activity may persist in some vegetation, particularly mid-story trees and tropical shrubs, and may enhance reproduction levels until limited by nutrient availability or climate factors such as drought frequency, rising temperatures, and reduced insolation (Pau et al. 2018).

2.2.5 Climate extremes and their impact on land functioning

Extreme weather events are generally defined as the upper or lower statistical tails of the observed range of values of climate variables or climate indicators (e.g., temperature/rainfall or drought/aridity indices respectively). Previous IPCC reports have reported with *high confidence* on the increase of many types of observed extreme temperature events (Seneviratne et al. 2012; Hartmann et al. 2013b; Hoegh-Guldberg et al. 2018). However, as a result of observational constraints, increases in precipitation extremes are less confident, except in observations-rich regions with dense, long-lived station networks, such as Europe and North America, where there have been likely increases in the frequency or intensity of heavy rainfall.

Extreme events occur across a wide range of time and space scales (Figure 2.3) and may include individual, relatively short-lived weather events (e.g., extreme thunderstorms storms) or a combination or accumulation of non-extreme events (Colwell et al. 2008b; Handmer et al. 2012), for example, moderate rainfall in a saturated catchment having the flood peak at mean high tide (Leonard et al. 2014). Combinatory processes leading to a significant impact are referred to as a compound event and are a function of the nature and number of physical climate and land variables, biological agents such as pests and disease, the range of spatial and temporal scales, the strength of dependence between processes and the perspective of the stakeholder who defines the impact (Leonard et al. 2014; Millar and Stephenson 2015). Currently, there is *low confidence* in the impact of compound events on land as the multi-disciplinary approaches needed to address the problem are few (Zscheischler et al. 2018) and the rarity of compound extreme climatic events renders the analysis of impacts difficult.

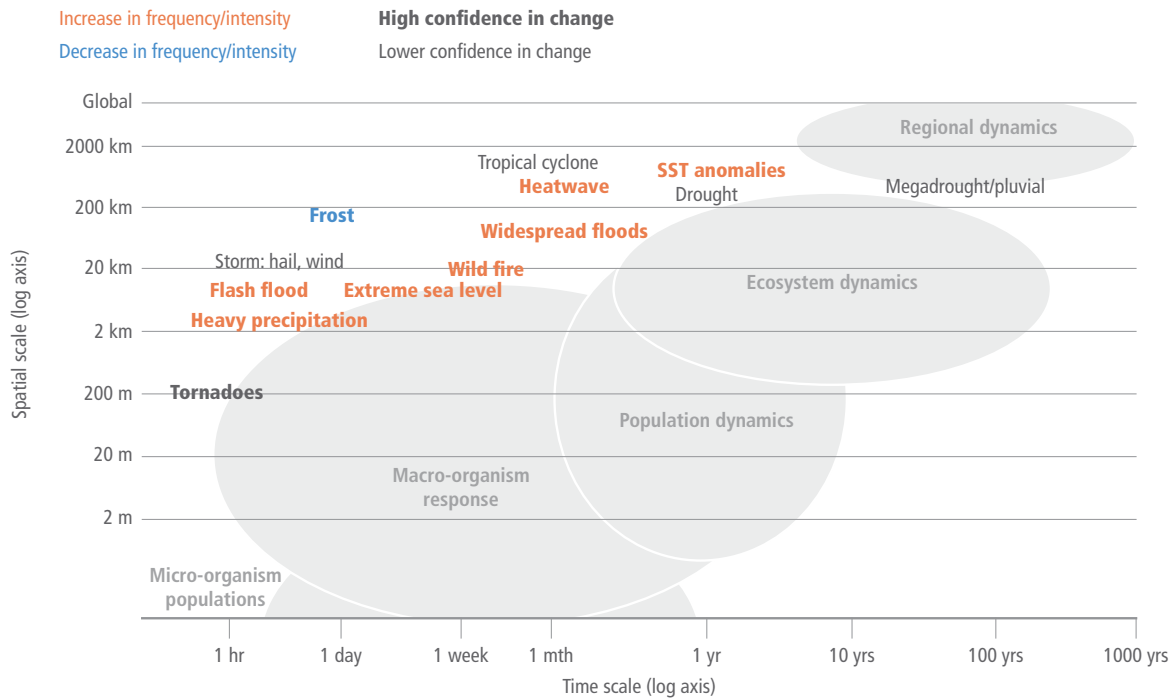


Figure 2.3 | Spatial and temporal scales of typical extreme weather and climate events and the biological systems they impact (shaded grey). Individuals, populations and ecosystems within these space-time ranges respond to relevant climate stressors. Orange (blue) labels indicate an increase (decrease) in the frequency or intensity of the event, with bold font reflecting confidence in the change. Non-bold black labels indicate low confidence in observed changes in frequency or intensity of these events. Each event type indicated in the figure is likely to affect biological systems at all temporal and spatial scales located to the left and below the specific event position in the figure. From Ummenhofer and Meehl (2017).

2.2.5.1 Changes in extreme temperatures, heatwaves and drought

It is *very likely* that most land areas have experienced a decrease in the number of cold days and nights, and an increase in the number of warm days and unusually hot nights (Orlowsky and Seneviratne 2012; Seneviratne et al. 2012; Mishra et al. 2015; Ye et al. 2018). Although there is no consensus definition of heatwaves, as some heatwave indices have relative thresholds and others absolute thresholds, trends between indices of the same type show that recent heat-related events have been made more frequent or more intense due to anthropogenic GHG emissions in most land regions (Lewis and Karoly 2013; Smith et al. 2013b; Scherer and Diffenbaugh 2014; Fischer and Knutti 2015; Ceccherini et al. 2016; King et al. 2016; Bador et al. 2016; Stott et al. 2016; King 2017; Hoegh-Guldberg et al. 2018). Globally, 50–80% of the land fraction is projected to experience significantly more intense hot extremes than historically recorded (Fischer and Knutti 2014; Diffenbaugh et al. 2015; Seneviratne et al. 2016). There is *high confidence* that heatwaves will increase in frequency, intensity and duration into the 21st century (Russo et al. 2016; Ceccherini et al. 2017; Herrera-Estrada and Sheffield 2017) and under high emission scenarios, heatwaves by the end of the century may become extremely long (more than 60 consecutive days) and frequent (once every two years) in Europe, North America, South America, Africa, Indonesia, the Middle East, South and Southeast Asia and Australia (Rusticucci 2012; Cowan et al. 2014; Russo et al. 2014;

Scherer and Diffenbaugh 2014; Pal and Eltahir 2016; Rusticucci et al. 2016; Schär 2016; Teng et al. 2016; Dosio 2017; Mora et al. 2017; Dosio et al. 2018; Lehner et al. 2018; Lhotka et al. 2018; Lopez et al. 2018; Tabari and Willems 2018). Furthermore, unusual heatwave conditions today will occur regularly by 2040 under the RCP 8.5 scenario (Russo et al. 2016). The intensity of heat events may be modulated by land cover and soil characteristics (Miralles et al. 2014; Lemordant et al. 2016; Ramarao et al. 2016). Where temperature increase results in decreased soil moisture, latent heat flux is reduced while sensible heat fluxes are increased, allowing surface air temperature to rise further. However, this feedback may be diminished if the land surface is irrigated through enhanced evapotranspiration (Mueller et al. 2015; Siebert et al. 2017) (Section 2.5.2.2).

Drought (IPCC 2013c), including megadroughts of the last century, for example, the Dustbowl drought (Hegerl et al. 2018) (Chapter 5), is a normal component of climate variability (Hoerling et al. 2010; Dai 2011) and may be seasonal, multi-year (Van Dijk et al. 2013) or multi-decadal (Hulme 2001) with increasing degrees of impact on regional activities. This inter-annual variability is controlled particularly through remote sea surface temperature (SST) forcings, such as the Inter-decadal Pacific Oscillation (IPO) and the Atlantic Multi-decadal Oscillation (AMO), El Niño/Southern Oscillation (ENSO) and Indian Ocean Dipole (IOD), that cause drought as a result of reduced rainfall (Kelley et al. 2015; Dai 2011; Hoell et al. 2017; Espinoza et al. 2018). In some cases however, large scale SST

modes do not fully explain the severity of drought some recent event attribution studies have identified a climate change fingerprint in several regional droughts, for example, the western Amazon (Erfanian et al. 2017), southern Africa (Funk et al. 2018; Yuan et al. 2018), southern Europe and the Mediterranean including North Africa (Kelley et al. 2015; Wilcox et al. 2018), parts of North America (Williams et al. 2015; Mote et al. 2016), Russia (Otto et al. 2012), India (Ramarao et al. 2015) and Australia (Lewis and Karoly 2013).

Long-term global trends in drought are difficult to determine because of this natural variability, potential deficiencies in drought indices (especially in how evapotranspiration is treated) and the quality and availability of precipitation data (Sheffield et al. 2012; Dai 2013; Trenberth et al. 2014; Nicholls and Seneviratne 2015; Mukherjee et al. 2018). However, regional trends in frequency and intensity of drought are evident in several parts of the world, particularly in low latitude land areas, such as the Mediterranean, North Africa and the Middle East (Vicente-Serrano et al. 2014; Spinoni et al. 2015a; Dai and Zhao 2017; Páscoa et al. 2017), many regions of sub-Saharan Africa (Masih et al. 2014; Dai and Zhao 2017), central China (Wang et al. 2017e), the southern Amazon (Fu et al. 2013; Espinoza et al. 2018), India (Ramarao et al. 2016), east and south Asia, parts of North America and eastern Australia (Dai and Zhao 2017). A recent analysis of 4500 meteorological droughts globally found increased drought frequency over the East Coast of the USA, Amazonia and north-eastern Brazil, Patagonia, the Mediterranean region, most of Africa and north-eastern China with decreased drought frequency over northern Argentina, Uruguay and northern Europe (Spinoni et al. 2019). The study also found drought intensity has become more severe over north-western USA, parts of Patagonia and southern Chile, the Sahel, the Congo River basin, southern Europe, north-eastern China, and south-eastern Australia, whereas the eastern USA, south-eastern Brazil, northern Europe, and central-northern Australia experienced less severe droughts. In addition to the IPCC SR15 assessment of medium confidence in increased drying over the Mediterranean region (Hoegh-Guldberg et al. 2018), it is further assessed with *medium confidence* that frequency and intensity of droughts in Amazonia, north-eastern Brazil, Patagonia, most of Africa, and north-eastern China has increased.

There is *low confidence* in how large-scale modes of variability will respond to a warming climate (Deser et al. 2012; Liu 2012; Christensen et al. 2013; Hegerl et al. 2015; Newman et al. 2016). Although, there is evidence for an increased frequency of extreme ENSO events, such as the 1997/98 El Niño and 1988/89 La Niña (Cai et al. 2014a, 2015) and extreme positive phases of the IOD (Christensen et al. 2013; Cai et al. 2014b). However, the assessment by the SR15 was retained on an increased regional drought risk (*medium confidence*), specifically over the Mediterranean and South Africa at both 1.5°C and 2°C warming levels compared to present day, with drought risk at 2°C being significantly higher than at 1.5°C (Hoegh-Guldberg et al. 2018).

2.2.5.2 Impacts of heat extremes and drought on land

There is *high confidence* that heat extremes such as unusually hot nights, extremely high daytime temperatures, heatwaves and drought are damaging to crop production (Chapter 5). Extreme heat

events impact a wide variety of tree functions including reduced photosynthesis, increased photooxidative stress, leaves abscise, a decreased growth rate of remaining leaves and decreased growth of the whole tree (Teskey et al. 2015). Although trees are more resilient to heat stress than grasslands (Teuling et al. 2010), it has been observed that different types of forest (e.g., needleleaf vs broadleaf) respond differently to drought and heatwaves (Babst et al. 2012). For example, in the Turkish Anatolian forests net primary productivity (NPP) generally decreased during drought and heatwave events between 2000 and 2010 but in a few other regions, NPP of needle leaf forests increased (Erşahin et al. 2016). However, forests may become less resilient to heat stress in future due to the long recovery period required to replace lost biomass and the projected increased frequency of heat and drought events (Frank et al. 2015a; McDowell and Allen 2015; Johnstone et al. 2016; Stevens-Rumann et al. 2018). Additionally, widespread regional tree mortality may be triggered directly by drought and heat stress (including warm winters) and exacerbated by insect outbreak and fire (Neuvonen et al. 1999; Breshears et al. 2005; Berg et al. 2006; Soja et al. 2007; Kurz et al. 2008; Allen et al. 2010).

Gross primary production (GPP) and soil respiration form the first and second largest carbon fluxes from terrestrial ecosystems to the atmosphere in the global carbon cycle (Beer et al. 2010; Bond-Lamberty and Thomson 2010). Heat extremes impact the carbon cycle through altering these and change ecosystem-atmosphere CO₂ fluxes and the ecosystem carbon balance. Compound heat and drought events result in a stronger carbon sink reduction compared to single-factor extremes as GPP is strongly reduced and ecosystem respiration less so (Reichstein et al. 2013; Von Buttlar et al. 2018). In forest biomes, however, GPP may increase temporarily as a result of increased insolation and photosynthetic activity as was seen during the 2015–2016 ENSO related drought over Amazonia (Zhu et al. 2018). Longer extreme events (heatwave or drought or both) result in a greater reduction in carbon sequestration and may also reverse long-term carbon sinks (Ciais et al. 2005; Phillips et al. 2009; Wolf et al. 2016b; Ummenhofer and Meehl 2017; Von Buttlar et al. 2018; Reichstein et al. 2013). Furthermore, extreme heat events may impact the carbon cycle beyond the lifetime of the event. These lagged effects can slow down or accelerate the carbon cycle: it will slow down if reduced vegetation productivity and/or widespread mortality after an extreme drought are not compensated by regeneration, or speed up if productive tree and shrub seedlings cause rapid regrowth after windthrow or fire (Frank et al. 2015a). Although some ecosystems may demonstrate resilience to a single heat climate stressor like drought (e.g., forests), compound effects of, for example, deforestation, fire and drought, potentially can result in changes to regional precipitation patterns and river discharge, losses of carbon storage and a transition to a disturbance-dominated regime (Davidson et al. 2012). Additionally, adaptation to seasonal drought may be overwhelmed by multi-year drought and their legacy effects (Brando et al. 2008; da Costa et al. 2010).

Under medium- and high-emission scenarios, global warming will exacerbate heat stress, thereby amplifying deficits in soil moisture and runoff despite uncertain precipitation changes (Ficklin and Novick 2017; Berg and Sheffield 2018; Cook et al. 2018; Dai et al. 2018; Engelbrecht et al. 2015; Ramarao et al. 2015; Grillakis 2019). This will

increase the rate of drying causing drought to set in quicker, become more intense and widespread, last longer and could result in an increased global aridity (Dai 2011; Prudhomme et al. 2014).

The projected changes in the frequency and intensity of extreme temperatures and drought is expected to result in decreased carbon sequestration by ecosystems and degradation of ecosystems health and loss of resilience (Trumbore et al. 2015). Also affected are many aspects of land functioning and type including agricultural productivity (Lesk et al. 2016), hydrology (Mosley 2015; Van Loon and Laaha 2015), vegetation productivity and distribution (Xu et al. 2011; Zhou et al. 2014), carbon fluxes and stocks, and other biogeochemical cycles (Frank et al. 2015b; Doughty et al. 2015; Schlesinger et al. 2016). Carbon stocks are particularly vulnerable to extreme events due to their large carbon pools and fluxes, potentially large lagged impacts and long recovery times to regain lost stocks (Frank et al. 2015a) (Section 2.2).

2.2.5.3 Changes in heavy precipitation

A large number of extreme rainfall events have been documented over the past decades (Coumou and Rahmstorf 2012; Seneviratne et al. 2012; Trenberth 2012; Westra et al. 2013; Espinoza et al. 2014; Guhathakurta et al. 2017; Taylor et al. 2017; Thompson et al. 2017; Zilli et al. 2017). The observed shift in the trend distribution of precipitation extremes is more distinct than for annual mean precipitation and the global land fraction experiencing more intense precipitation events is larger than expected from internal variability (Fischer and Knutti 2014; Espinoza et al. 2018; Fischer et al. 2013). As a result of global warming, the number of record-breaking rainfall events globally has increased significantly by 12% during the period 1981–2010 compared to those expected due to natural multi-decadal climate variability (Lehmann et al. 2015). The IPCC SR15 reports robust increases in observed precipitation extremes for annual maximum 1-day precipitation ($RX1day$) and consecutive 5-day precipitation ($RX5day$) (Hoegh-Guldberg et al. 2018; Schleussner et al. 2017). A number of extreme rainfall events have been attributed to human influence (Min et al. 2011; Pall et al. 2011; Sippel and Otto 2014; Trenberth et al. 2015; Krishnan et al. 2016) and the largest fraction of anthropogenic influence is evident in the most rare and extreme events (Fischer and Knutti 2014).

A warming climate is expected to intensify the hydrological cycle as a warmer climate facilitates more water vapour in the atmosphere, as approximated by the Clausius-Clapeyron (C-C) relationship, with subsequent effects on regional extreme precipitation events (Christensen and Christensen 2003; Pall et al. 2007; Berg et al. 2013; Wu et al. 2013; Guhathakurta et al. 2017; Thompson et al. 2017; Taylor et al. 2017; Zilli et al. 2017; Manola et al. 2018). Furthermore, changes to the dynamics of the atmosphere amplify or weaken future precipitation extremes at the regional scale (O’Gorman 2015; Pfahl et al. 2017). Continued anthropogenic warming is very likely to increase the frequency and intensity of extreme rainfall in many regions of the globe (Seneviratne et al. 2012; Mohan and Rajeevan 2017; Prein et al. 2017; Stott et al. 2016) although many general circulation models (GCMs) underestimate observed increased trends in heavy precipitation suggesting a substantially stronger intensification

of future heavy rainfall than the multi-model mean (Borodina et al. 2017; Min et al. 2011). Furthermore, the response of extreme convective precipitation to warming remains uncertain because GCMs and regional climate models (RCMs) are unable to explicitly simulate sub-grid scale processes such as convection, the hydrological cycle and surface fluxes and have to rely on parameterisation schemes for this (Crétat et al. 2012; Rossow et al. 2013; Wehner 2013; Kooperman et al. 2014; O’Gorman 2015; Larsen et al. 2016; Chawla et al. 2018; Kooperman et al. 2018; Maher et al. 2018; Rowell and Chadwick 2018). High-resolution RCMs that explicitly resolve convection have a better representation of extreme precipitation but are dependent on the GCM to capture the large scale environment in which the extreme event may occur (Ban et al. 2015; Prein et al. 2015; Kendon et al. 2017). Inter-annual variability of precipitation extremes in the convective tropics are not well captured by global models (Allan and Liu 2018).

There is *low confidence* in the detection of long-term observed and projected seasonal and daily trends of extreme snowfall. The narrow rain–snow transition temperature range at which extreme snowfall can occur is relatively insensitive to climate warming and subsequent large interdecadal variability (Kunkel et al. 2013; O’Gorman 2014, 2015).

2.2.5.4 Impacts of precipitation extremes on different land cover types

More intense rainfall leads to water redistribution between surface and ground water in catchments as water storage in the soil decreases (green water) and runoff and reservoir inflow increases (blue water) (Liu and Yang 2010; Ekhout et al. 2018). This results in increased surface flooding and soil erosion, increased plant water stress and reduced water security, which in terms of agriculture means an increased dependency on irrigation and reservoir storage (Nainggolan et al. 2012; Favis-Mortlock and Mullen 2011; García-Ruiz et al. 2011; Li and Fang 2016; Chagas and Chaffe 2018). As there is high confidence of a positive correlation between global warming and future flood risk, land cover and processes are likely to be negatively impacted, particularly near rivers and in floodplains (Kundzewicz et al. 2014; Alfieri et al. 2016; Winsemius et al. 2016; Arnell and Gosling 2016; Alfieri et al. 2017; Wobus et al. 2017).

In agricultural systems, heavy precipitation and inundation can delay planting, increase soil compaction and cause crop losses through anoxia and root diseases (Posthumus et al. 2009). In tropical regions, flooding associated with tropical cyclones can lead to crop failure from both rainfall and storm surge. In some cases, flooding can affect yield more than drought, particularly in tropical regions (e.g., India) and in some mid/high latitude regions such as China and central and northern Europe (Zampieri et al. 2017). Waterlogging of croplands and soil erosion also negatively affect farm operations and block important transport routes (Vogel and Meyer 2018; Kundzewicz and Germany 2012). Flooding can be beneficial in drylands if the floodwaters infiltrate and recharge alluvial aquifers along ephemeral river pathways, extending water availability into dry seasons and drought years, and supporting riparian systems and human communities (Kundzewicz and Germany 2012; Guan et al. 2015). Globally, the impact of rainfall extremes on agriculture

is less than that of temperature extremes and drought, although in some regions and for some crops, extreme precipitation explains a greater component of yield variability, for example, of maize in the Midwestern USA and southern Africa (Ray et al. 2015; Lesk et al. 2016; Vogel et al. 2019).

Although many soils on floodplains regularly suffer from inundation, the increases in the magnitude of flood events mean that new areas with no recent history of flooding are now becoming severely affected (Yellen et al. 2014). Surface flooding and associated soil saturation often results in decreased soil quality through nutrient loss, reduced plant productivity, stimulated microbial growth and microbial community composition, negatively impacted soil redox and increased GHG emissions (Bossio and Scow 1998; Niu et al. 2014; Barnes et al. 2018; Sánchez-Rodríguez et al. 2019). The impact of flooding on soil quality is influenced by management systems that may mitigate or exacerbate the impact. Although soils tend to recover quickly after floodwater removal, the impact of repeated extreme flood events over longer timescales on soil quality and function is unclear (Sánchez-Rodríguez et al. 2017).

Flooding in ecosystems may be detrimental through erosion or permanent habitat loss, or beneficial, as a flood pulse brings nutrients to downstream regions (Kundzewicz et al. 2014). Riparian forests can be damaged through flooding; however, increased flooding may also be of benefit to forests where upstream water demand has lowered stream flow, but this is difficult to assess and the effect of flooding

on forests is not well studied (Kramer et al. 2008; Pawson et al. 2013). Forests may mitigate flooding, however flood mitigation potential is limited by soil saturation and rainfall intensity (Pilaš et al. 2011; Ellison et al. 2017). Some grassland species under heavy rainfall and soil saturated conditions responded negatively with decreased reproductive biomass and germination rates (Gellesch et al. 2017), however overall productivity in grasslands remains constant in response to heavy rainfall (Grant et al. 2014).

Extreme rainfall alters responses of soil CO₂ fluxes and CO₂ uptake by plants within ecosystems, and therefore result in changes in ecosystem carbon cycling (Fay et al. 2008; Frank et al. 2015a). Extreme rainfall and flooding limits oxygen in soil which may suppress the activities of soil microbes and plant roots and lower soil respiration, therefore lowering carbon cycling (Knapp et al. 2008; Rich and Watt 2013; Philben et al. 2015). However, the impact of extreme rainfall on carbon fluxes in different biomes differs. For example, extreme rainfall in mesic biomes reduces soil CO₂ flux to the atmosphere and GPP whereas in xeric biomes the opposite is true, largely as a result of increased soil water availability (Knapp and Smith 2001; Heisler and Knapp 2008; Heisler-White et al. 2009; Zeppel et al. 2014; Xu and Wang 2016; Liu et al. 2017b; Connor and Hawkes 2018).

As shown above GHG fluxes between the land and atmosphere are affected by climate. The next section assesses these fluxes in greater detail and the potential for land as a carbon sink.

Cross-Chapter Box 3 | Fire and climate change

Raman Sukumar (India), Almut Arneth (Germany), Werner Kurz (Canada), Andrey Sirin (Russian Federation), Louis Verchot (Colombia/The United States of America)

Fires have been a natural part of Earth's geological past and its biological evolution since at least the late Silurian, about 400 million years ago (Scott 2000). Presently, roughly 3% of the Earth's land surface burns annually which affects both energy and matter exchanges between the land and atmosphere (Stanne et al. 2009). Climate is a major determinant of fire regimes through its control of fire weather, as well as through its interaction with vegetation productivity (fuel availability) and structure (fuel distribution and flammability) (Archibald et al. 2013) at the global (Krawchuk and Moritz 2011), regional (Pausas and Paula 2012) and local (Mondal and Sukumar 2016) landscape scales. Presently, humans are the main cause of fire ignition with lightning playing a lesser role globally (Bowman et al. 2017; Harris et al. 2016), although the latter factor has been predominantly responsible for large fires in regions such as the North American boreal forests (Veraverbeke et al. 2017). Humans also influence fires by actively extinguishing them, reducing spread and managing fuels.

Historical trends and drivers in land area burnt

While precipitation has been the major influence on fire regimes before the Holocene, human activities have become the dominant drivers since then (Bowman et al. 2011). There was less biomass burning during the 20th century than at any time during the past two millennia as inferred from charcoal sedimentary records (Doerr and Santin 2016), though there has been an increase in the most recent decades (Marlon et al. 2016). Trends in land area burnt have varied regionally (Giglio et al. 2013). Northern hemisphere Africa has experienced a fire decrease of 1.7 Mha yr⁻¹ (-1.4% yr⁻¹) since 2000, while southern hemisphere Africa saw an increase of 2.3 Mha yr⁻¹ (+1.8% yr⁻¹) during the same period. Southeast Asia witnessed a small increase of 0.2 Mha yr⁻¹ (+2.5% yr⁻¹) since 1997, while Australia experienced a sharp decrease of about 5.5 Mha yr⁻¹ (-10.7% yr⁻¹) during 2001–2011, followed by an upsurge in 2011 that exceeded the annual area burned in the previous 14 years. A recent analysis using the Global Fire Emissions Database v.4 (GFED4s) that includes small fires concluded that the net reduction in land area burnt globally during 1998–2015 was $-24.3 \pm 8.8\%$ ($-1.35 \pm 0.49\%$ yr⁻¹) (Andela et al. 2017). However, from the point of fire emissions it is important to consider the land cover types which have experienced changes in area burned; in this instance, most of the declines have come from grasslands, savannas and other non-forest land cover types (Andela et al. 2017). Significant increases in forest area burned (with higher fuel consumption per unit area) have been recorded in western and boreal

Cross-Chapter Box 3 (continued)

North America (Abatzoglou and Williams 2016; Ansmann et al. 2018) and in boreal Siberia (Ponomarev et al. 2016) in recent times. The 2017 and 2018 fires in British Columbia, Canada, were the largest ever recorded since the 1950s with 1.2 Mha and 1.4 Mha of forest burnt, respectively (Hanes et al. 2018) and smoke from these fires reaching the stratosphere over central Europe (Ansmann et al. 2018).

Climate variability and extreme climatic events such as severe drought, especially those associated with the El Niño Southern Oscillation (ENSO), play a major role in fire upsurges, as in equatorial Asia (Huijnen et al. 2016). Fire emissions in tropical forests increased by 133% on average during and following six El Niño years compared to six La Niña years during 1997–2016, due to reductions in precipitation and terrestrial water storage (Chen et al. 2017). The expansion of agriculture and deforestation in the humid tropics has also made these regions more vulnerable to drought-driven fires (Davidson et al. 2012; Brando et al. 2014). Even when deforestation rates were overall declining, as in the Brazilian Amazon during 2003–2015, the incidence of fire increased by 36% during the drought of 2015 (Aragão et al. 2018).

GHG emissions from fires

Emissions from wildfires and biomass burning are a significant source of GHGs (CO_2 , CH_4 , N_2O), carbon monoxide (CO), carbonaceous aerosols, and an array of other gases including non-methane volatile organic compounds (NMVOC) (Akagi et al. 2011; Van Der Werf et al. 2010). GFED4s has updated fire-related carbon emission estimates biome-wise (regionally and globally), using higher resolution input data gridded at 0.25° , a new burned area dataset with small fires, improved fire emission factors (Akagi et al. 2011; Urbanski 2014) and better fire severity characterisation of boreal forests (van der Werf et al. 2017). The estimates for the period 1997–2016 are 2.2 GtC yr^{-1} , being highest in the 1997 El Niño (3.0 GtC yr^{-1}) and lowest in 2013 (1.8 GtC yr^{-1}). Furthermore, fire emissions during 1997–2016 were dominated by savanna (65.3%), followed by tropical forest (15.1%), boreal forest (7.4%), temperate forest (2.3%), peatland (3.7%) and agricultural waste burning (6.3%) (van der Werf et al. 2017).

Fires not only transfer carbon from land to the atmosphere but also between different terrestrial pools: from live to dead biomass to soil, including partially charred biomass, charcoal and soot constituting $0.12\text{--}0.39 \text{ GtC yr}^{-1}$ or $0.2\text{--}0.6\%$ of annual terrestrial NPP (Doerr and Santin 2016). Carbon from the atmosphere is sequestered back into regrowing vegetation at rates specific to the type of vegetation and other environmental variables (Loehman et al. 2014). Fire emissions are thus not necessarily a net source of carbon into the atmosphere, as post-fire recovery of vegetation can sequester a roughly equivalent amount back into biomass over a time period of one to a few years (in grasslands and agricultural lands) to decades (in forests) (Landry and Matthews 2016). Fires from deforestation (for land use change) and on peatlands (which store more carbon than terrestrial vegetation) obviously are a net source of carbon from the land to the atmosphere (Turetsky et al. 2014); these types of fires were estimated to emit 0.4 GtC yr^{-1} in recent decades (van der Werf et al. 2017). Peatland fires dominated by smouldering combustion under low temperatures and high moisture conditions can burn for long periods (Turetsky et al. 2014).

Fires, land degradation/desertification and land-atmosphere exchanges

Flammable ecosystems are generally adapted to their specific fire regimes (Bond et al. 2005). A fire regime shift alters vegetation and soil properties in complex ways, both in the short- and the long-term, with consequences for carbon stock changes, albedo, fire-atmosphere-vegetation feedbacks and the ultimate biological capacity of the burnt land (Bond et al. 2004; Bremer and Ham 1999; MacDermott et al. 2016; Tepley et al. 2018; Moody et al. 2013; Veraverbeke et al. 2012) A fire-driven shift in vegetation from a forested state to an alternative stable state such as a grassland (Fletcher et al. 2014; Moritz 2015) with much less carbon stock is a distinct possibility. Fires cause soil erosion through action of wind and water (Moody et al. 2013) thus resulting in land degradation (Chapter 4) and eventually desertification (Chapter 3). Fires also affect carbon exchange between land and atmosphere through ozone (which retards photosynthesis) and aerosol (which slightly increases diffuse radiation) emissions. The net effect from fire on global GPP during 2002–2011 is estimated to be $-0.86 \pm 0.74 \text{ GtC yr}^{-1}$ (Yue and Unger 2018).

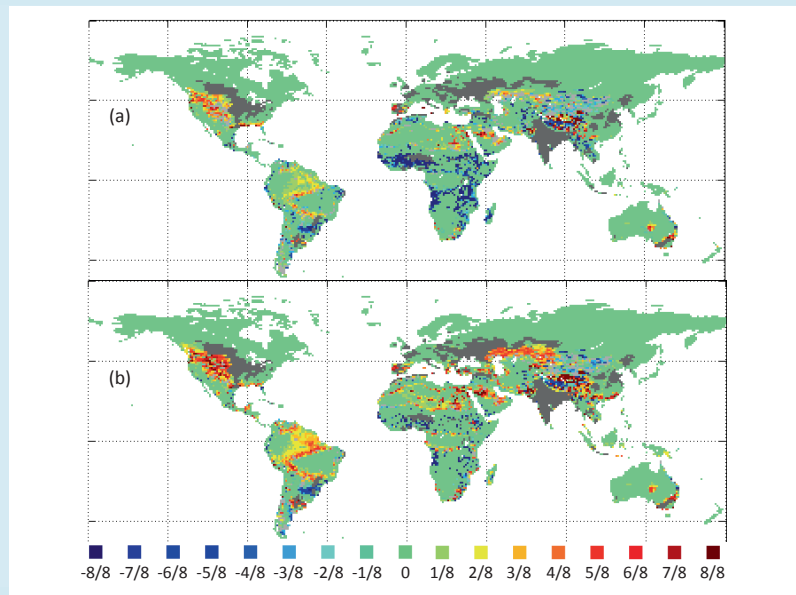
Fires under future climate change

Temperature increase and precipitation decline would be the major driver of fire regimes under future climates as evapotranspiration increases and soil moisture decreases (Pechony and Shindell 2010; Aldersley et al. 2011; Abatzoglou and Williams 2016; Fernandes et al. 2017). The risk of wildfires in future could be expected to change, increasing significantly in North America, South America, central Asia, southern Europe, southern Africa and Australia (Liu et al. 2010). There is emerging evidence that recent regional surges in wildland fires are being driven by changing weather extremes, thereby signalling geographical shifts in fire proneness (Jolly et al. 2015). Fire weather season has already lengthened by 18.7% globally between 1979 and 2013, with statistically significant increases across 25.3% but decreases only across 10.7% of Earth's land surface covered with vegetation. Even sharper changes have been observed during the second half of this period (Jolly et al. 2015). Correspondingly, the global area experiencing long fire weather seasons (defined as experiencing a fire weather season greater than one standard deviation (SD)

Cross-Chapter Box 3 (continued)

from the mean global value) has increased by 3.1% per annum or 108.1% during 1979–2013. Fire frequencies under 2050 conditions are projected to increase by approximately 27% globally, relative to the 2000 levels, with changes in future fire meteorology playing the most important role in enhancing global wildfires, followed by land cover changes, lightning activities and land use, while changes in population density exhibit the opposite effects (Huang et al. 2014).

However, climate is only one driver of a complex set of environmental, ecological and human factors in influencing fire regimes (Bowman et al. 2011). While these factors lead to complex projections of future burnt area and fire emissions (Knorr et al. 2016a, b), human exposure to wildland fires could still increase due to population expansion into areas already under high risk of fires (Knorr et al. 2016a, b). There are still major challenges in projecting future fire regimes and how climate, vegetation and socio/economic factors will interact (Hanson et al. 2016; Harris et al. 2016). There is also need for integrating various fire management strategies, such as fuel-reduction treatments in natural and planted forests, with other environmental and societal considerations to achieve the goals of carbon emissions reductions, maintain water quality, biodiversity conservation and human safety (Moritz et al. 2014; Gharun et al. 2017).



Cross-Chapter Box 3, Figure 1 | The probability of low-fire regions becoming fire prone (positive values), or of fire-prone areas changing to a low-fire state (negative values) between 1971–2000 and 2071–2100 based on eight-Earth system model (ESM) ensembles, two Shared Socio-economic Pathways (SSPs) and two Representative Concentration Pathways (RCPs). Light grey: areas where at least one ensemble simulation predicts a positive and one negative change (lack of agreement). Dark grey: area with >50% past or future cropland. Fire-prone areas are defined as having a fire frequency of $>0.01 \text{ yr}^{-1}$, (a) RCP4.5 emissions with SSP3 demographics, and (b) RCP8.5 emissions with SSP5 demographics (Knorr et al. 2016a).

In summary, climate change is playing an increasing role in determining wildfire regimes alongside human activity (*medium confidence*), with future climate variability expected to enhance the risk and severity of wildfires in many biomes, such as tropical rainforests (*high confidence*). Fire weather seasons have lengthened globally between 1979 and 2013 (*low confidence*). Global land area burned has declined in recent decades, mainly due to less burning in grasslands and savannas (*high confidence*). While drought remains the dominant driver of fire emissions, there has recently been increased fire activity in some tropical and temperate regions during normal to wetter-than-average years due to warmer temperatures that increase vegetation flammability (*medium confidence*). The boreal zone is also experiencing larger and more frequent fires, and this may increase under a warmer climate (*medium confidence*).

2.3 Greenhouse gas fluxes between land and atmosphere

Land is simultaneously a source and sink for several GHGs. Moreover, both natural and anthropogenic processes determine fluxes of GHGs, making it difficult to separate 'anthropogenic' and 'non-anthropogenic' emissions and removals. A meeting report by the IPCC (2010) divided the processes responsible for fluxes from land into three categories: (i) the *direct effects* of anthropogenic activity due to changing land cover and land management, (ii) the *indirect effects* of anthropogenic environmental change, such as climate change, carbon dioxide (CO₂) fertilisation, nitrogen deposition, and (iii) *natural* climate variability and natural disturbances (e.g., wildfires, windrow, disease). The meeting report (IPCC 2010) noted that it was impossible with any direct observation to separate direct anthropogenic effects from non-anthropogenic (indirect and natural) effects in the land sector.

As a result, different approaches and methods for estimating the anthropogenic fluxes have been developed by different communities to suit their individual purposes, tools and data availability.

The major GHGs exchanged between land and the atmosphere discussed in this chapter are CO₂ (Section 2.3.1), methane (CH₄) (Section 2.3.2) and nitrous oxide (N₂O) (Section 2.3.3). We estimate the total emissions from AFOLU to be responsible for approximately 23% of global anthropogenic GHG emissions over the period 2007–2016 (Smith et al. 2013a; Ciais et al. 2013a) (Table 2.2). The estimate is similar to that reported in AR5 (*high confidence*), with slightly more than half these emissions coming as non-CO₂ GHGs from agriculture. Emissions from AFOLU have remained relatively constant since AR4, although their relative contribution to anthropogenic emissions has decreased due to increases in emissions from the energy sector.

Table 2.2 | Net anthropogenic emissions due to Agriculture, Forestry, and other Land Use (AFOLU) and non-AFOLU (average for 2007–2016).¹ Positive value represents emissions; negative value represents removals.

		Direct anthropogenic							
Gas	Units	Net anthropogenic emissions due to Agriculture, Forestry, and Other Land Use (AFOLU)			Non-AFOLU anthropogenic GHG emissions ⁴	Total net anthropogenic emissions (AFOLU + non-AFOLU) by gas	AFOLU as a % of total net anthropogenic emissions, by gas	Natural response of land to human-induced environmental change ⁵	Net land – atmosphere flux from all lands
		FOLU	Agriculture	Total					
		A	B	C = A + B	D	E = C + D	F = (C/E) × 100	G	A + G
CO ₂ ²	GtCO ₂ yr ⁻¹	5.2 ± 2.6	No data	5.2 ± 2.6	33.9 ± 1.8	39.1 ± 3.2	13%	-11.2 ± 2.6	-6.0 ± 3.7
CH ₄ ^{3,6}	MtCH ₄ yr ⁻¹	19.2 ± 5.8	142 ± 43	161 ± 43	201 ± 101	362 ± 109			
	GtCO ₂ -eq yr ⁻¹	0.5 ± 0.2	4.0 ± 1.2	4.5 ± 1.2	5.6 ± 2.8	10.1 ± 3.1	44%		
N ₂ O ^{3,6}	MtN ₂ O yr ⁻¹	0.3 ± 0.1	8.3 ± 2.5	8.7 ± 2.5	2.0 ± 1.0	10.6 ± 2.7			
	GtCO ₂ -eq yr ⁻¹	0.09 ± 0.03	2.2 ± 0.7	2.3 ± 0.7	0.5 ± 0.3	2.8 ± 0.7	81%		
Total (GHG)	GtCO₂-eq yr⁻¹	5.8 ± 2.6	6.2 ± 1.4	12.0 ± 2.9	40.0 ± 3.4	52.0 ± 4.5	23%		

¹ Estimates are only given until 2016 as this is the latest date when data are available for all gases.

² Net anthropogenic flux of CO₂ due to land cover change such as deforestation and afforestation, and land management including wood harvest and regrowth, as well as peatland burning, based on two bookkeeping models as used in the Global Carbon Budget and for AR5. Agricultural soil carbon stock change under the same land use is not considered in these models.

³ Estimates show the mean and assessed uncertainty of two databases, FAOSTAT and USEPA 2012.

⁴ Total non-AFOLU emissions were calculated as the sum of total CO₂-eq emissions values for energy, industrial sources, waste and other emissions with data from the Global Carbon Project for CO₂, including international aviation and shipping and from the PRIMAP database for CH₄ and N₂O averaged over 2007–2014 only as that was the period for which data were available.

⁵ The natural response of land to human-induced environmental changes is the response of vegetation and soils to environmental changes such as increasing atmospheric CO₂ concentration, nitrogen deposition, and climate change. The estimate shown represents the average from Dynamic Global Vegetation Models.

⁶ All values expressed in units of CO₂-eq are based on AR5 100-year Global Warming Potential (GWP) values without climate-carbon feedbacks (N₂O = 265; CH₄ = 28). Note that the GWP has been used across fossil fuel and biogenic sources of methane. If a higher GWP for fossil fuel CH₄ (30 per AR5), then total anthropogenic CH₄ emissions expressed in CO₂-eq would be 2% greater.

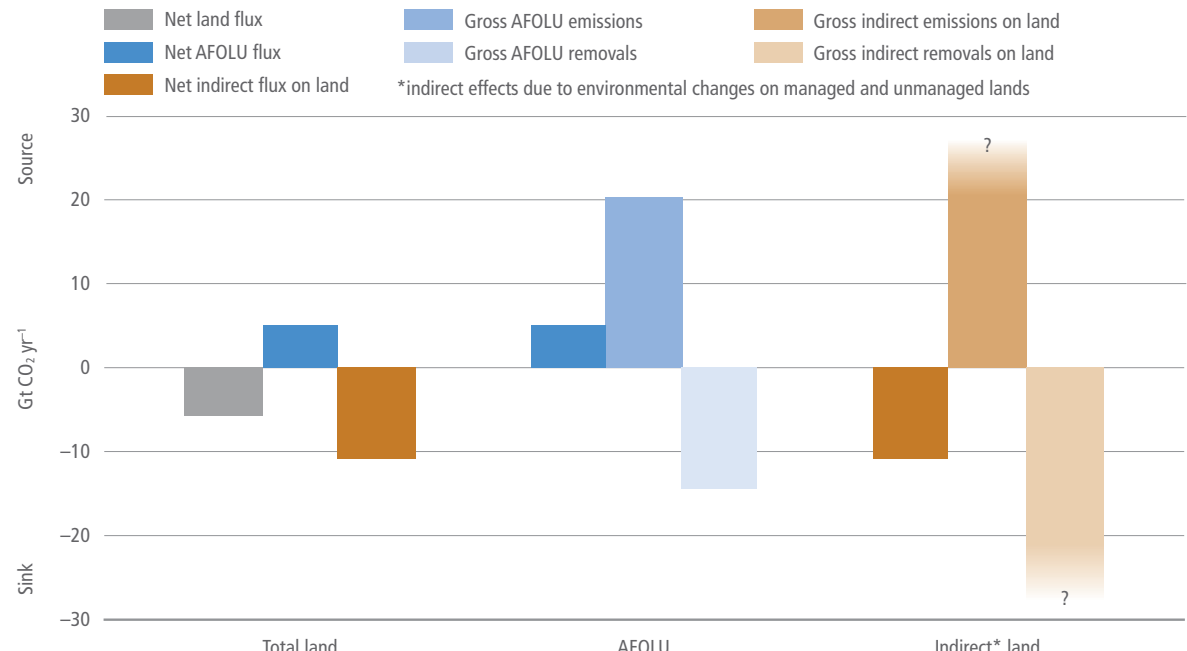


Figure 2.4 | Net and gross fluxes of CO_2 from land (annual averages for 2008–2017). Left: The total net flux of CO_2 between land and atmosphere (grey) is shown with its two component fluxes, (i) net AFOLU emissions (blue), and (ii) the net land sink (brown), due to indirect environmental effects and natural effects on managed and unmanaged lands. Middle: The gross emissions and removals contributing to the net AFOLU flux. Right: The gross emissions and removals contributing to the land sink.

2.3.1 Carbon dioxide

This section is divided into four sub-sections (Figure 2.4): (i) the total net flux of CO_2 between land and atmosphere, (ii) the contributions of AFOLU fluxes and the non-AFOLU land sink to that total net CO_2 flux, (iii) the gross emissions and removals comprising the net AFOLU flux, and (iv) the gross emissions and removals comprising the land sink. Emissions to the atmosphere are positive; removals from the atmosphere are negative.

2.3.1.1 The total net flux of CO_2 between land and atmosphere

The net effects of all anthropogenic and non-anthropogenic processes on managed and unmanaged land result in a net removal of CO_2 from the atmosphere (*high confidence*). This total net land-atmosphere removal (defined here as *the total net land flux*) is estimated to have averaged $6.0 \pm 2.0 \text{ GtCO}_2 \text{ yr}^{-1}$ (*likely range*) from 2007–2016 (Table 2.3). The estimate is determined from summing the AFOLU and non-AFOLU fluxes due to transient climate change, CO_2 fertilisation and nitrogen deposition calculated by models in the global carbon budget (Le Quéré et al. 2018), and is consistent with inverse modelling techniques based on atmospheric CO_2 concentrations and air transport (range: $5.1\text{--}8.8 \text{ GtCO}_2 \text{ yr}^{-1}$) (Peylin et al. 2013; Van Der Laan-Luijkx et al. 2017; Saeki and Patra 2017; Le Quéré et al. 2018) (see Box 2.2 for methods). A recent inverse analysis, considering carbon transport in rivers and oceans, found a net flux of CO_2 for land within this range, but a lower source from southern lands and a lower sink in northern lands (Resplandy et al. 2018).

The net removal of CO_2 by land has generally increased over the last 60 years in proportion to total emissions of CO_2 (*high confidence*). Although land has been a net sink for CO_2 since around the middle of last century, it was a net source to the atmosphere before that time, primarily as a result of emissions from AFOLU (Le Quéré et al. 2018).

2.3.1.2 Separation of the total net land flux into AFOLU fluxes and the land sink

The total net flux of carbon between land and the atmosphere can be divided into fluxes due to direct human activities (i.e., AFOLU) and fluxes due to indirect anthropogenic and natural effects (i.e., the land sink) (Table 2.3). These two components are less certain than their sums, the total net flux of CO_2 between atmosphere and land. The land sink, estimated with DGVMs, is least certain (Figure 2.5).

Fluxes attributed to AFOLU

The modelled AFOLU flux was a net emission of $5.2 \pm 2.6 \text{ GtCO}_2 \text{ yr}^{-1}$ (*likely range*) for 2007–2016, approximately 13% of total anthropogenic CO_2 emissions (Le Quéré et al. 2018) (Table 2.3). This net flux was due to direct anthropogenic activities, predominately tropical deforestation, but also afforestation/reforestation, and fluxes due to forest management (e.g., wood harvest) and other types of land management, as well as peatland drainage and burning. The AFOLU flux is the mean of two estimates from bookkeeping models (Hansis et al. 2015; Houghton and Nassikas 2017), and this estimated

Table 2.3 | Perturbation of the global carbon cycle caused by anthropogenic activities (GtCO₂ yr⁻¹). Source: Le Quéré et al. (2018).

	CO ₂ flux (GtCO ₂ yr ⁻¹), 10-year mean					
	1960–1969	1970–1979	1980–1989	1990–1999	2000–2009	2008–2017
Emissions						
Fossil CO ₂ emissions	11.4 ± 0.7	17.2 ± 0.7	19.8 ± 1.1	23.1 ± 1.1	28.6 ± 1.5	34. ± 1.8
AFOLU net emissions	5.5 ± 2.6	4.4 ± 2.6	4.4 ± 2.6	5.1 ± 2.6	4.8 ± 2.6	5.5 ± 2.6
Partitioning						
Growth in atmosphere	6.2 ± 0.3	10.3 ± 0.3	12.5 ± 0.07	11.4 ± 0.07	14.7 ± 0.07	17.2 ± 0.07
Ocean sink	3.7 ± 1.8	4.8 ± 1.8	6.2 ± 1.8	7.3 ± 1.8	7.7 ± 1.8	8.8 ± 1.8
Land sink (non-AFOLU)	4.4 ± 1.8	7.7 ± 1.5	6.6 ± 2.2	8.8 ± 1.8	9.9 ± 2.6	11.7 ± 2.6
Budget imbalance	2.2	-1.1	-1.1	0.7	0.7	1.8
Total net land flux (AFOLU – land sink)	+1.1 ± 3.2	-3.3 ± 3.0	-2.2 ± 3.4	-3.7 ± 2.2	-5.1 ± 3.2	-6.2 ± 3.7

mean is consistent with the mean obtained from an assemblage of DGVMs (Le Quéré et al. 2018) (Box 2.2 and Figure 2.5), although not all individual DGMVs include the same types of land use. Net CO₂ emissions from AFOLU have been relatively constant since 1900. AFOLU emissions were the dominant anthropogenic emissions until around the middle of the last century when fossil fuel emissions became dominant (Le Quéré et al. 2018). AFOLU activities have resulted in emissions of CO₂ over recent decades (*robust evidence, high agreement*) although there is a wide range of estimates from different methods and approaches (Smith et al. 2014; Houghton et al. 2012; Gasser and Ciais 2013; Pongratz et al. 2014; Tubiello et al. 2015; Grassi et al. 2018) (Box 2.2, Figure 2.5 and Figure 2.7).

DGVMs and one bookkeeping model (Hansis et al. 2015) used spatially explicit, harmonised land-use change data (LUH2) (Hurtt et al. 2017) based on HYDE 3.2. The HYDE data, in turn, are based on changes in the areas of croplands and pastures. In contrast, the Houghton bookkeeping approach (Houghton and Nassikas 2017) used primarily changes in forest area from the FAO Forest Resource Assessment (FAO 2015) and FAOSTAT to determine changes in land use. To the extent that forests are cleared for land uses other than crops and pastures, estimates from Houghton and Nassikas (2017, 2018) are higher than estimates from DGMVs. In addition, both bookkeeping models (Hansis et al. 2015; Houghton and Nassikas 2017) included estimates of carbon emissions in Southeast Asia from peat burning from GFED4s (Randerson et al. 2015) and from peat drainage (Hooijer et al. 2010).

Satellite-based estimates of CO₂ emissions from losses of tropical forests during 2000–2010 corroborate the modelled emissions but are quite variable; 4.8 GtCO₂ yr⁻¹ (Tyukavina et al. 2015), 3.0 GtCO₂ yr⁻¹ (Harris et al. 2015), 3.2 GtCO₂ yr⁻¹ (Achard et al. 2014) and 1.6 GtCO₂ yr⁻¹ (Baccini et al. 2017). Differences in estimates can be explained to a large extent by the different approaches used. For example, the analysis by Tyukavina et al. (2015) led to a higher estimate because they used a finer spatial resolution. Three of the estimates considered losses in forest area and ignored degradation and regrowth of forests. Baccini et al. (2017) in contrast, included both losses and gains in forest area and losses and gains of carbon within forests (i.e., forest degradation and growth). The four remote sensing studies cited above also reported committed emissions; in essence, all of the carbon lost from deforestation was assumed to

be released to the atmosphere in the year of deforestation. In reality, only some of the carbon in trees is released immediately to the atmosphere at the time of deforestation. The unburned portion is transferred to woody debris and wood products. Both bookkeeping models and DGVMs account for the delayed emissions in growth and decomposition. Finally, the satellite-based estimates do not include changes in soil carbon.

In addition to differences in land-cover data sets between models and satellites, there are many other methodological reasons for differences (Houghton et al. 2012; Gasser and Ciais 2013; Pongratz et al. 2014; Tubiello et al. 2015) (Box 2.2). There are different definitions of land-cover type, including forest (e.g., FAO uses a tree cover threshold for forests of 10%, Tyukavina et al. (2017) used 25%), different estimates of biomass and soil carbon density (MgC ha⁻¹), different approaches to tracking emissions through time (legacy effects) and different types of activity included (e.g., forest harvest, peatland drainage and fires). Most DGVMs only recently (since AR5) included forest management processes, such as tree harvesting and land clearing for shifting cultivation, leading to larger estimates of CO₂ emissions than when these processes are not considered (Arneth et al. 2017; Erb et al. 2018). Grazing management has likewise been found to have large effects (Sanderman et al. 2017), and is not included in most DGVMs (Pugh et al. 2015; Pongratz et al., 2018).

Nationally reported greenhouse gas inventories versus global model estimates

There are large differences globally between estimates of net anthropogenic land-atmosphere fluxes of CO₂ from national GHGs and from global models, and the same is true in many regions (Figure 2.5). Fluxes reported to the UNFCCC through country GHGs were noted as about 4.3 GtCO₂ yr⁻¹ lower (Grassi et al. 2018) than estimates from the bookkeeping model (Houghton et al. 2012) used in the carbon budget for AR5 (Ciais et al. 2013a). The anthropogenic emissions of CO₂ from AFOLU reported in countries' GHG inventories were 0.1 ± 1.0 GtCO₂ yr⁻¹ globally during 2005–2014 (Grassi et al. 2018) much lower than emission estimates from the two global bookkeeping models of 5.1 ± 2.6 GtCO₂ yr⁻¹ (*likely range*) over the same time period (Le Quéré et al. 2018). Transparency and comparability in estimates can support measuring, reporting and verifying GHG fluxes under the UNFCCC, and also the global

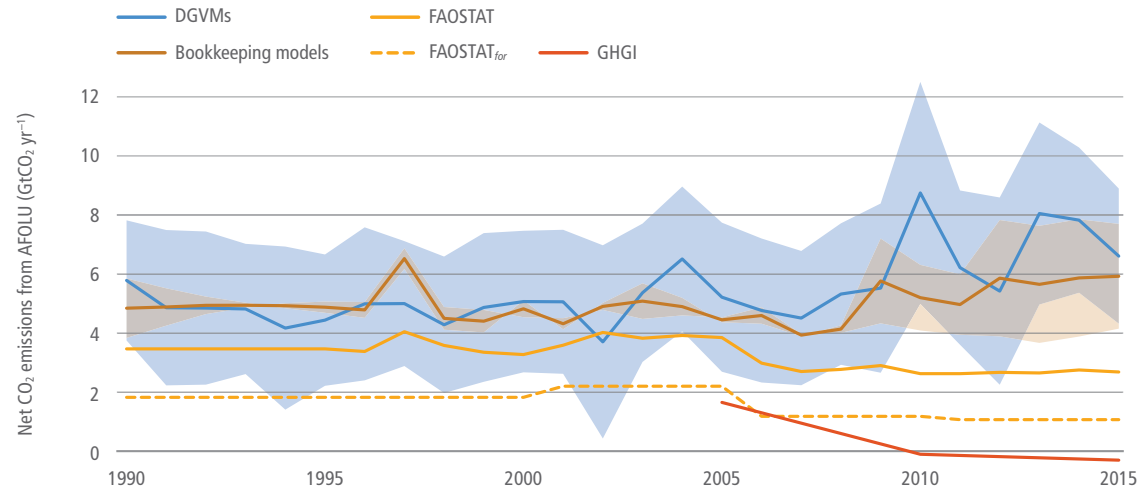


Figure 2.5 | Global net CO₂ emissions due to AFOLU from different approaches (in GtCO₂ yr⁻¹). Brown line: the mean and individual estimates (brown shading) from two bookkeeping models (Houghton and Nassikas 2017; Hansis et al. 2015). Blue line: the mean from DGVMs run with the same driving data with the pale blue shading showing the ±1 standard deviation range. Yellow line: data downloaded from FAOSTAT website (Tubiello et al. 2013); the dashed line is primarily forest-related emissions, while the solid yellow line also includes emissions from peat fires and peat draining. Orange line: Greenhouse Gas Inventories (GHGI) based on country reports to UNFCCC (Grassi et al. 2018), data are shown only from 2005 because reporting in many developing countries became more consistent/reliable after this date. For more details on methods see Box 2.2.

a) Effects of various factors on the forest CO₂ fluxes and where they occur

Direct-human induced effects

- Land use change
- Harvest and other management

Occur on managed land

Indirect-human induced effects

- Climate change induced change in T°, precipitation, length of growing season
- Atmospheric CO₂ fertilisation and N deposition, impact of air pollution
- Changes in natural disturbances regime

Occur on managed and unmanaged land

Natural effects

- Natural interannual variability
- Natural disturbances

b) Conceptual differences in defining the anthropogenic land CO₂ flux

IPCC AR5 and Global Carbon Budget:

Bookkeeping models: "Land Use Change"

	Managed land	Unmanaged land
Direct human induced effects	✓	
Indirect human induced effects		
Natural effects		

DGVMs: "Land Use Change" and "Land Sink"

	Managed land	Unmanaged land
Direct human induced effects	✓	
Indirect human induced effects	✓	✓
Natural effects	✓	✓

Country GHG inventories:

"AFOLU (LULUCF)"

	Managed land	Unmanaged land
Direct human induced effects	✓	
Indirect human induced effects	✓	
Natural effects	✓	

Figure 2.6 | Summary of the main conceptual differences between GHG Inventories and global models in considering what is the 'anthropogenic land CO₂ flux'. Adapted from Grassi et al. (2018), effects of key processes on the land flux as defined by IPCC (2010) including where these effects occur (in managed and/or unmanaged lands) and how these effects are captured in (a) bookkeeping models that do not explicitly model the effects of environmental change (although some is implicitly captured in data on carbon densities and growth and decay rates), (b) DGVMs that include the effects of environmental change on all lands, and run the models with and without land use change to diagnose 'land use change'. The 'land sink' is then conceptually assumed to be a natural response of land to the anthropogenic perturbation of environmental change, DGVMs include the effects of inter-annual climate variability, and some include fires but no other natural disturbances, and (c) GHG Inventories reported by countries to the UNFCCC that report all fluxes in areas the countries define as 'managed land' but do not report unmanaged land. This is the CO₂ flux due to Land Use Land Use Change and Forestry (LULUCF) which is a part of the overall AFOLU flux. The area of land considered as managed in the inventories is greater than that considered as subject to direct management activities (harvest and regrowth) in the models.

stocktake, which will assess globally the progress towards achieving the long-term goals of the Paris Agreement. These differences can be reconciled largely by taking account of the different approaches to defining ‘anthropogenic’ in terms of different areas of land and treatment of indirect environmental change (Grassi et al. 2018).

To date there has been one study that quantitatively reconciles the global model estimates with GHGIs (Grassi et al. 2018). The separation of anthropogenic from non-anthropogenic effects is impossible with direct observation (IPCC 2010). The different approaches of models and GHGIs to estimating anthropogenic emissions and removals are shown in (Figure 2.6). The difficulty is that *indirect* effects of environmental changes (e.g., climate change and rising atmospheric CO₂) affect both managed and unmanaged lands, and some approaches treat these as anthropogenic while others do not. Bookkeeping models (e.g., Houghton and Nassikas 2017) attempt to estimate the fluxes of CO₂ driven by direct anthropogenic effects alone. DGVMs model the *indirect* environmental effects of climate and CO₂. If the indirect effects happen on land experiencing anthropogenic land cover change or management (harvest and regrowth), DGVMs treat this as anthropogenic. Country GHGIs separately report fluxes due to land conversion (e.g., forests to croplands) and fluxes due to land management (e.g., forest land remaining forest land). The ‘managed land proxy’ is used as a pragmatic approach to estimate anthropogenic fluxes on managed lands, whereby countries define the areas they consider managed and include all of the emissions and removals that occur on those lands. Emissions and removals are caused simultaneously by direct, indirect and natural drivers and are captured in the reporting, which often relies on inventories.

Grassi et al. (2018) demonstrated that estimates of CO₂ emissions from global models and from nationally reported GHGIs were similar for deforestation and afforestation, but different for managed forests. Countries generally reported larger areas of managed forests than the models and the carbon removals by these managed forests were also larger. The flux due to indirect effects on managed lands was quantified using post-processing of results from DGVMs, looking at the *indirect* effects of CO₂ and climate change on secondary forest areas. The derived DGVM *indirect* managed forest flux was found to account for most of the difference between the bookkeeping models and the inventories.

Regional differences

Figure 2.7 shows regional differences in emissions due to AFOLU. Recent increases in deforestation rates in some tropical countries have been partially balanced by increases in forest area in India, China, the USA and Europe (FAO-FRA 2015). The trend in emissions from AFOLU since the 1990s is *uncertain* because some data suggest a declining rate of deforestation (FAO-FRA 2015), while data from satellites suggest an increasing rate (Kim 2014; Hansen et al. 2012). The disagreement results in part from differences in the definition of forest and approaches to estimating deforestation. The FAO defines deforestation as the conversion of forest to another land use (FAO-FRA 2015), while the measurement of forest loss by satellite may include wood harvests (forests remaining forests) and natural disturbances that are not directly caused by anthropogenic activity (e.g., forest mortality from droughts and fires). Trends in anthropogenic and natural disturbances

may be in opposite directions. For example, recent drought-induced fires in the Amazon have increased the emissions from wildfires at the same time that emissions from anthropogenic deforestation have declined (Aragão et al. 2018). Furthermore, there have been advances since AR5 in estimating the GHG effects of different types of forest management (e.g., Valade et al. 2017). Overall, there is *robust evidence* and *high agreement* for a net loss of forest area and tree cover in the tropics and a net gain, mainly of secondary forests and sustainably managed forests, in the temperate and boreal zones (Chapter 1).

Processes responsible for the land sink

Just over half of total net anthropogenic CO₂ emissions (AFOLU and fossil fuels) were taken up by oceanic and land sinks (*robust evidence, high agreement*) (Table 2.3). The land sink was referred to in AR5 as the ‘residual terrestrial flux’, as it was not estimated directly, but calculated by difference from the other directly estimated fluxes in the budget (Table 2.3). In the 2018 budget (Le Quéré et al. 2018), the land sink term was instead estimated directly by DGVMs, leaving a budget imbalance of 2.2 GtCO₂ yr⁻¹ (sources overestimated or sinks underestimated). The budget imbalance may result from variations in oceanic uptake or from uncertainties in fossil fuel or AFOLU emissions, as well as from land processes not included in DGVMs.

The land sink is thought to be driven largely by the indirect effects of environmental change (e.g., climate change, increased atmospheric CO₂ concentration, nitrogen deposition) on unmanaged and managed lands (*robust evidence, high agreement*). The land sink has generally increased since 1900 and was a net sink of 11.7 ± 3.7 GtCO₂ yr⁻¹ during the period 2008–2017 (Table 2.3), absorbing 29% of global anthropogenic emissions of CO₂. The land sink has slowed the rise in global land-surface air temperature by $0.09 \pm 0.02^\circ\text{C}$ since 1982 (*medium confidence*) (Zeng et al. 2017).

The rate of CO₂ removal by land accelerated from -0.026 ± 0.24 GtCO₂ yr⁻¹ during the warming period (1982–1998) to -0.436 ± 0.260 GtCO₂ yr⁻¹ during the warming hiatus (1998–2012). One explanation is that respiration rates were lower during the warming hiatus (Ballantyne et al. 2017). However, the lower rate of growth in atmospheric CO₂ during the warming hiatus may have resulted, not from lower rates of respiration, but from declining emissions from AFOLU (lower rates of tropical deforestation and increased forest growth in northern mid-latitudes) (Piao et al. 2018). Changes in the growth rate of atmospheric CO₂, by themselves, do not identify the processes responsible and the cause of the variation is uncertain.

While year-to-year variability in the indirect land sink is high in response to climate variability, DGVM fluxes are influenced far more on decadal timescales by CO₂ fertilisation. A DGVM intercomparison (Sitch et al. 2015) for 1990–2009 found that CO₂ fertilisation alone contributed a mean global removal of -10.54 ± 3.68 GtCO₂ yr⁻¹ (trend -0.444 ± 0.202 GtCO₂ yr⁻¹). Data from forest inventories around the world corroborate the modelled land sink (Pan et al. 2011). The geographic distribution of the non-AFOLU land sink is less certain. While it seems to be distributed globally, its distribution between the tropics and non-tropics is estimated to be between 1:1 (Pan et al. 2011) and 1:2 (Houghton et al. 2018).

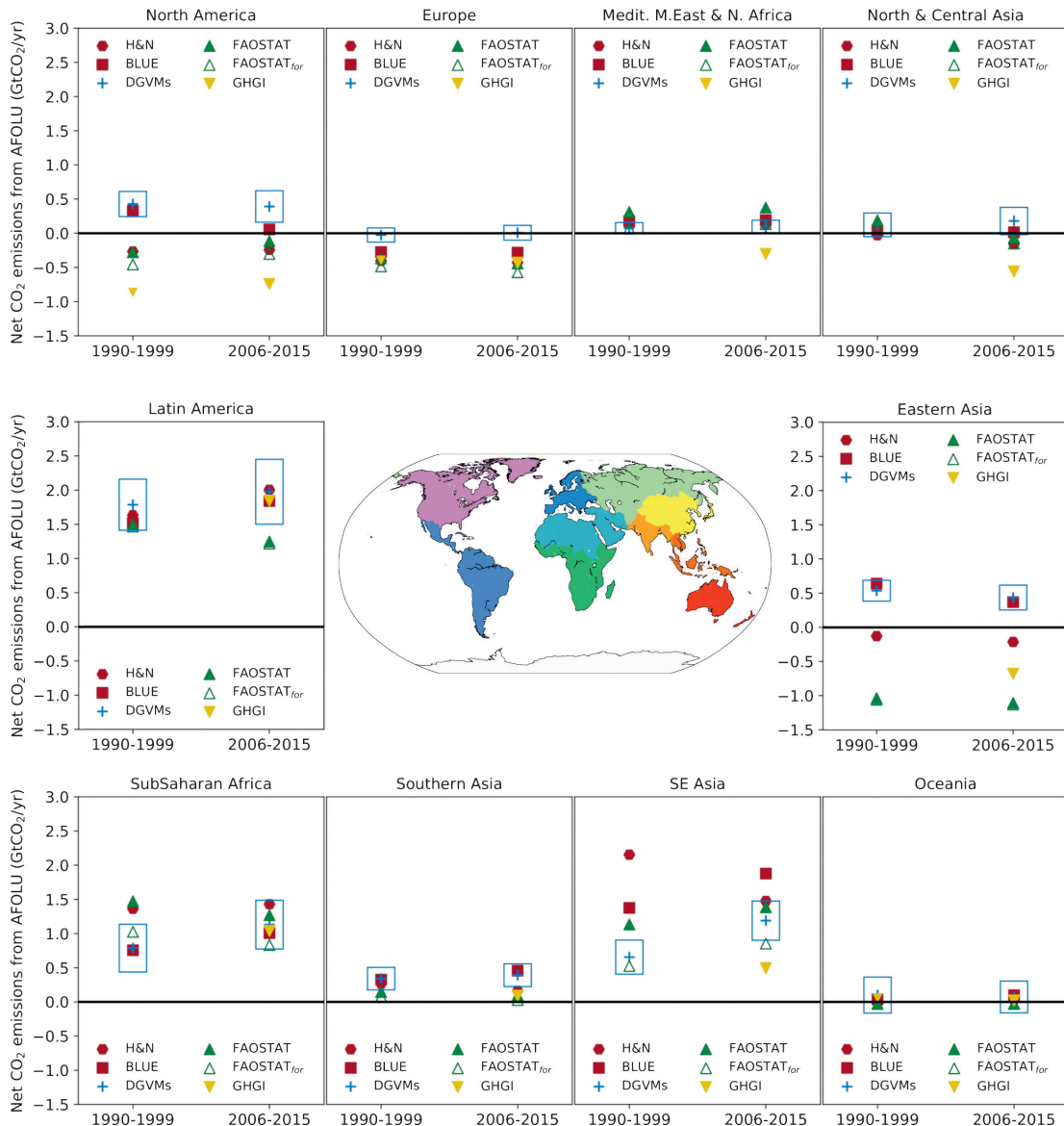


Figure 2.7 | Regional trends in net anthropogenic land-atmosphere CO₂ flux from a range of different approaches (in GtCO₂ yr⁻¹). Red symbols: bookkeeping models (hexagon: Houghton and Nassikas 2017; square: Hansis et al. 2015). Blue cross: the mean from DGVMs with the box showing the 1 standard deviation range. Green triangles: downloaded from FAOSTAT website; the open triangle is primarily forest-related emissions, while the closed triangle includes emission from peat fires and peat drainage. Yellow inverted triangle: GHGI LULUCF flux based on country reports to UNFCCC (Grassi et al. 2018). Data for developing countries are only shown for 2006–2015 because reporting in many developing countries became more consistent/reliable after 2005. For more details on methods see Box 2.2.

As described in Box 2.3, rising CO₂ concentrations have a fertilising effect on land, while climate has mixed effects; for example, rising temperature increases respiration rates and may enhance or reduce photosynthesis depending on location and season, while longer growing seasons might allow for higher carbon uptake. However, these processes are not included in DGVMs, which may account for at least some of the land sink. For example, a decline in the global area burned by fires each year (Andela et al. 2017) accounts for an estimated net sink (and/or reduced emissions) of 0.5 GtCO₂ yr⁻¹ (*limited evidence, medium agreement*) (Arora and Melton 2018).

Boreal forests represent an exception to this decline (Kelly et al. 2013). The reduction in burning not only reduces emissions, but also allows more growth of recovering forests. There is also an estimated net carbon sink of about the same magnitude (0.5 GtCO₂ yr⁻¹) as a result of soil erosion from agricultural lands and redeposition in anaerobic environments where respiration is reduced (*limited evidence, low agreement*) (Wang et al. 2017d). A recent study attributes an increase in land carbon to a longer-term (1860–2005) aerosol-induced cooling (Zhang et al. 2019). Recent evidence also suggests that DGVMs and ESMs underestimate the effects of

drought on CO₂ emissions (Humphrey et al. 2018; Green et al. 2019; Kolus et al. 2019).

2.3.1.3 Gross emissions and removals contributing to AFOLU emissions

The modelled AFOLU flux of $5.5 \pm 3.7 \text{ GtCO}_2 \text{ yr}^{-1}$ over the period 2008–2017 represents a net value. It consists of both gross emissions of CO₂ from deforestation, forest degradation and the oxidation of wood products, as well as gross removals of CO₂ in forests and soils recovering from harvests and agricultural abandonment (Figure 2.4). The uncertainty of these gross fluxes is high because few studies report gross fluxes from AFOLU. Houghton and Nassikas (2017) estimated gross emissions to be as high as 20.2 GtCO₂ yr⁻¹ (*limited evidence, low agreement*) (Figure 2.4), and even this may be an underestimate because the land-use change data used from FAOSTAT (Tubiello et al. 2013) is itself a net of all changes within a country.

Gross emissions and removals of CO₂ result from rotational uses of land, such as wood harvest and shifting cultivation, including regrowth. These gross fluxes are more informative for assessing the timing and potential for mitigation than estimates of net fluxes, because the gross fluxes include a more complete accounting of individual activities. Gross emissions from rotational land use in the tropics are approximately 37% of total CO₂ emissions, rather than 14%, as suggested by net AFOLU emissions (Houghton and Nassikas 2018). Further, if the forest is replanted or allowed to regrow, gross removals of nearly the same magnitude would be expected to continue for decades.

2.3.1.4 Gross emissions and removals contributing to the non-anthropogenic land sink

The *net* land sink averaged $11.2 \pm 2.6 \text{ GtCO}_2 \text{ yr}^{-1}$ (*likely range*) over 2007–2016 (Table 2.3.2), but its gross components have not been estimated at the global level. There are many studies that suggest increasing emissions of carbon are due to indirect environmental effects and natural disturbance, for example, temperature-induced increases in respiration rates (Bond-Lamberty et al. 2018), increased tree mortality (Brienen et al. 2015; Berdandler and Clark 2016; McDowell et al. 2018) and thawing permafrost (Schuur et al. 2015). The global carbon budget indicates that land and ocean sinks have *increased* over the last six decades in proportion to total CO₂ emissions (Le Quéré et al. 2018) (*robust evidence, high agreement*). That means that any emissions must have been balanced by even larger removals (likely driven by CO₂ fertilisation, climate change, nitrogen deposition, erosion and redeposition of soil carbon, a reduction in areas burned, aerosol-induced cooling and changes in natural disturbances) (Box 2.3).

Climate change is expected to impact terrestrial biogeochemical cycles via an array of complex feedback mechanisms that will act to either enhance or decrease future CO₂ emissions from land. Because the gross emissions and removals from environmental changes are not constrained at present, the balance of future positive and negative feedbacks remains uncertain. Estimates from climate models in Coupled Model Intercomparison Project 5 (CMIP5) exhibit large

differences for different carbon and nitrogen cycle feedbacks and how they change in a warming climate (Anav et al. 2013; Friedlingstein et al. 2006; Friedlingstein, et al. 2014). The differences are in large part due to the uncertainty regarding how primary productivity and soil respiration will respond to environmental changes, with many of the models not even agreeing on the sign of change. Furthermore, many models do not include a nitrogen cycle, which may limit the CO₂ fertilisation effect in the future (Box 2.3). There is an increasing amount of observational data available and methods to constrain models (e.g., Cox et al. 2013; Prentice, et al., 2015) which can reduce uncertainty.

2.3.1.5 Potential impact of mitigation on atmospheric CO₂ concentrations

If CO₂ concentrations decline in the future as a result of low emissions and large negative emissions, the global land and ocean sinks are expected to weaken (or even reverse). The oceans are expected to release CO₂ back to the atmosphere when the concentration declines (Ciais et al. 2013a; Jones et al. 2016). This means that to maintain atmospheric CO₂ and temperature at low levels, both the excess CO₂ from the atmosphere and the CO₂ progressively outgassed from the ocean and land sinks will need to be removed. This outgassing from the land and ocean sinks is called the ‘rebound effect’ of the global carbon cycle (Ciais et al. 2013a). It will reduce the effectiveness of negative emissions and increase the deployment level needed to achieve a climate stabilisation target (Jackson et al. 2017; Jones et al. 2016) (*limited evidence, high agreement*).

2.3.2 Methane

2.3.2.1 Atmospheric trends

In 2017, the globally averaged atmospheric concentration of CH₄ was $1850 \pm 1 \text{ ppbv}$ (Figure 2.8A). Systematic measurements of atmospheric CH₄ concentrations began in the mid-1980s and trends show a steady increase between the mid-1980s and early-1990s, slower growth thereafter until 1999, a period of no growth between 1999 and 2006, followed by a resumption of growth in 2007. The growth rates show very high inter-annual variability with a negative trend from the beginning of the measurement period until about 2006, followed by a rapid recovery and continued high inter-annual variability through 2017 (Figure 2.8B). The growth rate has been higher over the past 4 years (*high confidence*) (Nisbet et al. 2019). The trend in δ¹³C-CH₄ prior to 2000 with less depleted ratios indicated that the increase in atmospheric concentrations was due to thermogenic (fossil) CH₄ emissions; the reversal of this trend after 2007 indicates a shift to biogenic sources (Figure 2.8C).

Understanding the underlying causes of temporal variation in atmospheric CH₄ concentrations is an active area of research. Several studies concluded that inter-annual variability of CH₄ growth was driven by variations in natural emissions from wetlands (Rice et al. 2016; Bousquet et al. 2006; Bousquet et al. 2011). These modelling efforts concluded that tropical wetlands were responsible for between 50 and 100% of the inter-annual fluctuations and the renewed

growth in atmospheric concentrations after 2007. However, results were inconsistent for the magnitude and geographic distribution of the wetland sources between the models. Pison et al. (2013) used two atmospheric inversion models and the ORCHIDEE model and found greater uncertainty in the role of wetlands in inter-annual variability between 1990 and 2009 and during the 1999–2006 pause. Poulter et al. (2017) used several biogeochemical models and inventory-based wetland area data to show that wetland CH_4 emissions increases in the boreal zone have been offset by decreases in the tropics, and concluded that wetlands have not contributed significantly to renewed atmospheric CH_4 growth.

The models cited above assumed that atmospheric hydroxyl radical (OH) sink over the period analysed did not vary. OH reacts with CH_4 as the first step toward oxidation to CO_2 . In global CH_4 budgets,

the atmospheric OH sink has been difficult to quantify because its short lifetime (about 1 second) and its distribution is controlled by precursor species that have non-linear interactions (Taraborrelli et al., 2012; Prather et al., 2017). Understanding of the atmospheric OH sink has evolved recently. The development of credible time series of methyl chloroform (MCF: CH_3CCl_3) observations offered a way to understand temporal dynamics of OH abundance and applying this to global budgets further weakened the argument for the role of wetlands in determining temporal trends since 1990. Several authors used the MCF approach and concluded that changes in the atmospheric OH sink explained a large portion of the suppression in global CH_4 concentrations relative to the pre-1999 trend (Turner et al. 2017; Rigby et al. 2013; McNorton et al. 2016). These studies could not reject the null hypothesis that OH has remained constant in recent decades and they did not suggest a mechanism

2

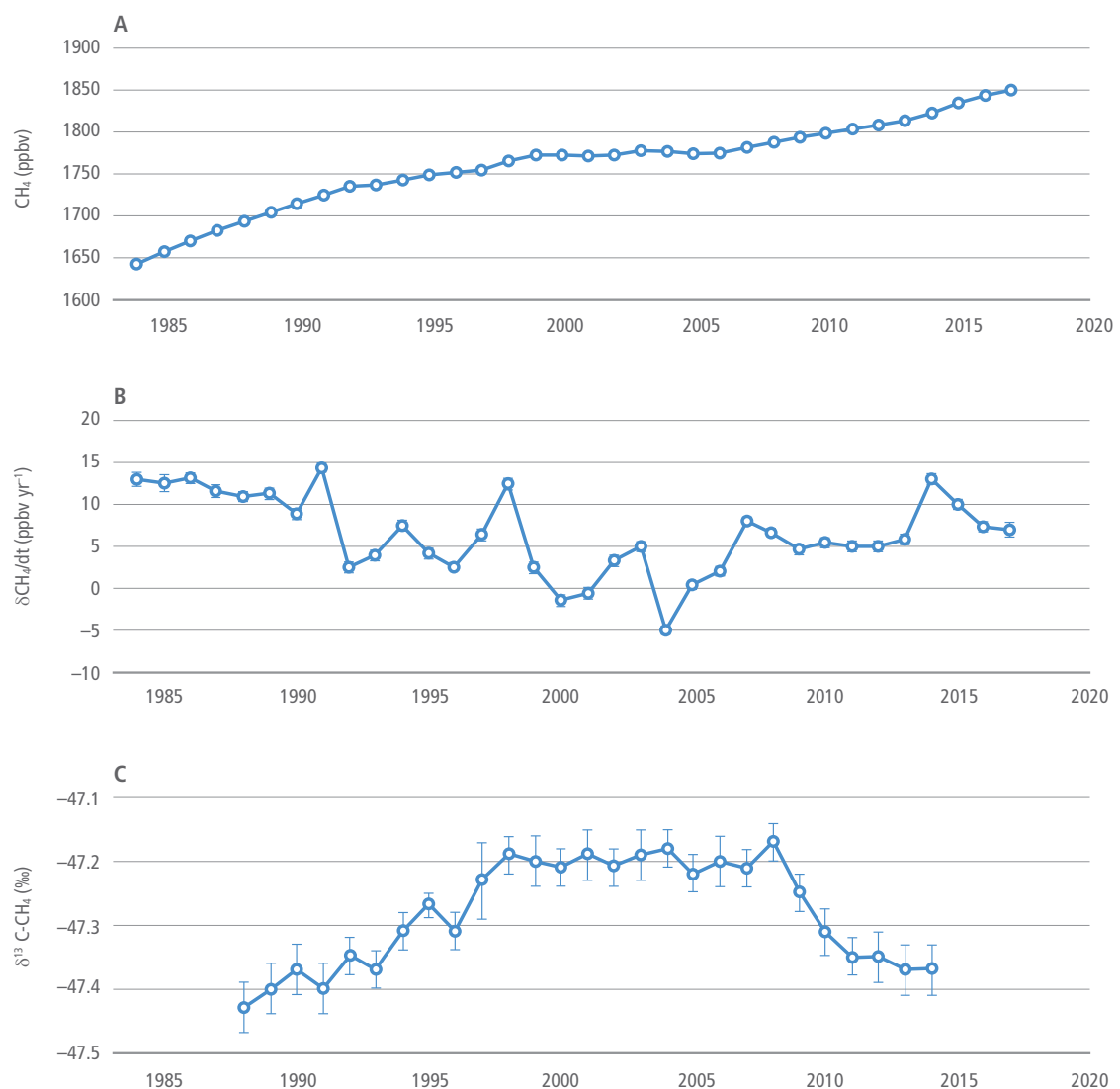


Figure 2.8 | Globally averaged atmospheric CH_4 mixing ratios (Frame A) and instantaneous rates of change (Frame B) and C isotope/variation (Frame C). Data sources: NOAA/ESRL (www.esrl.noaa.gov/gmd/ccgg/trends_ch4); Dlugokencky et al. (1994) and Schaefer et al. (2016).

for the inferred OH concentration changes (Nisbet et al. 2019). Nicely et al. (2018) used a mechanistic approach and demonstrated that variation in atmospheric OH was much lower than what MCF studies claimed that positive trends in OH due to the effects of water vapour, nitrogen oxides (NO_x), tropospheric ozone and expansion of the tropical Hadley cells offsets the decrease in OH that is expected from increasing atmospheric CH₄ concentrations.

The depletion of δ¹³C_{atm} beginning in 2009 could be due to changes in several sources. Decreased fire emissions combined with increased tropical wetland emissions compared to earlier years could explain the δ¹³C perturbations to atmospheric CH₄ sources (Worden et al. 2017; Schaefer et al. 2016). However, because tropical wetland emissions are higher in the southern hemisphere, and the remote sensing observations show that CH₄ emissions increases are largely in the north tropics (Bergamaschi et al. 2013; Melton et al. 2013; Houweling et al. 2014), an increased wetland source does not fit well with the southern hemisphere δ¹³C observations. New evidence shows that tropical wetland CH₄ emissions are significantly underestimated, perhaps by a factor of 2, because estimates do not account for release by tree stems (Pangala et al. 2017). Several authors have concluded that agriculture is a more probable source of increased emissions, particularly from rice and livestock in the tropics, which is consistent with inventory data (Wolf et al. 2017; Patra et al. 2016; Schaefer et al. 2016).

The importance of fugitive emissions in the global atmospheric accumulation rate is growing (*medium evidence, high agreement*). The increased production of natural gas in the US from the mid 2000s is of particular interest because it coincides with renewed atmospheric CH₄ growth (Rice et al. 2016; Hausmann et al. 2015). Reconciling increased fugitive emissions with increased isotopic depletion of atmospheric CH₄ indicates that there are *likely* multiple changes in emissions and sinks that affect atmospheric accumulation (*medium confidence*).

With respect to atmospheric CH₄ growth rates, we conclude that there is significant and ongoing accumulation of CH₄ in the atmosphere (*very high confidence*). The reason for the pause in growth rates and subsequent renewed growth is at least partially associated with land use and land use change. Evidence that variation in the atmospheric OH sink plays a role in the year-to-year variation of the CH₄ is accumulating, but results are contradictory (*medium evidence, low agreement*) and refining this evidence is constrained by lack of long-term isotopic measurements at remote sites, particularly in the tropics. Fugitive emissions *likely* contribute to the renewed growth after 2006 (*medium evidence, high agreement*). Additionally, the recent depletion trend of ¹³C isotope in the atmosphere indicates that growth in biogenic sources explains part of the current growth and that biogenic sources make up a larger proportion of the source mix compared to the period before 1997 (*robust evidence, high agreement*). In agreement with the findings of AR5, we conclude that wetlands are important drivers of inter-annual variability and current growth rates (*medium evidence, high agreement*). Ruminants and the expansion of rice cultivation are also important contributors to the current growth trend (*medium evidence, high agreement*).

2.3.2.2 Land use effects

Agricultural emissions are predominantly from enteric fermentation and rice, with manure management and waste burning contributing small amounts (Figure 2.9). Since 2000, livestock production has been responsible for 33% of total global emissions and 66% of agricultural emissions (EDGAR 4.3.2 database, May 2018; USEPA 2012; Tubiello et al. 2014; Janssens-Maenhout et al. 2017b). Asia has the largest livestock emissions (37%) and emissions in the region have been growing by around 2% per year over the same period. North America is responsible for 26% and emissions are stable; Europe is responsible for around 8% of emissions, and these are decreasing slightly (<1% per year). Africa is responsible for 14%, but emissions are growing fastest in this region at around 2.5% y⁻¹. In Latin America and the Caribbean, livestock emissions are decreasing at around 1.6% per year and the region makes up 16% of emissions. Rice emissions are responsible for about 24% of agricultural emissions and 89% of these are from Asia. Rice emissions are increasing by 0.9% per year in that region. These trends are predicted to continue through 2030 (USEPA 2013).

Upland soils are a net sink of atmospheric CH₄, but soils both produce and consume the gas. On the global scale, climatic zone, soil texture and land cover have an important effect on CH₄ uptake in upland soils (Tate 2015; Yu et al. 2017; Dutaur and Verchot 2007). Boreal soils take up less than temperate or tropical soils, coarse textured soils take up more CH₄ than medium and fine textured soils, and forests take up more than other ecosystems. Low levels of nitrogen fertilisation or atmospheric deposition can affect the soil microbial community and stimulate soil CH₄ uptake in nitrogen-limited soils, while higher fertilisation rates decrease uptake (Edwards et al. 2005; Zhuang et al., 2013). Globally, nitrogen fertilisation on agricultural lands may have suppressed CH₄ oxidation by as much as 26 Tg between 1998 and 2004 (*low confidence, low agreement*) (Zhuang et al., 2013). The effect of nitrogen additions is cumulative and repeated fertilisation events have progressively greater suppression effects (*robust evidence, high agreement*) (Tate 2015). Other factors such as higher temperatures, increased atmospheric concentrations and changes in rainfall patterns stimulate soil CH₄ consumption in unfertilised ecosystems. Several studies (Yu et al. 2017; Xu et al. 2016; Curry 2009) have shown that globally, uptake has been increasing during the second half of the 20th century and is expected to continue to increase by as much as 1 Tg in the 21st century, particularly in forests and grasslands (*medium evidence, high agreement*).

Northern peatlands (40–70°N) are a significant source of atmospheric CH₄, emitting about 48 TgCH₄, or about 10% of the total emissions to the atmosphere (Zhuang et al. 2006; Wuebbles and Hayhoe 2002). CH₄ emissions from natural northern peatlands are highly variable, with the highest rate from fens (*medium evidence, high agreement*). Peatland management and restoration alters the exchange of CH₄ with the atmosphere (*medium evidence, high agreement*). Management of peat soils typically converts them from CH₄ sources to sinks (Augustin et al. 2011; Strack and Waddington 2008; Abdalla et al. 2016) (*robust evidence, high agreement*). While restoration decreases CO₂ emissions (Section 4.9.4), CH₄ emissions often increase relative to the

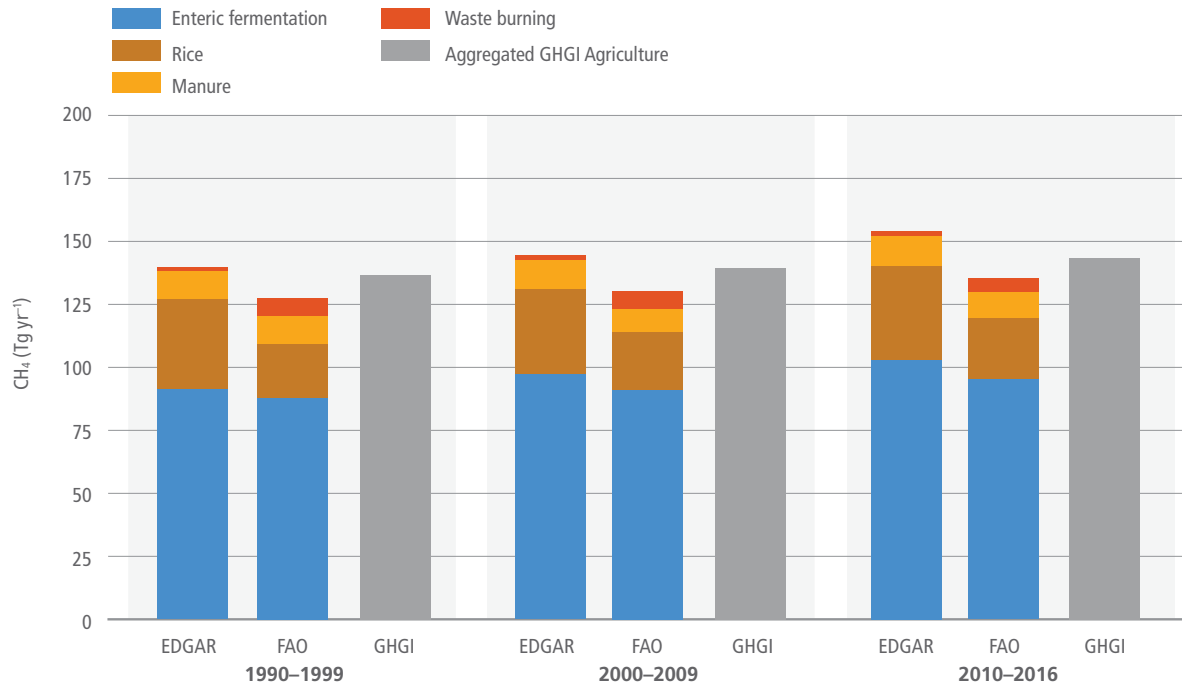


Figure 2.9 | Average agricultural CH₄ emissions estimates from 1990. Sub-sectorial agricultural emissions are based on the Emissions Database for Global Atmospheric Research (EDGAR v4.3.2; Janssens-Maenhout et al. 2017a); FAOSTAT (Tubiello et al. 2013); and National GHGI data (Grassi et al. 2018). GHGI data are aggregate values for the sector. Note that EDGAR data are complete only through 2012; the data in the right-hand panel represent the three years 2010–2012 and are presented for comparison.

drained conditions (*robust evidence, high agreement*) (Osterloh et al. 2018; Christen et al. 2016; Koskinen et al. 2016; Tuittila et al. 2000; Vanselow-Algan et al. 2015; Abdalla et al. 2016). Drained peatlands are usually considered to be negligible methane sources, but they emit CH₄ under wet weather conditions and from drainage ditches (Drösler et al. 2013; Sirin et al. 2012). While ditches cover only a small percentage of the drained area, emissions can be sufficiently high that drained peatlands emit comparable CH₄ as undrained ones (*medium evidence, medium agreement*) (Sirin et al. 2012; Wilson et al. 2016).

Because of the large uncertainty in the tropical peatland area, estimates of the global flux are highly uncertain. A meta-analysis of the effect of conversion of primary forest to rice production showed that emissions increased by a factor of four (*limited evidence, high agreement*) (Hergoualc'h and Verchot, 2012). For land uses that required drainage, emissions decreased by a factor of three (*limited evidence, high agreement*). There are no representative measurements of emissions from drainage ditches in tropical peatlands.

2.3.3 Nitrous oxide

2.3.3.1 Atmospheric trends

The atmospheric abundance of N₂O has increased since 1750, from a pre-industrial concentration of 270 ppbv to 330 ppbv in 2017 (*high agreement, robust evidence*) (US National Oceanographic and Atmospheric Agency, Earth Systems Research Laboratory)

(Figure 2.10). The rate of increase has also increased, from approximately 0.15 ppbv yr⁻¹ 100 years ago, to 0.85 ppbv yr⁻¹ over the period 2001–2015 (Wells et al. 2018). Atmospheric N₂O isotopic composition (¹⁴/¹⁵N) was relatively constant during the pre-industrial period (Prokopiou et al. 2018) and shows a decrease in the δ¹⁵N as the N₂O mixing ratio in the atmosphere has increased between 1940 and 2005. This recent decrease indicates that terrestrial sources are the primary driver of increasing trends and marine sources contribute around 25% (Snider et al. 2015). Microbial denitrification and nitrification processes are responsible for more than 80% of total global N₂O emissions, which includes natural soils, agriculture and oceans, with the remainder coming from non-biological sources such as biomass burning and fossil-fuel combustion (Fowler et al. 2015). The isotopic trend also indicates a shift from denitrification to nitrification as the primary source of N₂O as a result of the use of synthetic nitrogen fertiliser (*high evidence, high agreement*) (Park et al. 2012; Toyoda et al. 2013; Snider et al. 2015; Prokopiou et al. 2018).

The three independent sources of N₂O emissions estimates from agriculture at global, regional and national levels are: USEPA, EDGAR and FAOSTAT (USEPA 2013; Tubiello et al. 2015; Janssens-Maenhout et al. 2017a). EDGAR and FAOSTAT have temporal resolution beyond 2005 and these databases compare well with national inventory data (Figure 2.10). USEPA has historical estimates through 2005 and projections thereafter. The independent data use IPCC methods, with Tier 1 emission factors and national reporting of activity data. Tier 2 approaches are also available based on top-down and bottom-up approaches. Recent estimates using inversion modelling and process

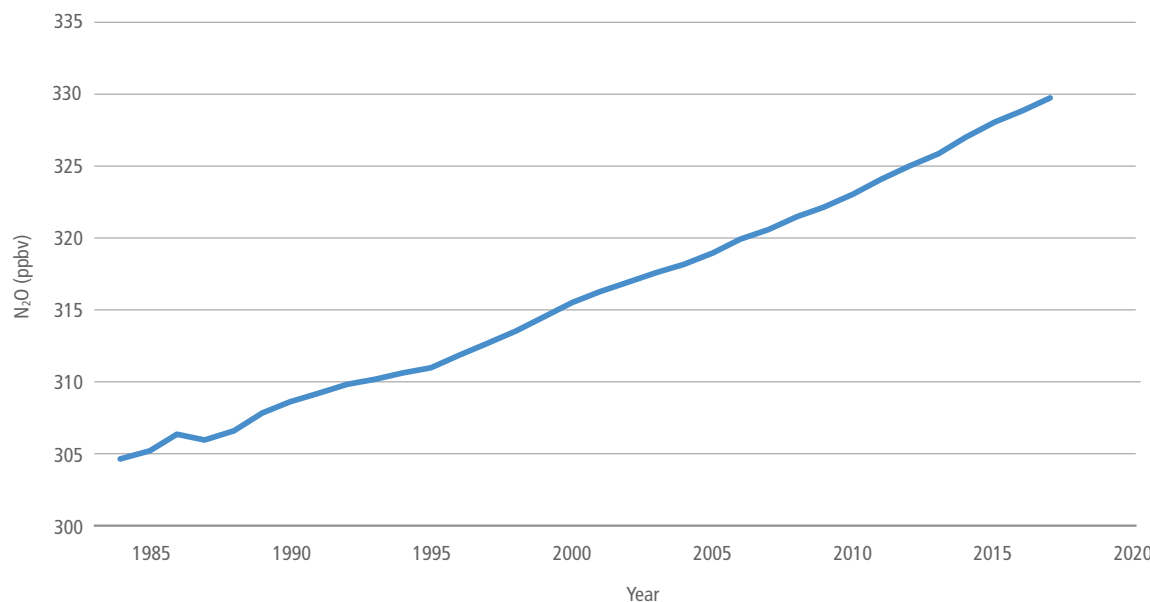


Figure 2.10 | Globally averaged atmospheric N_2O mixing ratios since 1984. Data source: NOAA/ESRL Global Monitoring Division ([www.esrl.noaa.gov/gmd/hats/combined/N₂O.html](http://www.esrl.noaa.gov/gmd/hats/combined/N2O.html)).

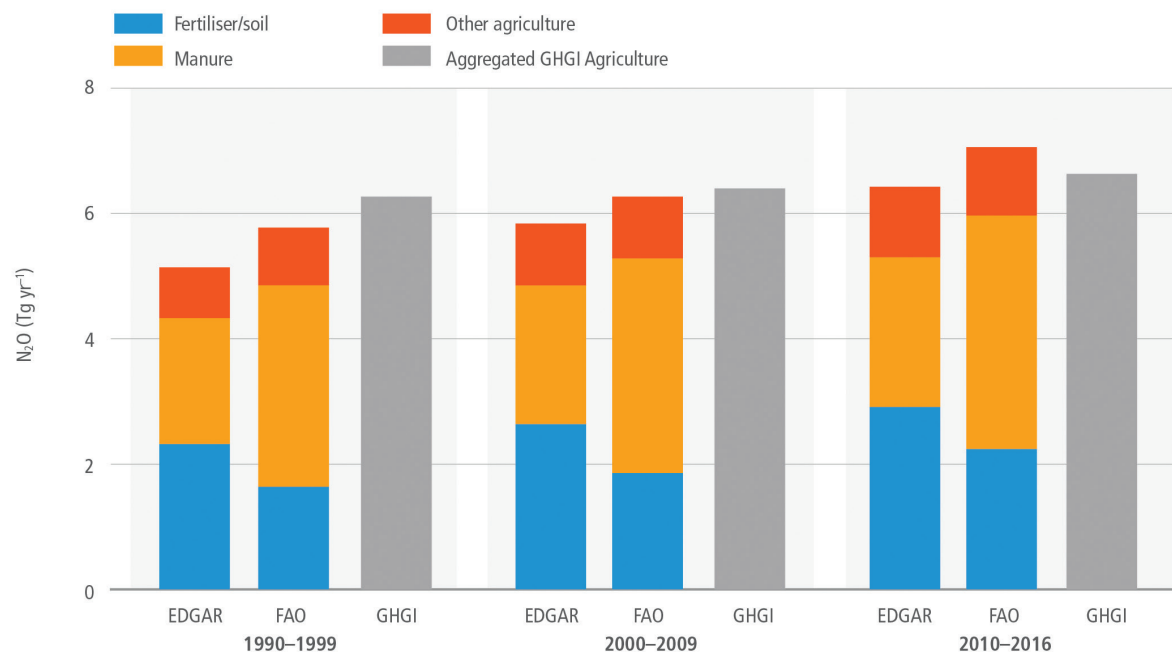


Figure 2.11 | Average agricultural N_2O emissions estimates from 1990. Sub-sectorial agricultural emissions are based on the Emissions Database for Global Atmospheric Research (EDGAR v4.3.2; Janssens-Maenhout et al. 2017a); FAOSTAT (Tubiello et al. 2013) and National GHGI data (Grassi et al. 2018). GHGI data are aggregate values for the sector. Note that EDGAR data are complete only through 2012; the EDGAR data in the right-hand panel represent the three years 2010–2012 and are presented for comparison. FAO data for the “other agriculture” category includes emissions from crop residues, cultivated organic soil, and burning of crop residues.

models estimate total annual global N₂O emissions of 16.1–18.7 (bottom-up) and 15.9–17.7 TgN (top-down), demonstrating relatively close agreement (Thompson et al. 2014). Agriculture is the largest source and has increased with extensification and intensification. Recent modelling estimates of terrestrial sources show a higher emissions range that is slightly more constrained than what was reported in AR5: approximately 9 (7–11) TgN₂O-N yr⁻¹ (Saikawa et al. 2014; Tian et al. 2016) compared to 6.6 (3.3–9.0) TgN₂O-N yr⁻¹ (Ciais et al. 2013a). Estimates of marine N₂O emissions are between 2.5 and 4.6 TgN₂O-N yr⁻¹ (Buitenhuis et al., 2018; Saikawa et al., 2014).

To conclude, N₂O is continuing to accumulate in the atmosphere at an increasingly higher rate (*very high confidence*), driven primarily by increases in manure production and synthetic nitrogen fertiliser use from the mid-20th century onwards (*high confidence*). Findings since AR5 have constrained regional and global estimates of annual N₂O emissions and improved our understanding of the spatio-temporal dynamics of N₂O emissions, including soil rewetting and freeze-thaw cycles which are important determinants of total annual emission fluxes in some regions (*medium confidence*).

2.3.3.2 Land use effects

Agriculture is responsible for approximately two-thirds of N₂O emissions (*robust evidence, high agreement*) (Janssens-Maenhout et al. 2017b). Total emissions from this sector are the sum of direct and indirect emissions. Direct emissions from soils are the result of mineral fertiliser and manure application, manure management, deposition of crop residues, cultivation of organic soils and inorganic nitrogen inputs through biological nitrogen fixation. Indirect emissions come from increased warming, enrichment of downstream water bodies from runoff, and downwind nitrogen deposition on soils. The main driver of N₂O emissions in croplands is a lack of synchronisation between crop nitrogen demand and soil nitrogen supply, with approximately 50% of nitrogen applied to agricultural land not taken up by the crop (Zhang et al. 2017). Cropland soils emit over 3 TgN₂O-N yr⁻¹ (*medium evidence, high agreement*) (Janssens-Maenhout et al. 2017b; Saikawa et al. 2014). Regional inverse modelling studies show larger tropical emissions than the inventory approaches and they show increases in N₂O emissions from the agricultural sector in South Asia, Central America, and South America (Saikawa et al. 2014; Wells et al. 2018).

Emissions of N₂O from pasturelands and rangelands have increased by as much as 80% since 1960 due to increased manure production and deposition (*robust evidence, high agreement*) (de Klein et al. 2014; Tian et al. 2018; Chadwick et al. 2018; Dangal et al. 2019; Cardenas et al. 2019). Studies consistently report that pasturelands and rangelands are responsible for around half of the total agricultural N₂O emissions (Davidson 2009; Oenema et al. 2014; Dangal et al. 2019). An analysis by Dangal et al. (2019) shows that, while managed pastures make up around one-quarter of the global grazing lands, they contribute 86% of the net global N₂O emissions from grasslands and that more than half of these emissions are related to direct deposition of livestock excreta on soils.

Many studies calculate N₂O emissions from a linear relationship between nitrogen application rates and N₂O emissions. New studies

are increasingly finding nonlinear relationships, which means that N₂O emissions per hectare are lower than the Tier 1 EFs (IPCC 2003) at low nitrogen application rates, and higher at high nitrogen application rates (*robust evidence, high agreement*) (Shcherbak et al. 2014; van Lent et al. 2015; Satria 2017). This not only has implications for how agricultural N₂O emissions are estimated in national and regional inventories, which now often use a linear relationship between nitrogen applied and N₂O emissions, it also means that in regions of the world where low nitrogen application rates dominate, increases in nitrogen fertiliser use would generate relatively small increases in agricultural N₂O emissions. Decreases in application rates in regions where application rates are high and exceed crop demand for parts of the growing season are likely to have very large effects on emissions reductions (*medium evidence, high agreement*).

Deforestation and other forms of land-use change alter soil N₂O emissions. Typically, N₂O emissions increase following conversion of native forests and grasslands to pastures or croplands (McDaniel et al. 2019; van Lent et al. 2015). This increase lasts from a few years to a decade or more, but there is a trend toward decreased N₂O emissions with time following land use change and, ultimately, lower N₂O emissions than had been occurring under native vegetation, in the absence of fertilisation (*medium evidence, high agreement*) (Meurer et al. 2016; van Lent et al. 2015) (Figure 2.12). Conversion of native vegetation to fertilised systems typically leads to increased N₂O emissions over time, with the rate of emission often being a function of nitrogen fertilisation rates, however, this response can be moderated by soil characteristics and water availability (*medium evidence, high agreement*) (van Lent et al. 2015; Meurer et al. 2016). Restoration of agroecosystems to natural vegetation, over the period of one to two decades does not lead to recovery of N₂O emissions to the levels of the original vegetation (McDaniel et al. 2019). To conclude, findings since AR5 increasingly highlight the limits of linear N₂O emission factors, particularly from field to regional scales, with emissions rising nonlinearly at high nitrogen application rates (*high confidence*). Emissions from unfertilised systems often increase and then decline over time with typically lower emissions than was the case under native vegetation (*high confidence*).

While soil emissions are the predominant source of N₂O in agriculture, other sources are important (or their importance is only just emerging). Biomass burning is responsible for approximately 0.7 TgN₂O-N yr⁻¹ (0.5–1.7 TgN₂O-N yr⁻¹) or 11% of total gross anthropogenic emissions due to the release of N₂O from the oxidation of organic nitrogen in biomass (UNEP 2013). This source includes crop residue burning, forest fires, household cook stoves and prescribed savannah, pasture and cropland burning. Aquaculture is currently not accounted for in most assessments or compilations. While it is currently responsible for less than 0.1 TgN₂O-N yr⁻¹, it is one of the fastest growing sources of anthropogenic N₂O emissions (Williams and Crutzen 2010; Bouwman et al. 2013) (*limited evidence, high agreement*). Finally, increased nitrogen deposition from terrestrial sources is leading to greater indirect N₂O emissions, particularly since 1980 (*moderate evidence, high agreement*) (Tian et al. 2018, 2016). In marine systems, deposition is estimated to have increased the oceanic N₂O source by 0.2 TgN₂O-N yr⁻¹ or 3% of total gross anthropogenic emissions (Suntharalingam et al. 2012).

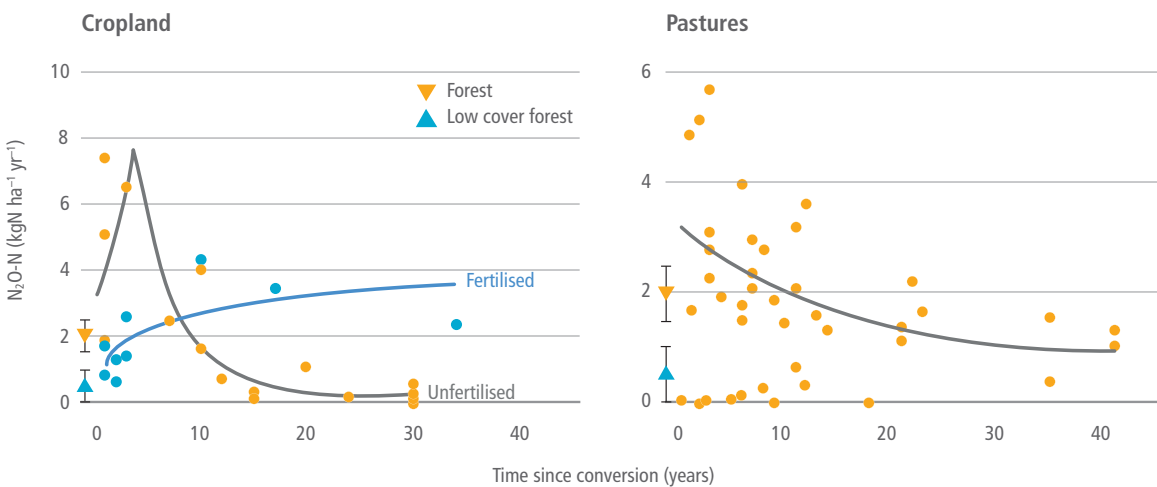


Figure 2.12 | Effect of time since conversion on N_2O fluxes in unfertilised (orange circles) and fertilised (blue circles) tropical croplands (left frame) and in unfertilised tropical pastures (right frame). Average N_2O flux and 95% confidence intervals are given for upland forests (orange inverted triangle) and low canopy forests (blue inverted triangle), for comparison. The solid lines represent the trends for unfertilised and fertilised cases. Data source: van Lent et al. (2015).

Box 2.2 | Methodologies for estimating national to global scale anthropogenic land carbon fluxes

Bookkeeping/accounting models calculate changes in biomass and soils that result from changes in land activity using data on biomass density and rates of growth/decomposition, typically from ground-based inventory data collection (field measurements of carbon in trees and soils) (Houghton et al. 2012; Hansis et al. 2015; Houghton and Nassikas 2017). The approach includes only those changes directly caused by major categories of land-use change and management. The models do not explicitly include the indirect effects to changing environmental conditions, although some effects are implicit in the biomass, growth rates and decay rates used. Thus, the models may overestimate past fluxes. The bookkeeping models include fluxes from peatland burning based on GFED estimates (Randerson et al. 2015).

DGVMs simulate ecological processes, such as photosynthesis, respiration, allocation, growth, decomposition etc., driven by environmental conditions (climate variability, climate change, CO_2 , nitrogen concentrations). Models vary with respect to the processes included, with many since AR5 now including forest management, fire, nitrogen and other management (Sitch et al. 2005; Le Quéré et al. 2018). Models are forced with increasing atmospheric CO_2 and changing climate, and run with and without 'land use change' (land cover and forest harvest) to differentiate the anthropogenic effects from the indirect effects of climate and CO_2 : the 'land sink'. Thus, indirect effects are explicitly included. This approach also includes a 'lost atmospheric sink capacity', or the carbon uptake due to environmental effects on forests that does not happen once the forests are removed (Pongratz et al. 2010).

Integrated assessment models (IAMs) use storylines to construct alternative future scenarios of GHG emissions and atmospheric concentrations within a global socio-economic framework, including projections of AFOLU based on assumptions of, for example, crop yields, population growth and bioenergy use (Cross-Chapter Box 1 and Chapter 1). Some models include simplified DGVMs, which may include climate and CO_2 effects, while others use AFOLU emissions from other sources.

ESMs couple DGVMs, surface hydrology, and energy exchange models with atmosphere, ocean, and sea ice models, enabling exploration of feedbacks between climate change and the carbon cycle (e.g., warming effects increase soil and plant respiration and lead to higher atmospheric CO_2 concentrations, which in turn promote plant growth) (Friedlingstein et al. 2014). They sometimes include numerical experiments with and without land-use change to diagnose the anthropogenic AFOLU flux (Lawrence et al. 2016).

Satellite data can be used as a proxy for plant activity (e.g., greenness) and to map land cover, vegetation fires and biomass density. Algorithms, models and independent data are used to calculate fluxes of CO_2 from satellite data, although calculating the net carbon flux is difficult because of the lack of information on the respiratory flux. Some active satellite sensors (LiDAR) are able to measure three-dimensional structure in woody vegetation, which is closely related to biomass density (Zarin et al. 2016; Baccini et al. 2012; Saatchi et al. 2011). Together with land-cover change data, these estimates of biomass density can be used to provide

Box 2.2 (continued)

observational-based estimates of fluxes due to changes in forest area (e.g., Tyukavina et al. (2015), Harris et al. (2015) and Baccini et al. (2012) or degradation (Baccini et al. 2017)). Satellite estimates of biomass vary considerably (Mitchard et al. 2013; Saatchi et al. 2015; Avitabile et al. 2016): data are available only for recent decades, methods generally assume that all losses of carbon are immediately released to the atmosphere and changes in soil carbon are generally ignored. The approach implicitly includes indirect and natural disturbance effects as well as direct anthropogenic effects.

Atmospheric inversions use observations of atmospheric concentrations with a model of atmospheric transport, based on data for wind speed and direction, to calculate implied emissions (Gatti et al. 2014; Liu et al. 2017; van der Laan-Luijkx et al. 2017). Since AR5, there has been an increase in availability of concentration data from flux tower networks and satellites, enabling better global coverage at finer spatial scales and some national estimates (e.g., in the UK inverse techniques are used together with national GHG inventories). A combination of concentrations of different gases and isotopes enables the separation of fossil, ocean and land fluxes. However, inversions give only the net flux of CO₂ from land; they cannot separate natural and anthropogenic fluxes.

Micrometeorological flux measurements data on CO₂ concentrations and air movements recorded on instrumented towers enable the calculation of CO₂ flux at the ecosystem scale. Global and regional Flux Networks (FluxNet (global), AsiaFlux, Ameriflux (North America), ICOS (EU), NEON (USA), and others) contribute to a global flux database, which is used to verify the results of modelling, inventory and remote sensing studies.

FAOSTAT has produced country level estimates of GHG emissions (Tubiello et al. 2013) from agriculture (1961–2016) and land use (1990–2016) using a globally consistent methodological approach based largely on IPCC Tier 1 methods of the 2006 IPCC Guidelines (FAO 2015). FAO emissions estimates were used as one of the three database inputs into the AR5 WGIII AFOLU chapter. Non-CO₂ emissions from agriculture are estimated directly from national statistics of activity data reported by countries to FAO. CO₂ emissions from land use and land-use change are computed mostly at Tier 1, albeit at fine geospatial scales to capture effects from peatland degradation and biomass fires (Rossi et al. 2016). Emissions from forest land and deforestation are based on the IPCC carbon stock change method, thus constituting a Tier 3 estimate relying on country statistics of carbon stocks and forest area collected through the FAO FRA. The carbon flux is estimated assuming instantaneous emissions in the year of forest area loss and changes in carbon stocks within extant forests, but does not distinguish ‘managed’ and ‘unmanaged’ forest areas, albeit it treats separately emissions from primary, secondary and planted forest (Federici et al. 2015).

Country Reporting of GHG Inventories (GHGIs): All parties to the UNFCCC are required to report national GHGIs of anthropogenic emissions and removals. Reporting requirements are differentiated between developed and developing countries. Because of the difficulty of separating direct anthropogenic fluxes from indirect or natural fluxes, the IPCC (2003) adopted the ‘managed land’ concept as a proxy to facilitate GHGI reporting. All GHG fluxes on ‘managed land’ are defined as anthropogenic, with each country applying their own definition of ‘managed land’ (i.e., ‘where human interventions and practices have been applied to perform production, ecological or social functions’ (IPCC 2006)). Fluxes may be determined on the basis of changes in carbon stocks (e.g., from forest inventories) or by activity data (e.g., area of land cover change management activity multiplied by emission factors or with modelled fluxes). Depending on the specific methods used, GHGIs include all direct anthropogenic effects and may include the indirect anthropogenic effects of environmental change (generally sinks) and natural effects (Section 2.3.1.2). GHG fluxes from ‘unmanaged land’ are not reported in GHGIs because they are assumed to be non-anthropogenic. The reported estimates may then be filtered through agreed ‘accounting rules’ (i.e., what countries actually count towards their mitigation targets (Cowie et al. 2007; Lee and Sanz 2017). The accounting aims to better quantify the additional mitigation actions by, for example, factoring out the impact of natural disturbances and forest age-related dynamics (Canadell et al. 2007; Grassi et al. 2018).

Box 2.3 | CO₂ fertilisation and enhanced terrestrial uptake of carbon

All DGVMs and ESMs represent the CO₂ fertilisation effect (Le Quéré et al. 2017; Hoffman et al. 2014). There is *high confidence* that elevated CO₂ results in increased short-term CO₂ uptake per unit leaf area (Swann et al. 2016; Field et al. 1995; Donohue et al. 2013), however, whether this increased CO₂ uptake at the leaf level translates into increased growth for the whole plant differs among plant species and environments, because growth is constrained by whole-plant resource allocation and nutrient limitation (e.g., nitrogen, phosphorus, potassium and soil water and light limitations (Körner 2006; Peñuelas et al. 2017; Friend et al. 2014a)). Interactions between plants and soil microbes further modulate the degree of nutrient limitation on CO₂ fertilisation (Terrer et al. 2017).

At the ecosystems level, enhanced CO₂ uptake at decadal or longer timescales depends on changes in plant community composition and ecosystem respiration, as well disturbance and natural plant mortality (De Kauwe et al., 2016; Farrior et al., 2015; Keenan et al., 2017; Sulman et al., 2019). The results of free-air carbon dioxide enrichment (FACE) experiments over two decades are highly variable because of these factors (Norby et al. 2010; Körner 2015; Feng et al. 2015; Paschalidis et al. 2017; Terrer et al. 2017; Du et al. 2019). Under higher atmospheric CO₂ concentrations, the ratio of CO₂ uptake to water loss (water use efficiency (WUE)), increases and enhances drought tolerance of plants (*high confidence*) (Berry et al., 2010; Ainsworth and Rogers 2007).

Long-term CO₂ and water vapour flux measurements show that WUE in temperate and boreal forests of the northern hemisphere has increased more than predicted by photosynthetic theory and models over the past two decades (*high confidence*) (Keenan et al. 2013; Laguë and Swann 2016). New theories have emerged on how CO₂ uptake by trees is related to water loss and to the risk of damaging xylem (water conducting tissues) in the trunk and branches (Wolf et al. 2016a; Anderegg et al. 2018a). Tree ring studies of stable carbon and oxygen isotopes also detected increased WUE in recent decades (Battipaglia et al. 2013; Silva and Anand 2013; van der Sleen et al. 2014). Yet, tree ring studies often fail to show acceleration of tree growth rates in support of CO₂ fertilisation, even when they show increased WUE (van der Sleen et al. 2014). The International Tree Ring Data Bank (ITRDB) indicated that only about 20% of the sites in the database showed increasing trends in tree growth that cannot be explained by climate variability, nitrogen deposition, elevation or latitude. Thus there is *limited evidence (low agreement)* among observations of enhanced tree growth due to CO₂ fertilisation of forests during the 20th century (Gedalof and Berg 2010).

In grasslands, although it is possible for CO₂ fertilisation to alleviate the impacts of drought and heat stress on net carbon uptake (Roy et al. 2016), there is *low confidence* about its projected magnitude. Because of its effect on water use efficiency, CO₂ fertilisation is expected to be pronounced in semi-arid habitats; and because of different metabolic pathways, C3 plants are expected to be more sensitive to elevated CO₂ concentrations than C4 grasses (Donohue et al. 2013; Morgan et al. 2011; Derner et al. 2003). Neither of these expectations was observed over a 12-year study of elevated CO₂ in a grassland system: enhanced growth was not observed during dry summers and growth of C4 grasses was unexpectedly stimulated, while growth of C3 grasses was not (Reich et al. 2014, 2018).

There is *medium confidence* that CO₂ fertilisation effects have increased water use efficiency in crops and thus reduced agricultural water use per unit of crop produced (Deryng et al. 2016; Nazemi and Wheater 2015; Elliott et al. 2014). This effect could lead to near-term continued greening of agricultural areas. However, current assessments of these effects are based on limited observations, mostly from the temperate zone (Deryng et al. 2016).

One line of evidence for CO₂ fertilisation is the increasing land sink ('the residual land sink' in AR5) over the last 50 years as the atmospheric CO₂ concentration has increased (Los 2013; Sitch et al. 2015; Campbell et al. 2017; Keenan and Riley 2018). A combined analysis of atmospheric inverse analyses, ecosystem models and forest inventory data concluded that 60% of the recent terrestrial carbon sink can be directly attributed to increasing atmospheric CO₂ (Schimel et al. 2015). A global analysis using a 'reconstructed vegetation index' (RVI) for the period 1901–2006 from MODIS satellite-derived normalised vegetation difference index (NDVI) showed that CO₂ fertilisation contributed at least 40% of the observed increase in the land carbon sink (Los 2013). Without CO₂ fertilisation, ESMs are unable to simulate the increasing land sink and the observed atmospheric CO₂ concentration growth rate since the middle of the 20th century (Sheviakova et al. 2013). There are other mechanisms that could explain enhanced land carbon uptake such as increased regional forest and shrub cover (Chen et al. 2019) (Cross-Chapter Box 2 and Chapter 1), and, at higher latitudes, increasing temperatures and longer growing seasons (Zhu et al. 2016).

In summary, there is *low confidence* about the magnitude of the CO₂ effect and other factors that may explain at least a portion of the land sink (e.g., nitrogen deposition, increased growing season, reduced burning, erosion and re-deposition or organic sediments, aerosol-induced cooling). Increases in atmospheric CO₂ result in increased water use efficiency and increase leaf-level photosynthesis (*high confidence*). The extent to which CO₂ fertilisation results in plant- or ecosystem-level carbon accumulation is highly variable and affected by other environmental constraints (*high confidence*). Even in ecosystems where CO₂ fertilisation has been detected in recent decades, those effects are found to weaken as a result of physiological acclimation, soil nutrient limitation and other constraints on growth (Friend et al., 2014; Körner, 2006; Peñuelas et al., 2017).

2.4 Emissions and impacts of short-lived climate forcers (SLCF) from land

While the rising atmospheric concentration of GHGs is the largest driver of anthropogenic changes in climate, the levels of short-lived climate forcers (SLCF) can significantly modulate regional climate by altering radiation exchanges and hydrological cycle and impact ecosystems (*high confidence*) (Boucher et al. 2013; Rogelj et al. 2014; Kok et al. 2018). This section assesses the current state of knowledge with respect to past and future emissions of the three major SLCFs and their precursors: mineral dust, carbonaceous aerosols (black carbon (BC) and organic carbon (OC)) and BVOCs. This section also reports on implications of changes in their emissions for climate. Aerosols particles with diameters between about 0.010 µm to about 20 µm are recognised as SLCFs, a term that refers to their short atmospheric lifetime (a few days). BVOCs are important precursors of ozone and OC, both important climate forcing agents with short atmospheric lifetimes.

While the AR5 did not assess land aerosols emissions in depth, their findings stated that although progress in quantifying regional emissions of anthropogenic and natural land aerosols has been made, considerable uncertainty still remains about their historical trends, their inter-annual and decadal variability and about any changes in the future (Calvo et al. 2013; Klimont et al. 2017). Some new and improved understanding of processes controlling emissions and atmospheric processing has been developed since AR5, for example, a better understanding of the climatic role of BC as well as the understanding of the role of BVOCs in formation of secondary organic aerosols (SOA).

Depending on the chemical composition and size, aerosols can absorb or scatter sunlight and thus directly affect the amount of absorbed and scattered radiation (Fuzzi et al. 2015; Nousiaainen 2011; de Sá et al. 2019) Aerosols affect cloud formation and development, and thus can also influence precipitation patterns and amounts (Suni et al. 2015). In addition, deposition of aerosols – especially BC – on snow and ice surfaces can reduce albedo and increase warming as a self-reinforcing feedback. Aerosols deposition also changes biogeochemical cycling in critical terrestrial ecosystems, with deposition of nutrients such as nitrogen and phosphorus (Andreae et al. 2002). Primary land aerosols are emitted directly into the atmosphere due to natural or anthropogenic processes and include mineral aerosols (or dust), volcanic dust, soot from combustion, organic aerosols from industry, vehicles or biomass burning, bioaerosols from forested regions and others. SOAs are particulates that are formed in the atmosphere by the gas-to-particles conversion processes from gaseous precursors, such as BVOCs, and account for a large fraction of fine mode (particles less than 2.5µm) aerosol mass (Hodzic et al. 2016; Manish et al. 2017). Land use change can affect the climate through changed emissions of SLCFs such as aerosols, ozone precursors and methane.

Aerosols from air pollution will decline in the coming years as a means for improving urban and regional air, but their removal will lead to additional warming (Boucher et al. 2013), with important regional variability, and partially offsetting projected mitigation effects for

two to three decades in 1.5°C consistent pathways (*high confidence*) (IPCC 2018). It is important to emphasise that changes in emissions can either be due to external forcing or through a feedback in the climate system (Box 2.1). For instance, enhanced dust emissions due to reduced vegetation could be a forcing if overgrazing is the cause of larger dust emission, or a feedback if drier climate is the cause. This distinction is important in terms of mitigation measures to be implemented.

2.4.1 Mineral dust

One of the most abundant atmospheric aerosols emitted into the atmosphere is mineral dust, a 'natural' aerosol that is produced by wind strong enough to initiate the emissions process of sandblasting. Mineral dust is preferentially emitted from dry and unvegetated soils in topographic depressions where deep layers of alluvium have been accumulated (Prospero et al. 2002). Dust is also emitted from disturbed soils by human activities, with a 25% contribution to global emissions based on a satellite-based estimate (Ginoux et al. 2012).

Dust is then transported over long distances across continents and oceans. The dust cycle, which consists of mineral dust emission, transport, deposition and stabilisation, has multiple interactions with many climate processes and biogeochemical cycles.

2.4.1.1 Mineral dust as a short-lived climate forcer from land

Depending on the dust mineralogy, mixing state and size, dust particles can absorb or scatter shortwave and longwave radiation. Dust particles serve as cloud condensation nuclei and ice nuclei. They can influence the microphysical properties of clouds, their lifetime and precipitation rate (Kok et al. 2018). New and improved understanding of processes controlling emissions and transport of dust, its regional patterns and variability, as well as its chemical composition, has been developed since AR5.

While satellites remain the primary source of information to locate dust sources and atmospheric burden, in-situ data remains critical to constrain optical and mineralogical properties of the dust (Di Biagio et al. 2017; Rocha-Lima et al. 2018). Dust particles are composed of minerals, including iron oxides which strongly absorb shortwave radiation and provide nutrients for marine ecosystems. Another mineral such as feldspar is an efficient ice nuclei (Harrison et al. 2016). Dust mineralogy varies depending on the native soils, so global databases were developed to characterise the mineralogical composition of soils for use in weather and climate models (Journet et al. 2014; Perlitz et al. 2015). New field campaigns, as well as new analyses of observations from prior campaigns, have produced insights into the role of dust in western Africa in climate system, such as long-ranged transport of dust across the Atlantic (Groß et al. 2015) and the characterisation of aerosol particles and their ability to act as ice and cloud condensation nuclei (Price et al. 2018). Size distribution at emission is another key parameter controlling dust interactions with radiation. Most models now use the parametrisation of Kok (2011) based on the theory of brittle material. It was shown that most models underestimate the size of the global dust cycle (Kok 2011).

Characterisation of spatial and temporal distribution of dust emissions is essential for weather prediction and climate projections (*high confidence*). Although there is a growing confidence in characterising the seasonality and peak of dust emissions (i.e., spring–summer (Wang et al. 2015)) and how the meteorological and soil conditions control dust sources, an understanding of long-term future dust dynamics, inter-annual dust variability and how they will affect future climate still requires substantial work. Dust is also important at high latitude, where it has an impact on snow-covered surface albedo and weather (Bullard et al. 2016).

2.4.1.2 Effects of past climate change on dust emissions and feedbacks

A limited number of model-based studies found that dust emissions have increased significantly since the late 19th century: by 25% from the preindustrial period to the present day (e.g., from 729 Tg yr⁻¹ to 912 Tg yr⁻¹) with about 50% of the increase driven by climate change and about 40% driven by land use cover change, such as conversion of natural land to agriculture (*low confidence*) (Stanelle et al. 2014). These changes resulted in a clear sky radiative forcing at the top of the atmosphere of -0.14 W m^{-2} (Stanelle et al. 2014). The authors found that, in North Africa, most dust is of natural origin, with a recent 15% increase in dust emissions attributed to climate change. In North America two-thirds of dust emissions take place on agricultural lands and both climate change and land-use change jointly drive the increase; between the pre-industrial period and the present day, the overall effect of changes in dust was -0.14 W m^{-2} cooling of clear sky net radiative forcing on top of the atmosphere, with -0.05 W m^{-2} from land use and -0.083 W m^{-2} from changes in climate.

The comparison of observations for vertically integrated mass of atmospheric dust per unit area (i.e., dust mass path (DMP)) obtained from the remotely sensed data and the DMP from CMIP5 models reveal that the model-simulate range of DMP was much lower than the estimates (Evan et al. 2014). ESMs typically do not reproduce inter-annual and longer timescales variability seen in observations (Evan et al. 2016). Analyses of the CMIP5 models (Evan 2018; Evan et al. 2014) reveal that all climate models systematically underestimate dust emissions, the amount of dust in the atmosphere and its inter-annual variability (*medium confidence*).

One commonly suggested reason for the lack of dust variability in climate models is the models' inability to simulate the effects of land surface changes on dust emission (Stanelle et al. 2014). Models that account for changes in land surface show more agreement with the satellite observations both in terms of aerosol optical depth and DMP (Kok et al. 2014). New prognostic dust emissions models are now able to account for both changes in surface winds and vegetation characteristics (e.g., leaf area index and stem area index) and soil water, ice and snow cover (Evans et al. 2016). As a result, new modelling studies (e.g., Evans et al. 2016) indicate that, in regions where soil and vegetation respond strongly to ENSO events, such as in Australia, inclusion of dynamic vegetation characteristics into dust emission parameterisations improves comparisons between the modelled and observed relationship with long-term climate variability (e.g., ENSO) and dust levels (Evans et al. 2016). Thus, there has been

progress in incorporating the effects of vegetation, soil moisture, surface wind and vegetation on dust emission source functions, but the number of studies demonstrating such improvement remains small (*limited evidence, medium agreement*).

2.4.1.3 Future changes of dust emissions

There is no agreement about the direction of future changes in dust emissions. Atmospheric dust loading is projected to increase over the southern edge of the Sahara in association with surface wind and precipitation changes (Pu and Ginoux, 2018), while Evan et al. (2016) project a decline in African dust emissions. Dust optical depth (DOD) is also projected to increase over the central Arabian peninsula in all seasons, and to decrease over northern China from March–April–May to September–October–November (Pu and Ginoux 2018). Climate models project rising drought risks over the south-western and central US in the 21st century. The projected drier regions largely overlay the major dust sources in the US. However, whether dust activity in the US will increase in the future is not clear, due to the large uncertainty in dust modelling (Pu and Ginoux 2017). Future trends of dust emissions will depend on changes in precipitation patterns and atmospheric circulation (*limited evidence, high agreement*). However, implication of changes in human activities, including mitigation (e.g., bioenergy production) and adaption (e.g., irrigation) are not characterised in the current literature.

2

2.4.2 Carbonaceous aerosols

Carbonaceous aerosols are one of the most abundant components of aerosol particles in continental areas of the atmosphere and a key land–atmosphere component (Contini et al. 2018). They can make up to 60–80% of PM2.5 (particulate matter with size less than 2.5 μm) in urban and remote atmospheres (Tsigaridis et al. 2014; Kulmala et al. 2011). It comprises an organic fraction (OC) and a refractory light-absorbing component, generally referred to as elemental carbon (EC), from which BC is the optically active absorption component of EC (Gilardoni et al. 2011; Bond et al. 2013).

2.4.2.1 Carbonaceous aerosol precursors of short-lived climate forcers from land

OC is a major component of aerosol mass concentration, and it originates from different anthropogenic (combustion processes) and natural (natural biogenic emissions) sources (Robinson et al. 2007). A large fraction of OC in the atmosphere has a secondary origin, as it can be formed in the atmosphere through condensation to the aerosol phase of low vapour pressure gaseous compounds emitted as primary pollutants or formed in the atmosphere. This component is SOA (Hodzic et al. 2016). A third component of the optically active aerosols is the so-called brown carbon (BrC), an organic material that shows enhanced solar radiation absorption at short wavelengths (Wang et al. 2016b; Laskin et al. 2015; Liu et al. 2016a; Bond et al. 2013; Saturno et al. 2018).

OC and EC have distinctly different optical properties, with OC being important for the scattering properties of aerosols and EC central for

the absorption component (Rizzo et al. 2013; Tsigaridis et al. 2014; Fuzzi et al. 2015). While OC is reflective and scatters solar radiation, it has a cooling effect on climate. On the other side, BC and BrC absorb solar radiation and they have a warming effect in the climate system (Bond et al. 2013).

OC is also characterised by a high solubility with a high fraction of water-soluble organic compounds (WSOC) and it is one of the main drivers of the oxidative potential of atmospheric particles. This makes particles loaded with oxidised OC an efficient cloud condensation nuclei (CCN) in most of the conditions (Pöhlker et al. 2016; Thalman et al. 2017; Schmale et al. 2018).

Biomass burning is a major global source of carbonaceous aerosols (Bowman et al. 2011; Harrison et al. 2010; Reddington et al. 2016; Artaxo et al. 2013). As knowledge of past fire dynamics improved through new satellite observations, new fire proxies' datasets (Marlon et al. 2013; van Marle et al. 2017a), process-based models (Hantson et al. 2016) and a new historic biomass burning emissions dataset starting in 1750 have been developed (van Marle et al. 2017b) (Cross-Chapter Box 3 in this chapter). Revised versions of OC biomass burning emissions (van Marle et al. 2017b) show, in general, reduced trends compared to the emissions derived by Lamarque et al. (2010) for CMIP5. CMIP6 global emissions pathways (Gidden et al. 2018; Hoesly et al. 2018) estimate global BC emissions in 2015 at 9.8 MtBC yr⁻¹, while global OC emissions are 35 MtOC yr⁻¹.

Land use change is critically important for carbonaceous aerosols, since biomass-burning emissions consist mostly of organic aerosol, and the undisturbed forest is also a large source of organic aerosols (Artaxo et al. 2013). Additionally, urban aerosols are also mostly carbonaceous because of the source composition (traffic, combustion, industry, etc.) (Fuzzi et al. 2015). Burning of fossil fuels, biomass-burning emissions and SOA from natural BVOC emissions are the main global sources of carbonaceous aerosols. Any change in each of these components directly influence the radiative forcing (Contini et al. 2018; Boucher et al. 2013; Bond et al. 2013).

One important component of carbonaceous aerosols is the primary biological aerosol particles (PBAP), also called bioaerosols, that correspond to a significant fraction of aerosols in forested areas (Fröhlich-Nowoisky et al. 2016; Pöschl and Shiraiwa 2015). They are emitted directly by the vegetation as part of the biological processes (Huffman et al. 2012). Airborne bacteria, fungal spores, pollen, archaea, algae and other bioparticles are essential for the reproduction and spread of organisms across various terrestrial ecosystems. They can serve as nuclei for cloud droplets, ice crystals and precipitation, thus influencing the hydrological cycle and climate (Whitehead et al. 2016; Scott et al. 2015; Pöschl et al. 2010).

2.4.2.2 Effects of past climate change on carbonaceous aerosols emissions and feedbacks

Annual global emission estimates of BC range from 7.2–7.5 Tg yr⁻¹ (using bottom-up inventories) (Bond et al. 2013; Klimont et al. 2017) up to 17.8 ± 5.6 Tg yr⁻¹ (using a fully coupled climate-aerosol-

urban model constrained by aerosol measurements) (Cohen and Wang 2014), with considerably higher BC emissions for Eastern Europe, southern East Asia, and Southeast Asia, mostly due to higher anthropogenic BC emissions estimates. A significant source of BC, the net trend in global burned area from 2000–2012 was a modest decrease of 4.3 Mha yr⁻¹ (-1.2% yr⁻¹).

Carbonaceous aerosols are important in urban areas as well as pristine continental regions, since they can be responsible for 50–85% of PM2.5 (Contini et al. 2018; Klimont et al. 2017). In boreal and tropical forests, carbonaceous aerosols originate from BVOC oxidation (Section 2.4.3). The largest global source of BC aerosols is open burning of forests, savannah and agricultural lands with emissions of about 2700 Gg yr⁻¹ in the year 2000 (Bond et al. 2013).

ESMs most likely underestimate globally averaged EC emissions (Bond et al. 2013; Cohen and Wang 2014), although recent emission inventories have included an upwards adjustment in these numbers (Hoesly et al. 2018). Vertical EC profiles have also been shown to be poorly constrained (Samset et al. 2014), with a general tendency of too much EC at high altitudes. Models differ strongly in the magnitude and importance of the coating-enhancement of ambient EC absorption (Boucher et al. 2016; Gustafsson and Ramanathan 2016) in their estimated lifetime of these particles, as well as in dry and wet removal efficiency (*limited evidence, medium agreement*) (Mahmood et al. 2016).

The equilibrium in emissions and concentrations between the scattering properties of organic aerosol versus the absorption component of BC is a key ingredient in the future climatic projections of aerosol effects (*limited evidence, high agreement*). The uncertainties in net climate forcing from BC-rich sources are substantial, largely due to lack of knowledge about cloud interactions with both BC and co-emitted OC. A strong positive forcing of about 1.1 wm^{-2} was calculated by Bond et al. (2013), but this forcing is balanced by a negative forcing of -1.45 wm^{-2} , and shows clearly a need to work on the co-emission issue for carbonaceous aerosols. The forcing will also depend on the aerosol-cloud interactions, where carbonaceous aerosol can be coated and change their CCN capability. It is difficult to estimate the changes in any of these components in a future climate, but this will strongly influence the radiative forcing (*high confidence*) (Contini et al. 2018; Boucher et al. 2013; Bond et al. 2013).

De Coninck et al. (2018) reported studies estimating a lower global temperature effect from BC mitigation (e.g., Samset et al. 2014; Boucher et al. 2016), although commonly used models do not capture properly observed effects of BC and co-emissions on climate (e.g., Bond et al. 2013). Regionally, the warming effects can be substantially larger, for example, in the Arctic (Sand et al. 2015) and high mountain regions near industrialised areas or areas with heavy biomass-burning impacts (*high confidence*) (Ming et al. 2013).

2.4.2.3 Future changes of carbonaceous aerosol emissions

Due to the short atmospheric lifetime of carbonaceous aerosols in the atmosphere, of the order of a few days, most studies dealing with the future concentration levels have a regional character (Cholakian

et al. 2018; Fiore et al. 2012). The studies agree that the uncertainties in changes in emissions of aerosols and their precursors are generally higher than those connected to climate change itself. Confidence in future changes in carbonaceous aerosol concentration projections is limited by the reliability of natural and anthropogenic emissions (including wildfires, largely caused by human activity) of primary aerosol as well as that of the precursors. The Aerosol Chemistry Model Intercomparison Project (AerChemMIP) is endorsed by the Coupled-Model Intercomparison Project 6 (CMIP6) and is designed to quantify the climate impacts of aerosols and chemically reactive gases (Lamarque et al. 2013). These simulations calculated future responses to SLCF emissions for the RCP scenarios in terms of concentration changes and radiative forcing. Carbonaceous aerosol emissions are expected to increase in the near future due to possible increases in open biomass-burning emissions (from forest, savannah and agricultural fires), and increase in SOA from oxidation of BVOCs (*medium confidence*) (Tsigaridis et al. 2014; van Marle et al. 2017b; Giglio et al. 2013).

More robust knowledge has been produced since the conclusions reported in AR5 (Boucher et al. 2013) and all lines of evidence now agree on a small effect on carbonaceous aerosol global burden due to climate change (*medium confidence*). The regional effects, however, are predicted to be much higher (Westervelt et al. 2015). With respect to possible changes in the chemical composition of PM as a result of future climate change, only a few sparse data are available in the literature and the results are, as yet, inconclusive. The co-benefits of reducing aerosol emissions due to air quality issues will play an important role in future carbonaceous aerosol emissions (*high confidence*) (Gonçalves et al. 2018; Shindell et al. 2017).

2.4.3 Biogenic volatile organic compounds

BVOCs are emitted in large amounts by forests (Guenther et al. 2012). They include isoprene, terpenes, alkanes, alkenes, alcohols, esters, carbonyls and acids (Peñuelas and Staudt 2010; Guenther et al. 1995, 2012). Their emissions represent a carbon loss to the ecosystem, which can be up to 10% of the carbon fixed by photosynthesis under stressful conditions (Bracho-Nunez et al. 2011). The global average emission for vegetated surfaces is $0.7\text{ g C m}^{-2}\text{ yr}^{-1}$ but can exceed $100\text{ g C m}^{-2}\text{ yr}^{-1}$ in some tropical ecosystems (Peñuelas and Llusia 2003).

2.4.3.1 BVOC precursors of short-lived climate forcers from land

BVOCs are rapidly oxidised in the atmosphere to form less volatile compounds that can condense and form SOA. In boreal and tropical forests, carbonaceous aerosols originate from BVOC oxidation, of which isoprene and terpenes are the most important precursors (Claeys et al. 2004; Hu et al. 2015; De Sá et al. 2017; de Sá et al. 2018; Liu et al. 2016b). See the following sub-section for more detail.

BVOCs are the most important precursors of SOA. The transformation process of BVOCs affects the aerosol size distribution both by

contributing to new particle formation and to the growth of larger pre-existing particles. SOA affects the scattering of radiation by the particles themselves (direct aerosol effect), but also changes the amount of CCN and the lifetime and optical properties of clouds (indirect aerosol effect).

High amounts of SOA are observed over forest areas, in particular in boreal and tropical regions where they have been found to mostly originate from BVOC emissions (Manish et al. 2017). In particular, isoprene epoxydiol-derived SOA (IEPOX-SOA) is being identified in recent studies in North America and Amazonian forest as a major component in the oxidation of isoprene (Allan et al. 2014; Schulz et al. 2018; De Sá et al. 2017). In tropical regions, BVOCs can be convected up to the upper atmosphere, where their volatility is reduced and where they become SOA. In some cases those particles are transported back to the lower atmosphere (Schulz et al. 2018; Wang et al. 2016a; Andreae et al. 2018). In the upper troposphere in the Amazon, SOA are important CCN and are responsible for the vigorous hydrological cycle (Pöhlker et al. 2018). This strong link between BVOC emissions by plants and the hydrological cycle has been discussed in a number of studies (Fuentes et al. 2000; Schmale et al. 2018; Pöhlker et al. 2018, 2016).

Changing BVOC emissions also affect the oxidant concentrations in the atmosphere. Their impact on the concentration of ozone depends on the NO_x concentrations. In polluted regions, high BVOC emissions lead to increased production of ozone, followed by the formation of more OH and a reduction in the methane lifetime. In more pristine regions (NO_x-limited), increasing BVOC emissions instead lead to decreasing OH and ozone concentrations, resulting in a longer methane lifetime. The net effect of BVOCs then can change over time if NO_x emissions are changing.

BVOCs' possible climate effects have received little attention because it was thought that their short lifetime would preclude them from having any significant direct influence on climate (Unger 2014a; Sporre et al. 2019). Higher temperatures and increased CO₂ concentrations are (separately) expected to increase the emissions of BVOCs (Jardine et al. 2011, 2015; Fuentes et al. 2016). This has been proposed to initiate negative climate feedback mechanisms through increased formation of SOA (Arneth et al. 2010; Kulmala 2004; Unger et al. 2017). More SOA can make clouds more reflective, which can provide a cooling effect. Furthermore, the increase in SOA formation has also been proposed to lead to increased aerosol scattering, resulting in an increase in diffuse radiation. This could boost GPP and further increase BVOC emissions (Kulmala et al. 2014; Cirino et al. 2014; Sena et al. 2016; Schafer et al. 2002; Ometto et al. 2005; Oliveira et al. 2007). This important feedback is starting to emerge (Sporre et al. 2019; Kulmala 2004; Arneth et al. 2017). However, there is evidence that this influence might be significant at different spatial scales, from local to global, through aerosol formation and through direct and indirect greenhouse effects (*limited evidence, medium agreement*). Most tropical forest BVOCs are primarily emitted from tree foliage, but soil microbes can also be a major source of some compounds including sesquiterpenes (Bourtsoukidis et al. 2018).

2.4.3.2 Historical changes of BVOCs and contribution to climate change

Climate warming over the past 30 years, together with the longer growing season experienced in boreal and temperate environments, have increased BVOC global emissions since the preindustrial times (*limited evidence, medium agreement*) (Peñuelas 2009; Sanderson et al. 2003; Pacifico et al. 2012). This was opposed by lower BVOC emissions caused by the historical conversion of natural vegetation and forests to cropland (*limited evidence, medium agreement*) (Unger 2013, 2014a; Fu and Liao 2014). The consequences of historical anthropogenic land cover change were a decrease in the global formation of SOA (−13%) (Scott et al. 2017) and tropospheric burden (−13%) (Heald and Geddes 2016). This has resulted in a positive radiative forcing (and thus warming) from 1850–2000 of 0.017 W m^{-2} (Heald and Geddes 2016), 0.025 W m^{-2} (Scott et al. 2017) and 0.09 W m^{-2} (Unger 2014b) through the direct aerosol effect. In present-day conditions, global SOA production from all sources spans between 13 and 121 Tg yr^{-1} (Tsigaridis et al. 2014). The indirect aerosol effect (change in cloud condensation nuclei), resulting from land use induced changes in BVOC emissions, adds an additional positive radiative forcing of 0.008 W m^{-2} (Scott et al. 2017). More studies with different model setups are needed to fully assess this indirect aerosol effect associated with land use change from the preindustrial to present. CMIP6 global emissions pathways (Hoesly et al. 2018; Gidden et al. 2018) estimates global VOCs emissions in 2015 at $230 \text{ MtVOC yr}^{-1}$. They also estimated that, from 2000–2015, emissions were up from $200\text{--}230 \text{ MtVOC yr}^{-1}$.

There is (*limited evidence, medium agreement*) that historical changes in BVOC emissions have also impacted on tropospheric ozone. At most surface locations where land use has changed, the NO_x concentrations are sufficiently high for the decrease in BVOC emissions to lead to decreasing ozone concentrations (Scott et al. 2017). However, in more pristine regions (with low NO_x concentrations), the imposed conversion to agriculture has increased ozone through decreased BVOC emissions and their subsequent decrease in OH (Scott et al. 2017; Heald and Geddes 2016). In parallel, the enhanced soil NO_x emissions from agricultural land can increase the ozone concentrations in NO_x limited regions (Heald and Geddes 2016).

Another impact of the historical decrease in BVOC emissions is the reduction in the atmospheric lifetime of methane (*limited evidence, medium agreement*), which results in a negative radiative forcing that ranges from -0.007 W m^{-2} (Scott et al. 2017) to -0.07 W m^{-2} (Unger 2014b). However, knowledge of the degree that BVOC emissions impact on oxidant concentrations, in particular OH (and thus methane concentrations), is still limited and therefore these numbers are very uncertain (Heald and Spracklen 2015; Scott et al. 2017). The effect of land use change on BVOC emissions are highly heterogeneous (Rosenkranz et al. 2015) and though the global values of forcing described above are small, the local or regional values can be higher, and even of opposite sign, than the global values.

2.4.3.3 Future changes of BVOCs

Studies suggest that increasing temperature will change BVOC emissions through change in species composition and rate of BVOC production. A further $2^\circ\text{C}\text{--}3^\circ\text{C}$ rise in the mean global temperature could increase BVOC global emissions by an additional 30–45% (Peñuelas and Llusià 2003). In two modelling studies, the impact on climate from rising BVOC emissions was found to become even larger with decreasing anthropogenic aerosol emissions (Kulmala et al. 2013; Sporre et al. 2019). A negative feedback on temperature, arising from the BVOC-induced increase in the first indirect aerosol effect, has been estimated by two studies to be in the order of $-0.01 \text{ W m}^{-2} \text{ K}$ (Scott et al. 2018b; Paasonen et al. 2013). Enhanced aerosol scattering from increasing BVOC emissions has been estimated to contribute to a global gain in BVOC emissions of 7% (Rap et al. 2018). In a warming planet, BVOC emissions are expected to increase but magnitude of this increase is unknown and will depend on future land use change, in addition to climate (*limited evidence, medium agreement*).

There is a very limited number of studies investigating the climate impacts of BVOCs using future land use scenarios (Ashworth et al. 2012; Pacifico et al. 2012). Scott et al. (2018a) found that a future deforestation according to the land use scenario in RCP8.5 leads to a 4% decrease in BVOC emissions at the end of the century. This resulted in a direct aerosol forcing of $+0.006 \text{ W m}^{-2}$ (decreased reflection by particles in the atmosphere) and a first indirect aerosol forcing of -0.001 W m^{-2} (change in the amount of CCN). Studies not including future land use scenarios but investigating the climate feedbacks leading to increasing future BVOC emissions, have found a direct aerosol effect of -0.06 W m^{-2} (Sporre et al. 2019) and an indirect aerosol effect of -0.45 W m^{-2} (Makkonen et al. 2012; Sporre et al. 2019). The stronger aerosol effects from the feedback compared to the land use are, at least partly, explained by a much larger change in the BVOC emissions.

A positive climate feedback could happen in a future scenario with increasing BVOC emissions, where higher ozone and methane concentrations could lead to an enhanced warming which could further increase BVOC emissions (Arneth et al. 2010). This possible feedback is mediated by NO_x levels. One recent study including dynamic vegetation, land use change, CO₂ and climate change found no increase and even a slight decrease in global BVOC emissions at the end of the century (Hantson et al. 2017). There is a lack of understanding concerning the processes governing the BVOC emissions, the oxidation processes in the atmosphere, the role of the BVOC oxidation products in new particle formation and particle growth, as well as general uncertainties in aerosol–cloud interactions. There is a need for continued research into these processes, but the current knowledge indicates that changing BVOC emissions need to be taken into consideration when assessing the future climate and how land use will affect it. In summary, the magnitude and sign of net effect of BVOC emissions on the radiation budget and surface temperature is highly uncertain.

2.5 Land impacts on climate and weather through biophysical and GHG effects

The focus of this section is summarised in Figure 2.13. We report on what we know regarding the influence land has on climate via biophysical and biogeochemical exchanges. Biogeochemical effects herein only refer to changes in net emissions of CO₂ from land. The influence of land on atmospheric composition is discussed in Section 2.3.

All sections discuss impacts of land on global and regional climate, and climate extremes, whenever the information is available. Section 2.5.1 presents effects of historical and future land use scenarios, Section 2.5.2 is devoted to impacts of specific anthropogenic land uses such as forestation, deforestation, irrigation, crop and forest management, Section 2.5.3 focuses on how climate-driven land changes feedback on climate, and Section 2.5.4 puts forward the theory that land use changes in one region can affect another region.

2.5.1 Impacts of historical and future anthropogenic land cover changes

The studies reported below focus essentially on modelling experiments, as there is no direct observation of how historical land use changes have affected the atmospheric dynamics and physics at the global and regional scales. Moreover, the climate modelling experiments only assess the impacts of anthropogenic land cover

changes (e.g., deforestation, urbanisation) and neglect the effects of changes in land management (e.g., irrigation, use of fertilisers, choice of species varieties among managed forests or crops). Because of this restricted accounting for land use changes, we will use the term 'land cover changes' in Sections 2.5.1.1 and 2.5.1.2.

Each section starts by describing changes at the global scale and regional scale, and ends with what we know about the impacts of those scenarios on extreme weather events, whenever the information is available.

2.5.1.1 Impacts of global historical land cover changes on climate

At the global level

The contribution of anthropogenic land cover changes to the net global warming throughout the 20th century has been derived from few model-based estimates that account simultaneously for biogeochemical and biophysical effects of land on climate (Table 2.4). The simulated net change in mean global annual surface air temperature, averaged over all the simulations, is a small warming of $0.078 \pm 0.093^\circ\text{C}$, ranging from small cooling simulated by two models (-0.05°C and -0.02°C respectively in Brovkin et al. (2004) and Simmons and Matthews (2016), to larger warming simulated by three models ($>+0.14^\circ\text{C}$; Shevlakova et al. 2013; Pongratz et al. 2010; Matthews et al. 2004). When starting from the Holocene period, He et al. (2014) estimated an even larger net warming effect of anthropogenic land cover changes ($+0.72^\circ\text{C}$).

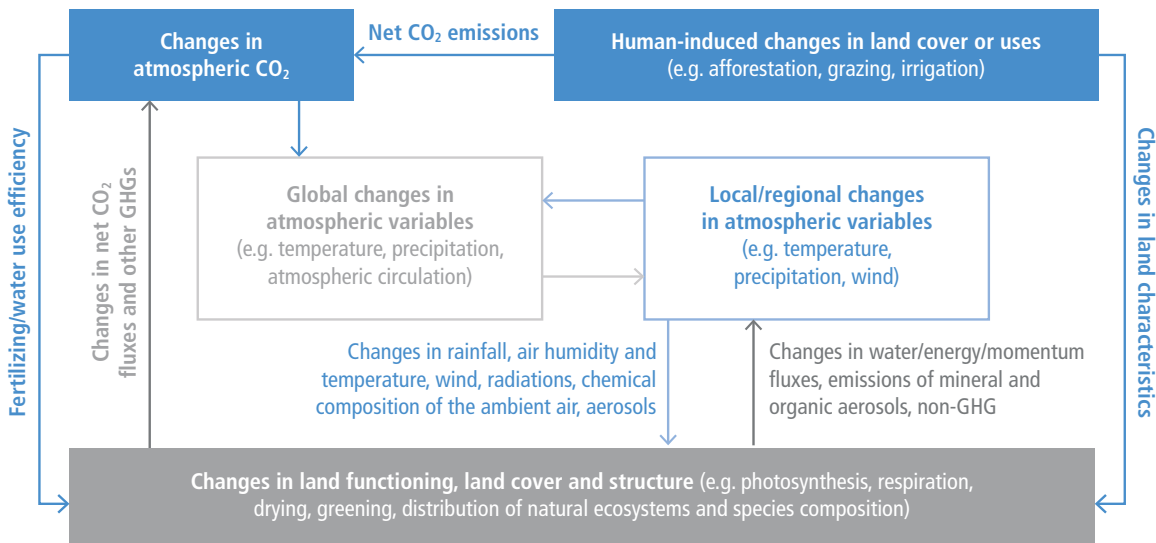


Figure 2.13 | Global, local and regional climate changes are the focus of this section. They are examined through changes in climate states (e.g., changes in air temperature and humidity, rainfall, radiation) as well as through changes in atmospheric dynamics (e.g., circulation patterns). Changes in land that influence climate are either climate- or human-driven. Dark-blue arrows and boxes refer to what we consider imposed changes (forcings). Dark-grey arrows and boxes refer to responses of land to forcings (blue boxes and blue-outline box) and feedbacks on those initial forcings. Pale-grey and pale-blue arrows and boxes refer respectively to global and local/regional climate changes and their subsequent changes on land.

Table 2.4 | Change in mean global annual surface air temperature resulting from anthropogenic land cover change over the historical period. This historical period varies from one simulation to another (middle column).

Reference of the study	Time period	Mean global annual change in surface air temperature (°C)
Simmons and Matthews (2016)	1750–2000	-0.02
Shevlakova et al. (2013)	1861–2005	+0.17
Pongratz et al. (2010)	1900–2000	+0.14
Matthews et al. (2004)	1700–2000	+0.15
Brovkin et al. (2004)	1850–2000	-0.05
Mean ± standard deviation		0.078 ± 0.093

This net small warming signal results from the competing effects of biophysical cooling (*medium confidence*) and biogeochemical warming (*very high confidence*) (Figure 2.14¹). The global biophysical cooling alone has been estimated by a larger range of climate models and is $-0.10 \pm 0.14^\circ\text{C}$; it ranges from -0.57°C to $+0.06^\circ\text{C}$ (e.g., Zhang et al. 2013a; Hua and Chen 2013; Jones et al. 2013b; Simmons and Matthews 2016) (Table A2.1). This cooling is essentially dominated by increases in surface albedo; historical land cover changes have generally led to a dominant brightening of land as discussed in AR5 (Myhre et al. 2013). Reduced incoming longwave radiation at the surface from reduced evapotranspiration and thus less water vapour in the atmosphere has also been reported as a potential contributor to this cooling (Claussen et al. 2001). The cooling is, however, damped by decreases in turbulent fluxes, leading to decreased loss of heat and water vapour from the land through convective processes. Those non-radiative processes are well-known to often oppose the albedo-induced surface temperature changes (e.g., Davin and de Noblet-Ducoudré (2010), Boisier et al. (2012)).

Historical land cover changes have contributed to the increase in atmospheric CO₂ content (Section 2.3) and thus to global warming (biogeochemical effect, *very high confidence*). The global mean biogeochemical warming has been calculated from observation-based estimates ($+0.25 \pm 0.10^\circ\text{C}$) (e.g., Li et al. (2017a), Avitabile et al. (2016), Carvalhais et al. (2014), Le Quéré et al. (2015)), or estimated from DGVMs ($+0.24 \pm 0.12^\circ\text{C}$) (Peng et al. 2017; Arneth et al. 2017; Pugh et al. 2015; Hansis et al. 2015) and global climate models ($+0.20 \pm 0.05^\circ\text{C}$) (Pongratz et al. 2010; Brovkin et al. 2004; Matthews et al. 2004; Simmons and Matthews 2016).

The magnitude of these simulated biogeochemical effects may, however, be underestimated as they do not account for a number of processes such as land management, nitrogen/phosphorus cycles, changes in the emissions of CH₄, N₂O and non-GHG emissions from land (Ward et al. 2014; Arneth et al. 2017; Cleveland et al. 2015; Pongratz et al. 2018). Two studies have accounted for those compounds and found a global net positive radiative forcing in response to historical anthropogenic land cover changes, indicating a net surface warming (Mahowald et al. 2017; Ward et al. 2014). However, first the estimated biophysical radiative forcing in those studies only accounts for changes in albedo and not for changes in turbulent fluxes. Secondly, the combined estimates also depend on other several key modelling estimates such as climate sensitivity, CO₂ fertilisation caused by land use emissions, possible synergistic

effects, validity of radiative forcing concept for land forcing. The comparison with the other above-mentioned modelling studies is thus difficult.

In addition, most of those estimates do not account for the evolution of natural vegetation in unmanaged areas, while observations and numerical studies have reported a greening of the land in boreal regions resulting from both extended growing season and poleward migration of tree lines (Lloyd et al. 2003; Lucht et al. 1995; Section 2.2). This greening enhances global warming via a reduction of surface albedo (winter darkening of the land through the snow-albedo feedbacks; e.g., Forzieri et al. 2017). At the same time, cooling occurs due to increased evapotranspiration during the growing season, along with enhanced photosynthesis, in essence, increased CO₂ sink (Qian et al. 2010). When feedbacks from the poleward migration of treeline are accounted for, together with the biophysical effects of historical anthropogenic land cover change, the biophysical annual cooling (about -0.20°C to -0.22°C on land, -0.06°C globally) is significantly damped by the warming (about $+0.13^\circ\text{C}$) resulting from the movements of natural vegetation (Strengers et al. 2010). Accounting simultaneously for both anthropogenic and natural land cover changes reduces the cooling impacts of historical land cover change in this specific study.

At the regional level

The global and annual estimates reported above mask out very contrasted regional and seasonal differences. Biogeochemical effects of anthropogenic land cover change on temperature follow the spatial patterns of GHG-driven climate change with stronger warming over land than ocean, and stronger warming in northern high latitudes than in the tropics and equatorial regions (Arctic amplification). Biophysical effects on the contrary are much stronger where land cover has been modified than in their surroundings (see Section 2.5.4 for a discussion on non-local effects). Very contrasted regional temperature changes can thus result, depending on whether biophysical processes dampen or exacerbate biogeochemical impacts.

Figure 2.15 compares, for seven climate models, the biophysical effects of historical anthropogenic land cover change in North America and Eurasia (essentially cooling) to the regional warming resulting from the increased atmospheric CO₂ content since pre-industrial times (De Noblet-Ducoudré et al. 2012; comparing

¹ The detailed list of all values used to construct this figure is provided in Table A2.1 in the Appendix at the end of the chapter.

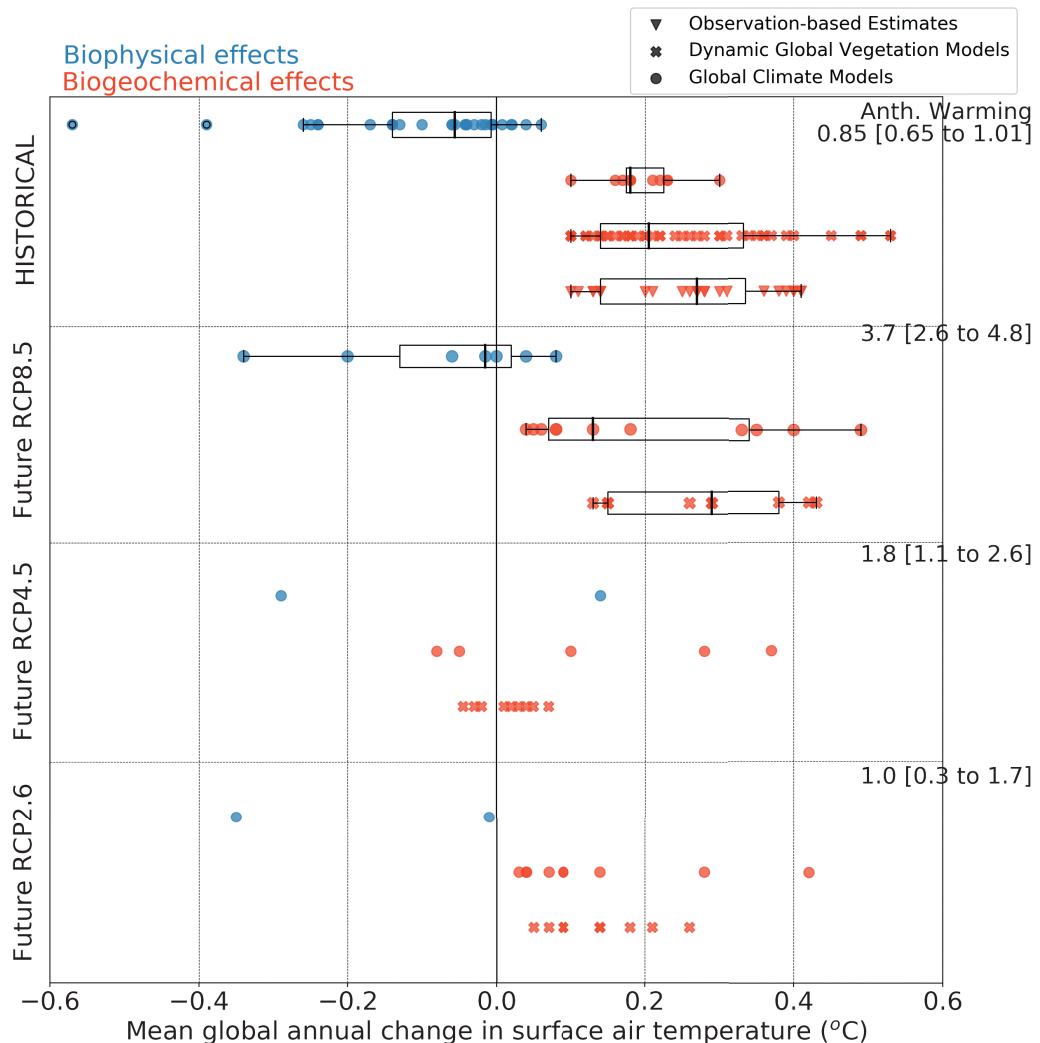


Figure 2.14 | Changes in mean global annual surface air temperature (°C) in response to historical and future anthropogenic land cover changes as estimated from a range of studies. See Table A2.1 in the Appendix for detailed information. Temperature changes resulting from biophysical processes (e.g., changes in physical land surface characteristics such as albedo, evapotranspiration and roughness length) are illustrated using blue symbols and temperature changes resulting from biogeochemical processes (e.g., changes in atmospheric CO₂ composition) use red symbols. Future changes are shown for three distinct scenarios: RCP8.5, RCP4.5 and RCP2.6. The markers 'filled circle', 'filled cross' and 'filled triangle down' represent estimates from global climate models, DGVMs and observations respectively. When the number of estimates is sufficiently large, box plots are overlaid; they show the ensemble minimum, first quartile (25th percentile), median, third quartile (75th percentile), and the ensemble maximum. Scatter points beyond the box plot are the outliers. Details about how temperature change is estimated from DGVMs and observations is provided in the Appendix. Numbers on the right-hand side give the mean and the range of simulated mean global annual warming from various climate models.

1973–2002 to 1871–1900). It shows a dominant biophysical cooling effect of changes in land cover, at all seasons, as large as the regional footprint of anthropogenic global warming. Averaged over all agricultural areas of the world (Pongratz et al. 2010) reported a 20th century biophysical cooling of -0.10°C , and Strengers et al. (2010) reported a land induced cooling as large as -1.5°C in western Russia and eastern China between 1871 and 2007. There is thus *medium confidence* that anthropogenic land cover change has dampened warming in many regions of the world over the historical period.

Very few studies have explored the effects of historical land cover changes on seasonal climate. There is, however, evidence that the seasonal magnitude and sign of those effects at the regional level are strongly related to soil-moisture/evapotranspiration and snow regimes, particularly in temperate and boreal latitudes (Teuling et al. 2010; Pitman and de Noblet-Ducoudré 2012; Alkama and Cescatti 2016). Quesada et al. (2017a) showed that atmospheric circulation changes can be significantly strengthened in winter for tropical and temperate regions. However, the lack of studies underlines the need for a more systematic assessment of seasonal, regional and other-than-mean-temperature metrics in the future.

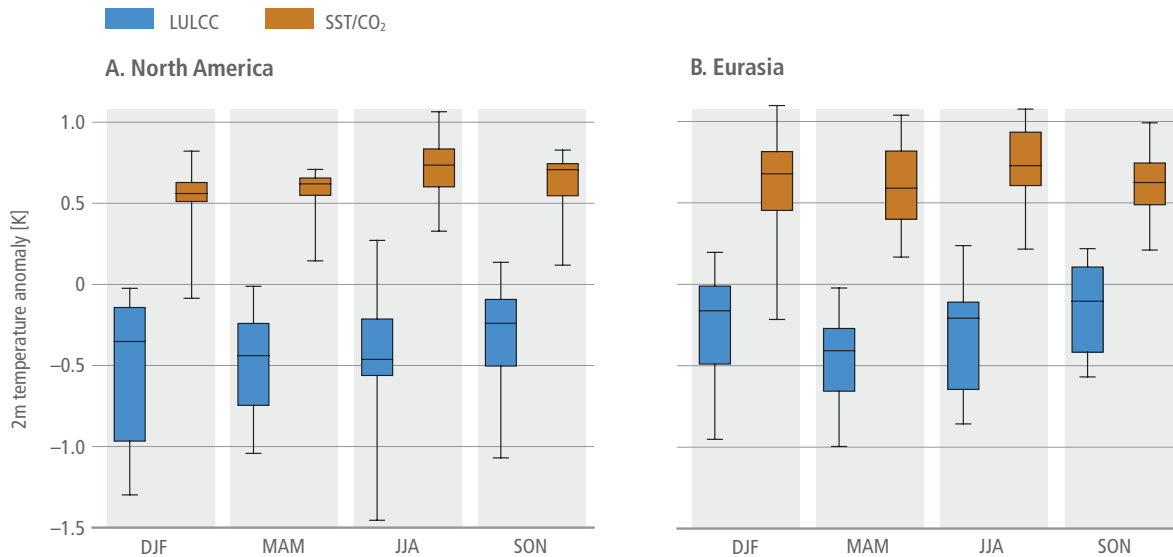


Figure 2.15 | Simulated changes in mean surface air temperature ($^{\circ}\text{C}$) between the pre-industrial period (1870–1900) and the present-day (1972–2002) for all seasons and for (A) North America and (B) Eurasia. Source: De Noblet-Ducoudré et al. (2012). Brown boxes are the changes simulated in response to increased atmospheric GHG content between both time periods and subsequent changes in sea-surface temperature and sea-ice extent (SST/CO₂). The CO₂ changes accounted for include emissions from all sources, including land use. Blue boxes are the changes simulated in response to the biophysical effects of historical land cover changes. The box-and-whisker plots have been drawn using results from seven climate models and ensembles of 10 simulations per model and time period. The bottom and top of each grey box are the 25th and 75th percentiles, and the horizontal line within each box is the 50th percentile (the median). The whiskers (straight lines) indicate the ensemble maximum and minimum values. Seasons are respectively December–January–February (DJF), March–April–May (MAM), June–July–August (JJA) and September–October–November (SON). North America and Eurasia are extended regions where land-use changes are the largest between the two time periods considered (their contours can be found in Figure 1 of De Noblet-Ducoudré et al. (2012)).

Effects on extremes

The effect of historical deforestation on extreme temperature trends is intertwined with the effect of other climate forcings, thus making it difficult to quantify based on observations. Based on results from four climate models, the impact of historical anthropogenic land cover change on temperature and precipitation extremes was found to be locally as important as changes arising from increases in atmospheric CO₂ and sea-surface temperatures, but with a lack of model agreement on the sign of changes (Pitman et al. 2012). In some regions, the impact of land cover change masks or amplifies the effect of increased CO₂ on extremes (Avila et al. 2012; Christidis et al. 2013). Using an observational constraint for the local biophysical effect of land cover change applied to a set of CMIP5 climate models, Lejeune et al. (2018) found that historical deforestation increased extreme hot temperatures in northern mid-latitudes. The results also indicate a stronger impact on the warmest temperatures compared to mean temperatures. Findell et al. (2017) reached similar conclusions, although using only a single climate model. Importantly, the climate models involved in these three studies did not consider the effect of management changes, which have been shown to be important, as discussed in Section 2.5.2.

Based on the studies discussed above, there is *limited evidence* but *high agreement* that land cover change affects local temperature extremes more than mean values. Observational studies assessing the role of land cover on temperature extremes are still very limited (Zaitchik et al. 2006; Renaud and Rebetez 2008), but suggest that

trees dampen seasonal and diurnal temperature variations at all latitudes, and even more so in temperate regions compared to short vegetation (Chen et al. 2018; Duveiller et al. 2018; Li et al. 2015a; Lee et al. 2011). Furthermore, trees also locally dampen the amplitude of heat extremes (Renaud and Rebetez 2008; Zaitchik et al. 2006) although this result depends on the forest type, coniferous trees providing less cooling effect than broadleaf trees (Renaud et al. 2011; Renaud and Rebetez 2008).

2.5.1.2 Impacts of future global land cover changes on climate

At the global level

The most extreme CMIP5 emissions scenario, RCP8.5, has received the most attention in the literature with respect to how projected future anthropogenic land use land cover changes (Hurt et al. 2011) will affect the highest levels of global warming.

Seven model-based studies have examined both the biophysical and biogeochemical effects of anthropogenic changes in land cover, as projected in RCP8.5, on future climate change (Simmons and Matthews 2016; Davies-Barnard et al. 2014; Boysen et al. 2014) (Table 2.5). They all agree on a biogeochemical warming, ranging from +0.04°C to +0.35°C, in response to land cover change. Two models predict an additional biophysical warming, while the others agree on a biophysical cooling that dampens (or overrules) the biogeochemical warming. Using a wider range of global

Table 2.5 | Change in mean global annual surface air temperature resulting from anthropogenic land cover changes projected for the future, according to three different scenarios: RCP8.5, RCP4.5 and RCP2.6. Temperature changes resulting from biophysical and biogeochemical effects of land cover change are examined.

Reference of the study	Time period	Mean global annual change in surface air temperature (°C)			
		Biophysical/biogeochemical	RCP2.6	RCP4.5	RCP8.5
Simmons and Matthews (2016)	2000–2100		-0.35/+0.42	-0.29/+0.37	-0.34/+0.35
Davies-Barnard et al. (2014)	2005–2100		-0.01/+0.04	+0.14/-0.08	-0.015/+0.04
Boysen et al. (2014)	2005–2100				+0.04/+0.08 0/+0.05 +0.08/+0.06 -0.20/+0.13 -0.06/+0.33

climate models, the biogeochemical warming (*high confidence*) is $+0.20 \pm 0.15^\circ\text{C}$ whereas it is $+0.28 \pm 0.11^\circ\text{C}$ when estimated from DGVMs (Pugh et al. 2015; Stocker et al. 2014). This biogeochemical warming is compensated for by a biophysical cooling (*medium confidence*) of $-0.10 \pm 0.14^\circ\text{C}$ (Quesada et al. 2017a; Davies-Barnard et al. 2015; Boysen et al. 2014). The estimates of temperature changes resulting from anthropogenic land cover changes alone remain very small compared to the projected mean warming of $+3.7^\circ\text{C}$ by the end of the 21st century (ranging from 2.6°C – 4.8°C depending on the model and compared to 1986–2005; Figure 2.14).

Two other projected land cover change scenarios have been examined (RCP4.5 and RCP2.6; Table 2.5; Figure 2.14) but only one climate modelling experiment has been carried out for each, to estimate the biophysical impacts on climate of those changes (Davies-Barnard et al. 2015). For RCP2.6, ESMs and DGVMs agree on a systematic biogeochemical warming resulting from the imposed land cover changes, ranging from $+0.03$ to $+0.28^\circ\text{C}$ (Brovkin et al. 2013), which is significant compared to the projected mean climate warming of $+1^\circ\text{C}$ by the end of the 21st century (ranging from 0.3°C – 1.7°C depending on the models, compared to 1986–2005). A very small amount of biophysical cooling is expected from the one estimate. For RCP4.5, biophysical warming is expected from only one estimate, and results from a projected large forestation in the temperate and high latitudes. There is no agreement on the sign of the biogeochemical effect: there are as many studies predicting cooling as warming, whichever the method to compute those effects (ESMs or DGVMs).

Previous scenarios – Special Report on Emission Scenarios (SRES) results of climate studies using those scenarios were reported in AR4 – displayed larger land use changes than the more recent ones (RCP, AR5). There is *low confidence* from some of those previous scenarios (SRES A2 and B1) of a small warming effect ($+0.2$ to $+0.3^\circ\text{C}$) of anthropogenic land cover change on mean global climate, this being dominated by the release of CO_2 in the atmosphere from land conversions (Sitch et al. 2005). This additional warming remains quite small when compared to the one resulting from the combined anthropogenic influences ($+1.7^\circ\text{C}$ for SRES B1 and $+2.7^\circ\text{C}$ for SRES A2). A global biophysical cooling of -0.14°C is estimated in response to the extreme land cover change projected in SRES A2, a value that far exceeds the impacts of historical land use changes (-0.05°C) calculated using the same climate model (Davin et al. 2007). The authors derived a biophysical climatic sensitivity to land use change of about $-0.3^\circ\text{C W.m}^{-2}$ for their

model, whereas a warming of about 1°C W.m^{-2} is obtained in response to changes in atmospheric CO_2 concentration.

Those studies generally do not report on changes in atmospheric variables other than surface air temperature, thereby limiting our ability to assess the effects of anthropogenic land cover changes on regional climate (Sitch et al. 2005). However, small reductions reported in rainfall via changes in biophysical properties of the land, following the massive tropical deforestation in SRES A2 ($+0.5$ and $+0.25 \text{ mm day}^{-1}$ respectively in the Amazon and Central Africa). They also report opposite changes – that is, increased rainfall of about 0.25 mm day^{-1} across the entire tropics and subtropics, triggered by biogeochemical effects of this same deforestation.

At the regional level

In regions that will undergo land cover changes, dampening of the future anthropogenic warming can be as large as -26% while enhancement is always smaller than 9% within RCP8.5 by the end of the 21st century (Boysen et al. 2014). Volodko (2006) shows that, by 2050, and following the SRES B2 scenario, the contribution of land cover changes to the total temperature change can be as large as 15% in many boreal regions, and as large as 40% in south-western tropical Africa. Feddema et al. (2005) simulate large decreases in the diurnal temperature range in the future (2050 and 2100 in SRES B1 and A2) following tropical deforestation in both scenarios. In the Amazon, for example, the diurnal temperature range is lowered by 2.5°C due to increases in minimum temperature, while little change is obtained for the maximum value.

There is thus *medium evidence* that future anthropogenic land cover change will have a significant effect on regional temperature via biophysical effects in many regions of the world. There is, however, *no agreement* on whether warming will be damped or enhanced, and there is *no agreement* on the sign of the contribution across regions.

There are very few studies that go beyond analysing the changes in mean surface air temperature. Some studies attempted to look at global changes in rainfall and found no significant influence of future land cover changes (Brovkin et al. 2013; Sitch et al. 2005; Feddema et al. 2005). Quesada et al. (2017a, b) however carried out a systematic multi-model analysis of the response of a number of atmospheric, radiative and hydrological variables (e.g., rainfall, sea level pressure,

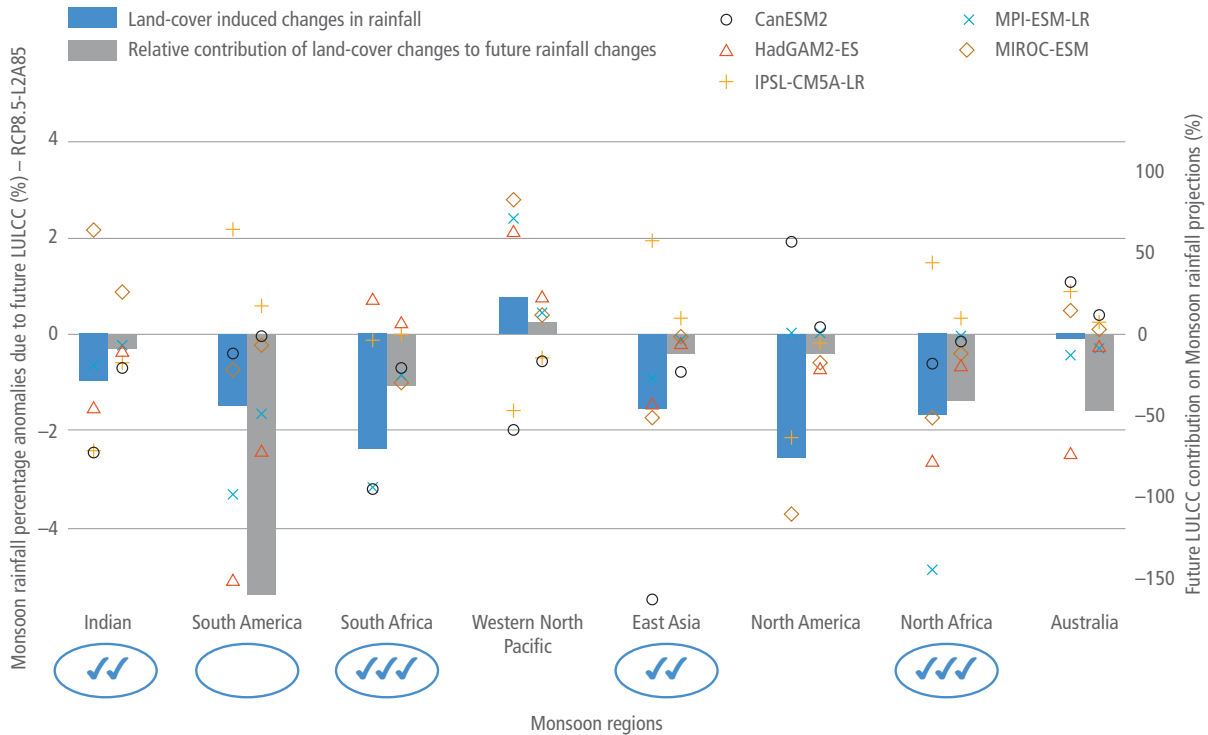


Figure 2.16 | Changes in monsoon rainfall in RCP8.5 scenario resulting from projected changes in anthropogenic land cover, in eight monsoon regions (%; blue bars). Differences are calculated between the end of the 21st century (2071–2100) and the end of the 20th century (1976–2005), and the percent change is calculated with reference to 1976–2005. Grey bars refer to the relative contribution of land-cover changes (in %) to future rainfall projections: it is the ratio between the change in rainfall responding to land cover changes and the one responding to all anthropogenic changes (Quesada et al. 2017b). Negative values mean that changes in land cover have an opposite effect (dampening) on rainfall compared to the effects of all anthropogenic changes. Monsoon regions have been defined following Yim et al. (2014). The changes have been simulated by five climate models (Brovkin et al. 2013). Results are shown for December–January–February for southern hemisphere regions, and for June–July–August for northern hemisphere regions. Statistical significance is given by blue tick marks and circles: one, two and three blue tick marks are displayed for the regions where at least 80% of the climate models have regional changes significant at the 66th, 75th and 80th confidence level, respectively; blue circles are added when the regional values are also significant at 90th confidence level. Note that future land cover change impacts on South American monsoon are neither significant nor robust among models, along with very small future projected changes in South American monsoon rainfall.

geopotential height, wind speed, soil-moisture, turbulent heat fluxes, shortwave and longwave radiation, cloudiness) to RCP8.5 land cover scenario. In particular, they found a significant reduction of rainfall in six out of eight monsoon regions studied (Figure 2.16) of about 1.9–3% (which means more than -0.5 mm day^{-1} in some areas) in response to future anthropogenic land cover changes. Including those changes in global climate models reduces the projected increase in rainfall by about 9–41% in those same regions, when all anthropogenic forcings are accounted for (30% in the global monsoon region as defined by Wang and Ding (2008)). In addition, they found a shortening of the monsoon season of one to four days. They conclude that the projected future increase in monsoon rains may be overestimated by those models that do not yet include biophysical effects of land cover changes. Overall, the regional hydrological cycle was found to be substantially reduced and wind speed significantly strengthened in response to regional deforestation within the tropics, with magnitude comparable to projected changes with all forcings (Quesada et al. 2017b).

Effects on extremes

Results from a set of climate models have shown that the impact of future anthropogenic land cover change on extreme temperatures can be of similar magnitude as the changes arising from half a degree global mean annual surface temperature change (Hirsch et al. 2018). However, this study also found a lack of agreement between models with respect to the magnitude and sign of changes, thus making land cover change a factor of uncertainty in future climate projections.

2.5.2 Impacts of specific land use changes

2.5.2.1 Impacts of deforestation and forestation

Deforestation or forestation,² wherever it occurs, triggers simultaneously warming and cooling of the surface and of the atmosphere via changes in its various characteristics (Pitman 2003; Strengers et al. 2010; Bonan 2008). Following deforestation, warming results from (i) the release of

² The term ‘forestation’ is used herein as this chapter does not distinguish between afforestation and reforestation. In model-based studies, simulations with and without trees are compared; in observation-based estimates, sites with and without trees are compared.

CO_2 and other GHGs in the atmosphere (biogeochemical impact) and subsequent increase in incoming infrared radiation at surface (greenhouse effect), (ii) a decrease in the total loss of energy through turbulent fluxes (latent and sensible heat fluxes) resulting from reduced surface roughness, (iii) an increased incoming solar radiation following reduced cloudiness that often (but not always) accompanies the decreased total evapotranspiration. Cooling occurs in response to (iv) increased surface albedo that reduces the amount of absorbed solar radiation, (v) reduced incoming infrared radiation triggered by the decreased evapotranspiration and subsequent decrease in atmospheric water vapour. Points ii–v are referred to as biophysical effects. Deforestation and forestation also alter rainfall and winds (horizontal as well as vertical, as will be further discussed below).

The literature that discusses the effects of forestation on climate is more limited than for deforestation, but they reveal a similar climatic response with opposite sign, as further discussed below. For each latitudinal band (tropical, temperate and boreal) we look at how very large-scale deforestation or forestation impacts on the global mean climate, followed by an examination of the large-scale changes in the specific latitudinal band, and finally more regionally focused analysis. Large-scale idealised deforestation or forestation experiments are often carried out with global or regional climate models as they allow us to understand and measure how sensitive climate is to very large changes

in land cover (similar to the instant doubling of CO_2 in climate models to calculate the climatic sensitivity to GHGs). Details of the model-based studies discussed below can be found in Table A2.2 in the Appendix.

Global and regional impacts of deforestation/forestation in tropical regions

A pan-tropical deforestation would lead to the net release of CO_2 from land, and thus to mean global annual warming, with model-based estimates of biogeochemical effects ranging from $+0.19$ to $+1.06^\circ\text{C}$, with a mean value of $+0.53 \pm 0.32^\circ\text{C}$ (Ganopolski et al. 2001; Snyder et al. 2004; Devaraju et al. 2015a; Longobardi et al. 2016; Perugini et al. 2017). There is, however, *no agreement* between models on the magnitude and sign of the biophysical effect of such changes at the global scale (the range spans from -0.5°C to $+0.7^\circ\text{C}$ with a mean value of $+0.1 \pm 0.27^\circ\text{C}$) (e.g., Devaraju et al. (2015b), Snyder (2010), Longobardi et al. (2016a)) (Figure 2.17). This is the result of many compensation effects in action: increased surface albedo following deforestation, decreased atmospheric water vapour content due to less tropical evapotranspiration, and decreased loss of energy from tropical land in the form of latent and sensible heat fluxes.

There is, however, *high confidence* that such large land cover change would lead to a mean biophysical warming when averaged over the

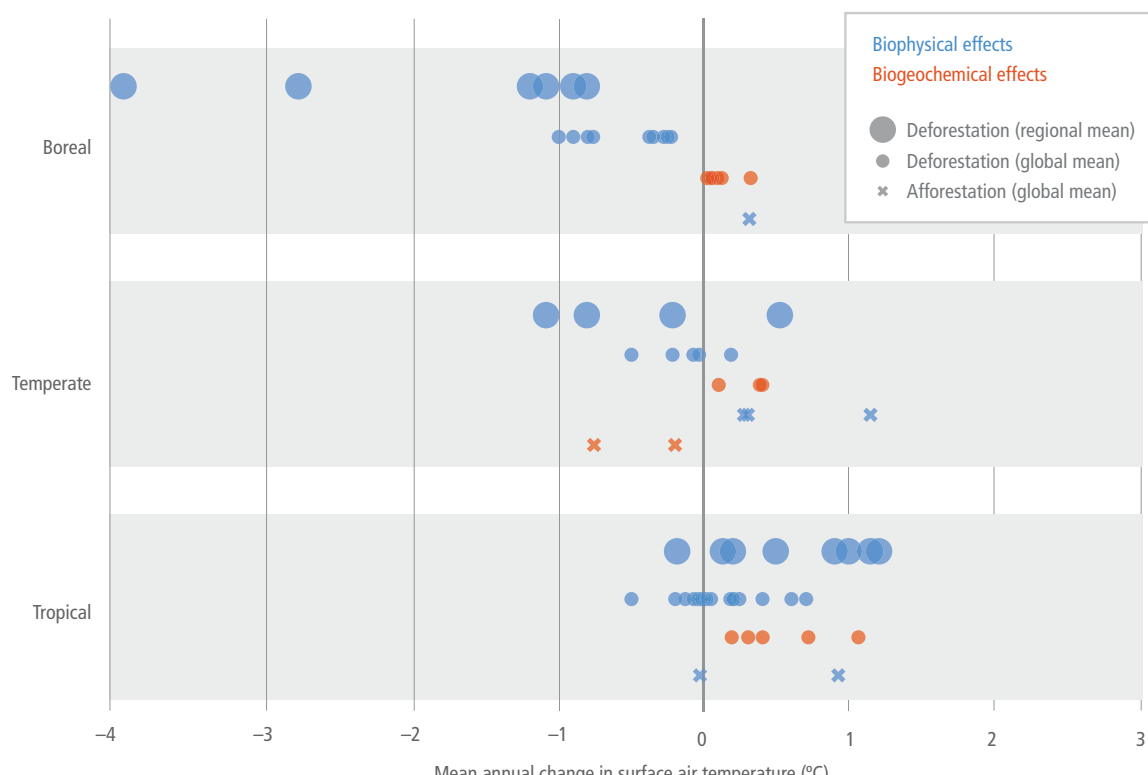


Figure 2.17 | Changes in mean annual surface air temperature ($^\circ\text{C}$) in response to idealised large-scale deforestation (circles) or forestation (crosses). Estimated from a range of studies (see Table A2.2 in the Appendix for detailed information and references to the studies). Temperature changes resulting from biophysical processes (e.g., changes in physical land surface characteristics such as albedo, evapotranspiration, and roughness length) are illustrated using blue symbols and temperature changes resulting from biogeochemical processes (e.g., changes in atmospheric CO_2 composition) use orange symbols. Small blue and orange circles and crosses are model-based estimates of changes in temperature averaged globally. Large circles are estimates averaged only over the latitudinal band where deforestation is imposed.

Chapter 2

deforested land. A mean warming of $+0.61 \pm 0.48^\circ\text{C}$ is found over the entire tropics. On the other hand, biophysical regional cooling and global warming is expected from forestation (Wang et al. 2014b; Bathiany et al. 2010).

Large-scale deforestation (whether pan-tropical or imposed at the sub-continent level, e.g., the Amazon) results in significant mean rainfall decrease (Lawrence and Vandecar 2015; Lejeune et al. 2015; Perugini et al. 2017). In their review, Perugini et al. (2017) reported an average simulated decrease of $-288 \pm 75 \text{ mm yr}^{-1}$ (95% confidence interval). Inversely large-scale forestation increases tropical rainfall by $41 \pm 21 \text{ mm yr}^{-1}$. The magnitude of the change in precipitation strongly depends on the type of land cover conversion. For instance, conversion of tropical forest to bare soil causes larger reductions in regional precipitation than conversion to pasture (respectively $-470 \pm 60 \text{ mm yr}^{-1}$ and $-220 \pm 100 \text{ mm yr}^{-1}$). Biogeochemical effects in response to pan-tropical deforestation, particularly CO₂ release, are generally not taken into account in those studies, but could intensify the hydrological cycle and thus precipitation (Kendra Gotangco Castillo and Gurney 2013).

Specific model-based deforestation studies have been carried out for Africa (Hagos et al. 2014; Boone et al. 2016; Xue et al. 2016; Nogherotto et al. 2013; Hartley et al. 2016; Klein et al. 2017; Abiodun et al. 2012), southern America (Butt et al. 2011; Wu et al. 2017; Spracklen and Garcia-Carreras 2015; Lejeune et al. 2015) and Southeast Asia (Ma et al. 2013b; Werth and Avissar 2005; Mabuchi et al. 2005; Tölle et al. 2017). All found decreases in evapotranspiration following deforestation (*high agreement*), resulting in surface warming, despite the competing effect from increased surface albedo (*high agreement*). Changes in thermal gradients between deforested and adjacent regions, between land and ocean, affect horizontal surface winds (*high agreement*) and thus modify the areas where rain falls, as discussed in Section 2.5.4. An increase in the land-sea thermal contrast has been found in many studies as surface friction is reduced by deforestation, thus increasing the monsoon flow in Africa and South America (Wu et al. 2017).

Observation-based estimates all agree that deforestation increases local land-surface and ambient air temperatures in the tropics, while forestation has the reverse effect (*very high confidence*) (Prevedello et al. 2019; Schultz et al. 2017; Li et al. 2015b; Alkama and Cescatti 2016). There is *very high confidence* that forests are cooler than any shorter vegetation (crops, grasses, bare soil) during daytime due to larger transpiration rates, and there is *high confidence* that the amplitude of the diurnal cycle is smaller in the presence of forests.

Large-scale forestation scenarios of West Africa (Abiodun et al. 2012), eastern China (Ma et al. 2013a) or the Saharan and Australian deserts (Ornstein et al. 2009; Kemen et al. 2017) all concluded that regional surface cooling is simulated wherever trees are grown (-2.5°C in the Sahel, -1°C in the savanna area of West Africa, up to -8°C in the western Sahara and -1.21°C over land in eastern China) while cooling of the ambient air is smaller (-0.16°C). In the case of savanna forestation, this decrease entirely compensates the GHG-induced future warming ($+1^\circ\text{C}$ following the SRES A1B scenario). West African countries thus have the potential to reduce, or even totally cancel in

Land-climate interactions

some places, the GHG-induced warming in the deforested regions (Abiodun et al. 2012). However, this is compensated by enhanced warming in adjacent countries (non-local effect).

Global and regional impacts of deforestation/forestation in temperate regions

As for the tropics, model-based experiments show that large-scale temperate deforestation would induce a small mean global annual warming through the net release of CO₂ into the atmosphere (ranging from $+0.10$ to $+0.40^\circ\text{C}$ with a mean value of $+0.20 \pm 0.13^\circ\text{C}$) (Figure 2.17), whereas there is less agreement on the sign of the mean global annual temperature change resulting from biophysical processes: estimates range from -0.5°C to $+0.18^\circ\text{C}$ with a mean value of $-0.13 \pm 0.22^\circ\text{C}$. There is also *very low agreement* on the mean annual temperature change in the temperate zone ($-0.4 \pm 0.62^\circ\text{C}$; Phillips et al. 2007; Snyder et al. 2004; Longobardi et al. 2016a; Devaraju et al. 2015a, 2018). There is *medium agreement* on a global and latitudinal biophysical warming in response to forestation (Laguë and Swann 2016; Swann et al. 2012; Gibbard et al. 2005; Wang et al. 2014b) (Figure 2.17), but this is based on a smaller number of studies.

The lack of agreement at the annual scale among the climate models is, however, masking *rising agreement* regarding seasonal impacts of deforestation at those latitudes. There is *high agreement* that temperate deforestation leads to summer warming and winter cooling (Bright et al. 2017; Zhao and Jackson 2014; Gálos et al. 2011, 2013; Wickham et al. 2013; Ahlsweide and Thomas 2017; Anderson-Teixeira et al. 2012; Anderson et al. 2011; Chen et al. 2012; Strandberg and Kjellström 2018). The winter cooling is driven by the increased surface albedo, amplified by the snow-albedo feedback. In some models, and when deforestation is simulated for very large areas, the cooling is further amplified by high latitude changes in sea-ice and snow extent (polar amplification). Summer warming occurs because the latent and sensible heat fluxes that take energy out of the surface diminish with the smaller roughness length and lower evapotranspiration efficiency of low vegetation, as compared to tree canopies (Davin and de Noblet-Ducoudre 2010; Anav et al. 2010). Conversely, there is *high agreement* that forestation in North America or in Europe cools surface climate during summer time, especially in regions where water availability can support large evapotranspiration rates. In temperate regions with water deficits, the simulated change in evapotranspiration following forestation will be insignificant, while the decreased surface albedo will favour surface warming.

Observation-based estimates confirm the existence of a seasonal pattern of response to deforestation, with colder winters any time there is snow on the ground and in any place where soils are brighter than the trees, and warmer summers (Schultz et al. 2017; Wickham et al. 2014; Juang et al. 2007; Tang et al. 2018; Peng et al. 2014; Zhang et al. 2014b; Prevedello et al. 2019; Li et al. 2015b; Alkama and Cescatti 2016). In contrast, forestation induces cooler summers wherever trees have access to sufficient soil moisture to transpire. The magnitude of the cooling depends on the wetness of the area of concern (Wickham et al. 2013) as well as on the original and targeted species and varieties implicated in the vegetation conversion (Peng et al. 2014; Juang et al. 2007).

There is also *high confidence* from observation-based estimates that mean annual daytime temperatures are warmer following deforestation, while night-time temperatures are cooler (Schultz et al. 2017; Wickham et al. 2014; Juang et al. 2007; Tang et al. 2018; Prevedello et al. 2019; Peng et al. 2014; Zhang et al. 2014b; Li et al. 2015b; Alkama and Cescatti 2016). Deforestation then increases the amplitude of diurnal temperature variations while forestation reduces it (*high confidence*). Two main reasons have been put forward to explain why nights are warmer in forested areas: their larger capacity to store heat and the existence of a nocturnal temperature inversion bringing warmer air from the higher atmospheric levels down to the surface.

In addition to those seasonal and diurnal fluctuations, Lejeune et al. (2018) found systematic warming of the hottest summer days following historical deforestation in the northern mid-latitudes, and this echoes Strandberg and Kjellström (2018) who argue that the August 2003 and July 2010 heatwaves could have been largely mitigated if Europe had been largely forested.

In a combined modelling of large-scale forestation of western Europe and climate change scenario (SRES A2), Gálos et al. (2013) found relatively small dampening potential of additional forest on ambient air temperature at the end of the 21st century when compared to the beginning (the cooling resulting from land cover changes is -0.5°C whereas the GHG-induced warming exceeds 2.5°C). Influence on rainfall was, however, much larger and significant. Projected annual rainfall decreases following warming were cancelled in Germany and significantly reduced in both France and Ukraine through forestation. In addition, forestation decreased the number of warming-induced dry days but increased the number of extreme precipitation events.

The net impact of forestation, combining both biophysical and biogeochemical effects, has been tested in the warmer world predicted by RCP 8.5 scenario (Sonntag et al. 2016, 2018). The cooling effect from the addition of 8 Mkm^2 of forests following the land use RCP 4.5 scenario was too small (-0.27°C annually) to dampen the RCP 8.5 warming. However, it reached about -1°C in some temperate regions and -2.5°C in boreal ones. This is accompanied by a reduction in the number of extremely warm days.

Global and regional impacts of deforestation/forestation in boreal regions

Consistent with what we have previously discussed for temperate and tropical regions, large-scale boreal deforestation induces a biogeochemical warming of $+0.11 \pm 0.09^{\circ}\text{C}$ (Figure 2.17). But contrary to those other latitudinal bands, the biophysical effect is a consistent cooling across all models ($-0.55 \pm 0.29^{\circ}\text{C}$ when averaged globally). It is also significantly larger than the biogeochemical warming (e.g., Dass et al. (2013), Longobardi et al. (2016a), Devaraju et al. (2015a), Bathiany et al. (2010), Devaraju et al. (2018)) and is driven by the increased albedo, enhanced by the snow-albedo feedback as well as by an increase in sea-ice extent in the Arctic. Over boreal lands, the cooling is as large as $-1.8 \pm 1.2^{\circ}\text{C}$. However, this means that annual cooling masks a seasonal contrast, as discussed in Strandberg and Kjellström (2018) and Gao et al. (2014): during summer time, following the removal of forest, the decreased

evapotranspiration results in a significant summer warming that outweighs the effect of an increased albedo effect.

The same observation-based estimates (as discussed in the previous subsection) show similar patterns for the temperate latitudes: seasonal and daily contrasts. Schultz et al. (2017), however, found that mean annual night-time changes are as large as daytime ones in those regions (mean annual nocturnal cooling of $-1.4 \pm 0.10^{\circ}\text{C}$, balanced by mean annual daytime warming of $1.4 \pm 0.04^{\circ}\text{C}$). This contrasts with both temperate and tropical regions where daytime changes are always larger than the night-time ones.

Arora and Montenegro (2011) combined large-scale forestation and climate change scenario (SRES A2): forestation of either 50% or 100% of the total agricultural area was gradually prescribed between years 2011 and 2060 everywhere. In addition, boreal, temperate and tropical forestation have been tested separately. Both biophysical and biogeochemical effects were accounted for. The net simulated impact of forestation was a cooling varying from -0.04°C to -0.45°C , depending on the location and magnitude of the additional forest cover. It was, however, quite marginal compared to the large global warming resulting from anthropogenic GHG emissions ($+3^{\circ}\text{C}$ at the end of the 21st century). In their experiment, forestation in boreal regions led to biophysical warming and biogeochemical cooling that compensated each other, whereas forestation in the tropics led to both biophysical and biogeochemical cooling. The authors concluded that tropical forestation is three times more effective at cooling down climate than boreal or temperate forestation.

Conclusion

In conclusion, planting trees will always result in capturing more atmospheric CO_2 , and thus will mean annual cooling of the globe (*very high confidence*). At the regional level, however, the magnitude and sign of the local temperature change depends on (i) where forestation occurs, (ii) its magnitude, (iii) the level of warming under which the land cover change is applied, and (iv) the land conversion type. This is because the background climatic conditions (e.g., precipitation and snow regimes, mean annual temperature) within which the land cover changes occur vary across regions (Pitman et al. 2011; Montenegro et al. 2009; Juang et al. 2007; Wickham et al. 2014; Hagos et al. 2014; Voldoire 2006; Feddema et al. 2005; Strandberg and Kjellström 2018). In addition, there is *high confidence* that estimates of the influence of any land cover or land use change on surface temperature from the sole consideration of the albedo and the CO_2 effects is incorrect as changes in turbulent fluxes (i.e., latent and sensible heat fluxes) are large contributors to local temperature change (Bright et al. 2017).

There is *high confidence* that, in boreal and temperate latitudes, the presence of forest cools temperature in warmer locations and seasons (provided that the soil is not dry), whereas it warms temperature in colder locations and seasons (provided the soil is brighter than the trees or covered with snow). In the humid tropics, forestation increases evapotranspiration year-round and thus decreases temperature (*high confidence*). In tropical areas with a strong seasonality of rainfall, forestation will also increase evapotranspiration year-round, unless

Chapter 2

the soil becomes too dry. In all regions there is *medium confidence* that the diurnal temperature range decreases with increasing forest cover, with potentially reduced extreme values of temperature.

Although there is not enough literature yet that rigorously compares both biophysical and biogeochemical effects of realistic scenarios of forestation, there is *high confidence* that, at the local scale (that is where the forest change occurs), biophysical effects on surface temperature are far more important than the effects resulting from the changes in emitted CO₂.

What is lacking in the literature today is an estimate of the impacts that natural disturbances in forests will have on local climates and on the build-up of atmospheric CO₂ (O'Halloran et al. 2012), illustrated with many examples that changes in albedo following disturbances can result in radiative forcing changes opposite to, and as large as, the ones resulting from the associated changes in the net release of CO₂ by land. The resulting climate effects depend on the duration of the perturbation and of the following recovery of vegetation.

2.5.2.2 Impacts of changes in land management

There have been little changes in net cropland area over the past 50 years (at the global scale) compared to continuous changes in land management (Erb et al. 2017). Similarly, in Europe, change in forest management has resulted in a very significant anthropogenic land change. Management affects water, energy and GHG fluxes exchanged between the land and the atmosphere, and thus affects temperature and rainfall, sometimes to the same extent as changes in land cover do (as discussed in Luyssaert et al. (2014)).

The effects of irrigation, which is a practice that has been substantially studied, including one attempt to manage solar radiation via increases in cropland albedo (geoengineering the land) are assessed, along with a discussion of recent findings on the effects of forest management on local climate, although there is not enough literature yet on this topic to carry out a thorough assessment. The effects of urbanisation on climate are assessed in a specific cross-chapter box within this chapter (Cross-Chapter Box 4 in this chapter).

There are a number of other practices that exist whose importance for climate mitigation has been examined (some are reported in Section 2.6 and Chapter 6). There is, however, not enough literature available for assessing their biophysical effect on climate. Few papers are generally found per agricultural practice, for example, Jeong et al. (2014b) for double cropping, Bagley et al. (2017) for the timing of the growing season and Erb et al. (2017) for a review of 10 management practices.

Similarly, there are very few studies that have examined how choosing species varieties and harvesting strategies in forest management impacts on climate through biophysical effects, and how those effects compare to the consequences of the chosen strategies on the net CO₂ sink of the managed forest. The modelling studies highlight the existence of competing effects, for example, between the capacity of certain species to store more carbon than others (thus inducing cooling) while at the same time reducing the total evapotranspiration

Land–climate interactions

loss and absorbing more solar radiation via lower albedo (thus inducing warming) (Naudts et al. 2016a; Luyssaert et al. 2018).

Irrigation

There is substantial literature on the effects of irrigation on local, regional and global climate as this is a major land management issue. There is *very high confidence* that irrigation increases total evapotranspiration, increases the total amount of water vapour in the atmosphere and decreases mean surface daytime temperature within the irrigated area and during the time of irrigation (Bonfils and Lobell 2007; Alter et al. 2015; Chen and Jeong 2018; Christy et al. 2006; Im and Eltahir 2014; Im et al. 2014; Mueller et al. 2015). Decreases in maximum daytime temperature can locally be as large as -3°C to -8°C (Cook et al. 2015; Han and Yang 2013; Huber et al. 2014; Alter et al. 2015; Im et al. 2014). Estimates of the contribution of irrigation to past historical trends in ambient air temperature vary between -0.07°C and -0.014°C/decade in northern China (Han and Yang 2013; Chen and Jeong 2018) while being quite larger in California, USA (-0.14°C to -0.25°C/decade) (Bonfils and Lobell 2007). Surface cooling results from increased energy being taken up from the land via larger evapotranspiration rates. In addition, there is growing evidence from modelling studies that such cooling can locally mitigate the effect of heatwaves (Thiery et al. 2017; Mueller et al. 2015).

There is *no agreement* on changes in night-time temperatures, as discussed in Chen and Jeong (2018) who summarised the findings from observations in many regions of the world (India, China, North America and eastern Africa) (Figure 2.18). Where night-time warming is found (Chen and Jeong 2018; Christy et al. 2006), two explanations are put forward, (i) an increase in incoming longwave radiation in response to increased atmospheric water vapour content (greenhouse effect), and (ii) an increased storage of heat in the soil during daytime. Because of the larger heat capacity of moister soil, heat is then released to the atmosphere at night.

There is *robust evidence* from modelling studies that implementing irrigation enhances rainfall, although there is *very low confidence* on where this increase occurs. When irrigation occurs in Sahelian Africa during the monsoon period, rainfall is decreased over irrigated areas (*high agreement*), increased in the southwest if the crops are located in western Africa (Alter et al. 2015) and increased in the east/northeast when crops are located further east in Sudan (Im and Eltahir 2014; Im et al. 2014) The cooler irrigated surfaces in the Sahel, because of their greater evapotranspiration, inhibit convection and create an anomalous descending motion over crops that suppresses rainfall but influences the circulation of monsoon winds. Irrigation in India occurs prior to the start of the monsoon season and the resulting land cooling decreases the land-sea temperature contrast. This can delay the onset of the Indian monsoon and decrease its intensity (Niyogi et al. 2010; Guimbretie et al. 2012). Results from a modelling study by De Vrese et al. (2016) suggest that part of the excess rainfall triggered by Indian irrigation falls westward, in the horn of Africa. The theory behind those local and downwind changes in rainfall support the findings from the models, but we do not yet have sufficient literature to robustly assess the magnitude and exact location of the expected changes driven by irrigation.

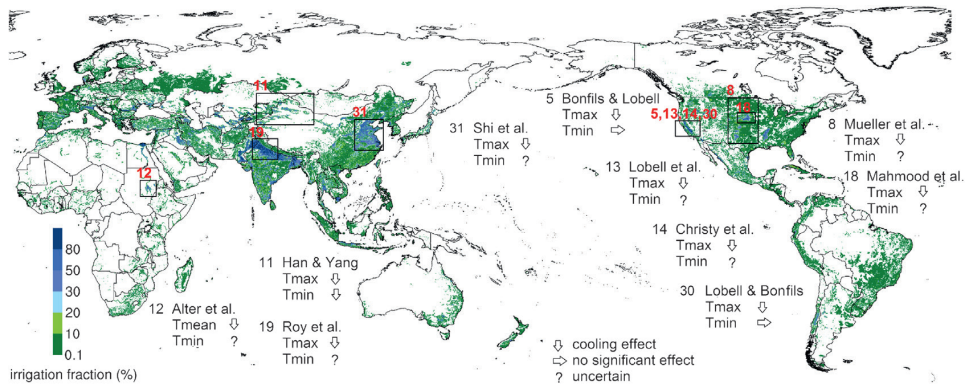


Figure 2.18 | Global map of areas equipped for irrigation (colours), expressed as a percentage of total area, or irrigation fraction. Source: Siebert et al. (2013). Numbered boxes show regions where irrigation causes cooling (down arrow) of surface mean (T_{mean}), maximum (T_{max}) or minimum (T_{min}) temperature, or else no significant effect (right arrow) or where the effect is uncertain (question mark), based on observational studies as reviewed in Chen and Jeong (2018). T_{max} refers to the warmest daily temperature while T_{min} to the coldest one, which generally occurs at night (Alter et al. 2015; Han and Yang 2013; Roy et al. 2007; Shi et al. 2013; Bonfils and Lobell 2007; Lobell et al. 2008; Lobell and Bonfils 2008; Christy et al. 2006; Mahmood et al. 2006; Mueller et al. 2015).

2

Cropland albedo

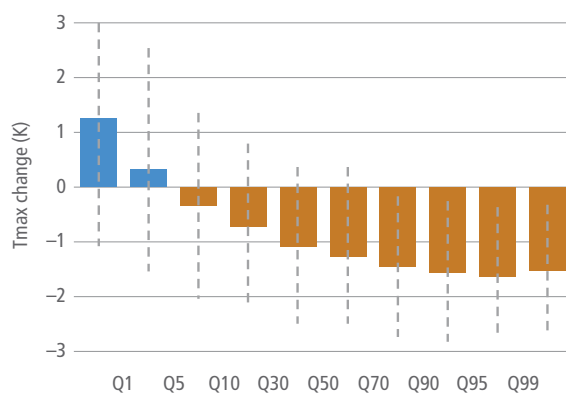
Various methods have been proposed to increase surface albedo in cropland and thus reduce local surface temperature (*high confidence*): choose 'brighter' crop varieties (Ridgwell et al. 2009; Crook et al. 2015; Hirsch et al. 2017; Singarayer et al. 2009; Singarayer and Davies-Barnard 2012), abandon tillage (Lobell et al. 2006; Davin et al. 2014), include cover crops into rotation in areas where soils are darker than vegetation (Carrer et al. 2018; Kaye and Quemada 2017) or use greenhouses (as in Campra et al. (2008)). See Seneviratne et al. (2018) for a review.

Whatever the solution chosen, the induced reduction in absorbed solar radiation cools the land – more specifically during the hottest summer days (*low confidence*) (Davin et al. 2014; Wilhelm et al. 2015;

Figure 2.19. Changes in temperature are essentially local and seasonal (limited to crop growth season) or sub-seasonal (when resulting from inclusion of cover crop or tillage suppression). Such management action on incoming solar radiation thus holds the potential to counteract warming in cultivated areas during crop growing season.

Introducing cover crops into a rotation can also have a warming effect in areas where vegetation has a darker albedo than soil, or in winter during snow periods if the cover crops or their residues are tall enough to overtop the snow cover (Kaye and Quemada 2017; Lombardozzi et al. 2018). In addition, evapotranspiration greater than that of bare soil during this transitional period reduces soil temperature (Ceschia et al. 2017). Such management strategy can have another substantial mitigation effect as it allows carbon to be stored in the soil and to reduce both direct and indirect N_2O

A Albedo effect – southern Europe



B Albedo effect – northern Europe

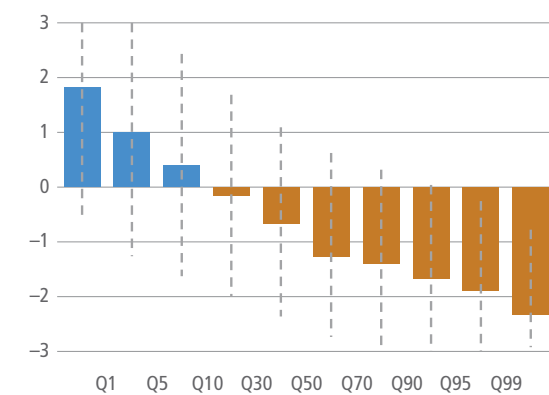


Figure 2.19 | Change in summer (July–August) daily maximum temperature (°C) resulting from increased surface albedo in unploughed versus ploughed land, in (A) southern, and (B) northern Europe, during the period 1986–2009. Changes are simulated for different quantiles of the daily maximum temperature distribution, where Q1 represents the coolest 1% and Q99 the warmest 1% of summer days. Only grid cells with more than 60% of their area in cropland are included. The dashed bars represent the standard deviation calculated across all days and grid points. Southern Europe refers to Europe below 45°N, and northern Europe refers to Europe above 45°N (Davin et al. 2014).

emissions (Basche et al. 2014; Kaye and Quemada 2017), in particular if fertilisation of the subsequent crop is reduced (Constantin et al. 2010, 2011). The use of cover crops thus substantially improves the GHG budget of croplands (Kaye and Quemada 2017; Tribouillois et al. 2018). More discussion on the role of management practices for mitigation can be found in Section 2.6 and Chapter 6.

Only a handful of modelling studies have looked at effects other than changes in atmospheric temperature in response to increased cropland albedo. Seneviratne et al. (2018) have found significant changes in rainfall following an idealised increase in cropland albedo, especially within the Asian monsoon regions. The benefits of cooler temperature on production, resulting from increased albedo, is cancelled out by decreases in rainfall that are harmful for crop productivity. The rarity of a concomitant evaluation of albedo management impact on crop productivity prevents us from providing a robust assessment of this practice in terms of both climate mitigation and food security.

2.5.3 Amplifying/dampening climate changes via land responses

Section 2.1 and Box 2.1 illustrate the various ways through which land can affect the atmosphere and thereby climate and weather. Section 2.2 illustrates the many impacts that climate changes have on the functioning of land ecosystems. Section 2.3 discusses the effects that future climatic conditions have on the capacity of the land to absorb anthropogenic CO₂, which then controls the sign

of the feedback to the initial global warming. Sections 2.5.1 and 2.5.2 show the effects of changes in anthropogenic land cover or land management on climate variables or processes. Therefore, land has the potential to dampen or amplify the GHG-induced global climate warming, or can be used as a tool to mitigate regional climatic consequences of global warming such as extreme weather events, in addition to increasing the capacity of land to absorb CO₂ (Figure 2.20).

Land-to-climate feedbacks are difficult to assess with global or regional climate models, as both types of models generally omit a large number of processes. Among these are (i) the response of vegetation to climate change in terms of growth, productivity, and geographical distribution, (ii) the dynamics of major disturbances such as fires, (iii) the nutrients dynamics, and (iv) the dynamics and effects of short-lived chemical tracers such as biogenic volatile organic compounds (Section 2.4). Therefore, only those processes that are fully accounted for in climate models are considered here.

2.5.3.1 Effects of changes in land cover and productivity resulting from global warming

In boreal regions, the combined northward migration of the treeline and increased growing season length in response to increased temperatures in those regions (Section 2.2) will have positive feedbacks both on global and regional annual warming (*high confidence*) (Garnaud and Sushama 2015; Jeong et al. 2014a; O’ishi and Abe-Ouchi 2009; Port et al. 2012; Strengers et al. 2010). The warming resulting from the decreased surface albedo remains

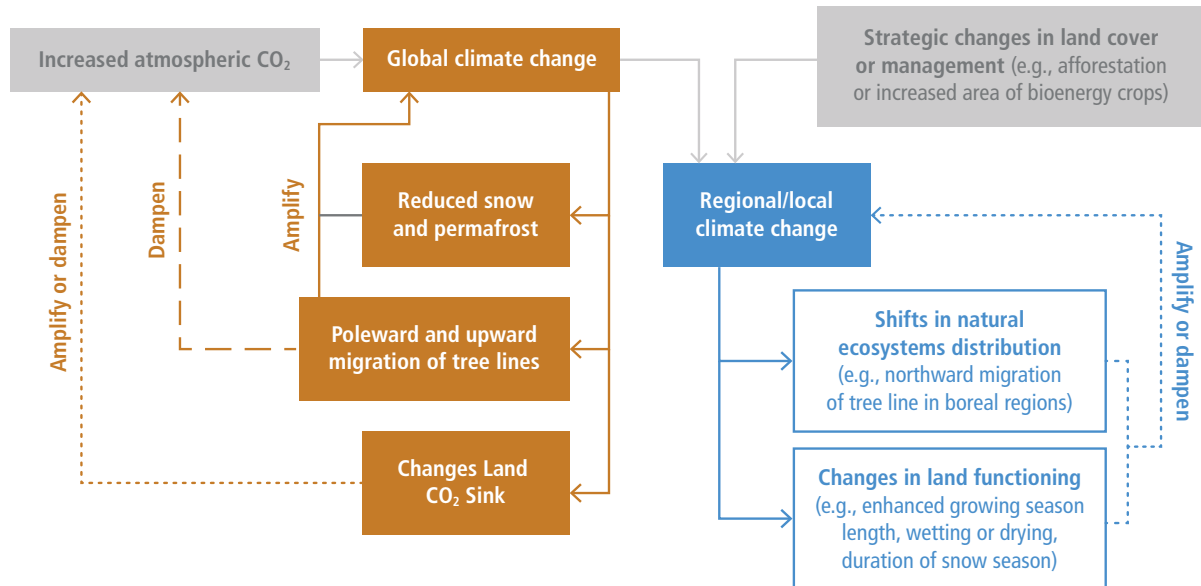


Figure 2.20 | Schematics of the various ways land has been shown in the literature to either amplify or dampen the initial GHG-induced climatic change. Brown arrows and boxes represent the global scale and blue arrows and boxes represent the regional/local level. Grey arrows and boxes refer to what we consider herein as imposed changes – that is, the initial atmospheric GHG content as well as anthropogenic land cover change and land management. Dampening feedbacks are represented with dashed lines, amplifying ones with solid lines and feedbacks where the direction may be variable are represented using dotted lines. The feedbacks initiated by changes in snow and permafrost areas in boreal regions are discussed in Section 2.5.3.2, the ones initiated by changes in ecosystem distribution are discussed in Sections 2.5.3.1, 2.5.1 and 2.5.2, and the feedbacks related to changes in the land functioning are discussed in Sections 2.5.3.3 and 2.5.1, as well as in Sections 2.3 and 2.5 (for changes in net CO₂ fluxes). References supporting this figure can be found in each of those sections.

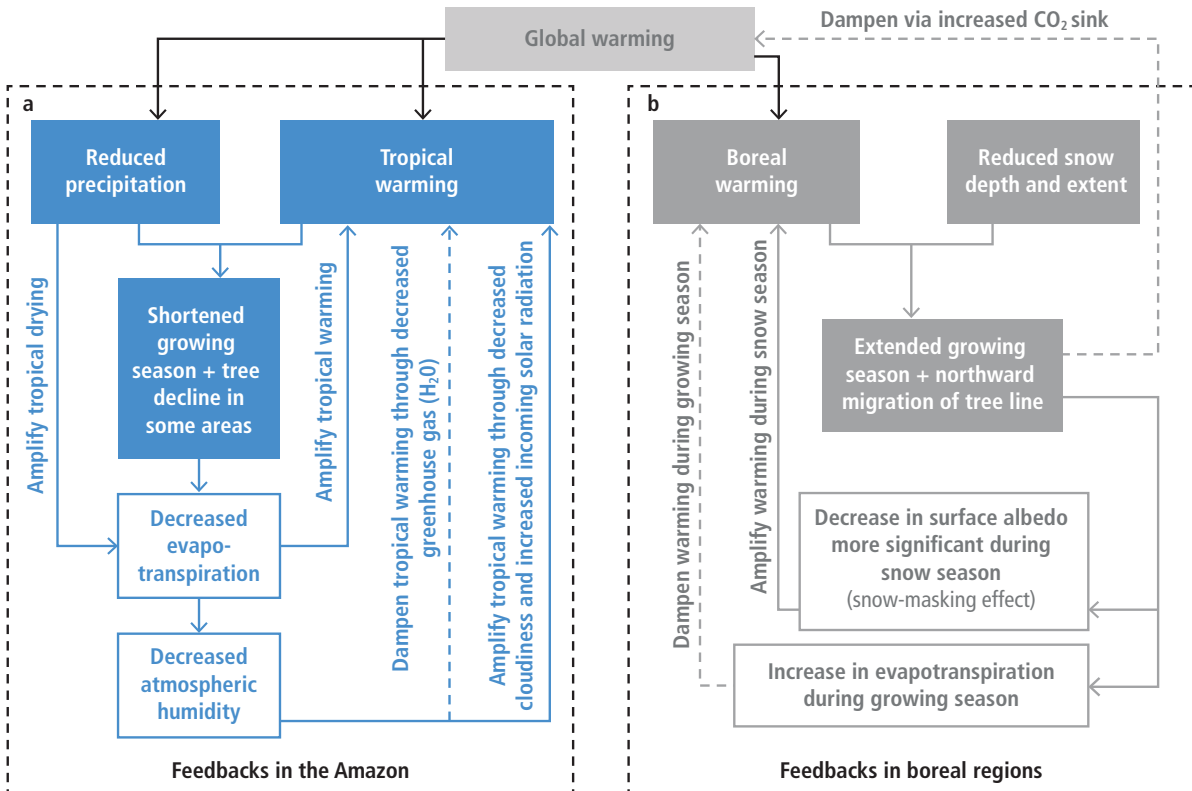


Figure 2.21 | Schematic illustration of the processes through which the effects of global warming in (a) the Amazon (blue arrows and boxes), and (b) boreal regions (grey arrows and boxes) feedback on the regional climate change. In boreal regions, the sign of the feedbacks depends on the season, although annually global warming is further enhanced in those regions. Dashed lines illustrate negative feedbacks, while solid lines indicate positive feedbacks. References supporting this figure can be found in the text.

the dominant signal in all modelling studies at the annual timescale and during the snow season, while cooling is obtained during the growing season (Section 2.5.2.1 and Figure 2.21, right panel).

In the tropics, climate change will cause both greening and browning (Section 2.2). Where global warming provokes a decrease in rainfall, the induced decrease in biomass production leads to increased local warming (*high confidence*) (Port et al. 2012; Wu et al. 2016; Yu et al. 2016). The reverse is true where warming generates increases in rainfall and thus greening. As an example, Port et al. (2012) simulated decreases in tree cover and shortened growing season in the Amazon, despite the CO_2 fertilisation effects, in response to both future tropical warming and reduced precipitation (Figure 2.21, left panel). This browning of the land decreases both evapotranspiration and atmospheric humidity. The warming driven by the drop in evapotranspiration is enhanced via a decrease in cloudiness, increasing solar radiation, and is damped by reduced water vapour greenhouse radiation.

There is *very low confidence* on how feedbacks affect rainfall in the tropics where vegetation changes may occur, as the sign of the change in precipitation depends on where the greening occurs and on the season (as discussed in Section 2.5.2). There is, however, *high confidence* that increased vegetation growth in the southern Sahel increases African monsoon rains (Yu et al. 2016; Port et al. 2012;

Wu et al. 2016). Confidence on the direction of such feedbacks is also based on a significant number of paleoclimate studies that analysed how vegetation dynamics helped maintain a northward position of the African monsoon during the Holocene time period (9–6 kyr BP) (de Noblet-Ducoudré et al. 2000; Rachmayani et al. 2015).

2.5.3.2 Feedbacks to climate from high-latitude land-surface changes

In high latitudes, snow albedo and permafrost carbon feedbacks are the most well-known and most important surface-related climate feedbacks because of their large-scale impacts.

In response to ongoing and projected decrease in seasonal snow cover (Derksen and Brown 2012; Brutel-Vuilmet et al. 2013) warming is, and will continue to be, enhanced in boreal regions (*high confidence*) (Brutel-Vuilmet et al. 2013; Perket et al. 2014; Thackeray and Fletcher 2015; Mudryk et al. 2017). One reason for this is the large reflectivity (albedo) the snow exerts on shortwave radiative forcing: the all-sky global land snow shortwave radiative effect is evaluated to be around $-2.5 \pm 0.5 \text{ W m}^{-2}$ (Flanner et al. 2011; Singh et al. 2015). In the southern hemisphere, perennial snow on the Antarctic is the dominant contribution, while in the northern hemisphere, this is essentially attributable to seasonal snow, with a smaller contribution

from snow on glaciated areas. Another reason is the sensitivity of snow cover to temperature: Mudryk et al. (2017) recently showed that, in the high latitudes, climate models tend to correctly represent this sensitivity, while in mid-latitude and alpine regions, the simulated snow cover sensitivity to temperature variations tends to be biased low. In total, the global snow albedo feedback is about $0.1 \text{ W m}^{-2} \text{ K}^{-1}$, which amounts to about 7% of the strength of the globally dominant water vapour feedback (e.g., Thackeray and Fletcher (2015)). While climate models do represent this feedback, a persistent spread in the modelled feedback strength has been noticed (Qu and Hall 2014) and, on average, the simulated snow albedo feedback strength tends to be somewhat weaker than in reality (*medium confidence*) (Flanner et al. 2011; Thackeray and Fletcher 2015). Various reasons for the spread and biases of the simulated snow albedo feedback have been identified, notably inadequate representations of vegetation masking snow in forested areas (Loranty et al. 2014; Wang et al. 2016c; Thackeray and Fletcher 2015).

The second most important potential feedback from land to climate relates to permafrost decay. There is *high confidence* that, following permafrost decay from a warming climate, the resulting emissions of CO_2 and/or CH_4 (caused by the decomposition of organic matter in previously frozen soil) will produce additional GHG-induced warming. There is, however, substantial uncertainty on the magnitude of this feedback, although recent years have seen large progress in its quantification. Lack of agreement results from several critical factors that carry large uncertainties. The most important are (i) the size of the permafrost carbon pool, (ii) its decomposability, (iii) the magnitude, timing and pathway of future high-latitude climate change, and (iv) the correct identification and model representation of the processes at play (Schuur et al. 2015). The most recent comprehensive estimates establish a total soil organic carbon storage in permafrost of about $1500 \pm 200 \text{ PgC}$ (Hugelius et al. 2014, 2013; Olefeldt et al. 2016), which is about 300 Pg C lower than previous estimates (*low confidence*). Important progress has been made in recent years at incorporating permafrost-related processes in complex ESMs (e.g., McGuire et al. (2018)), but representations of some critical processes such as thermokarst formation are still in their infancy (Schuur et al. 2015). Recent model-based estimates of future permafrost carbon release (Koven et al. 2015; McGuire et al. 2018) have converged on an important insight. Their results suggest that substantial net carbon release of the coupled vegetation-permafrost system will probably not occur before about 2100 because carbon uptake by increased vegetation growth will initially compensate for GHG releases from permafrost (*limited evidence, high agreement*).

2.5.3.3 Feedbacks related to changes in soil moisture resulting from global warming

There is *medium evidence* but *high agreement* that soil moisture conditions influence the frequency and magnitude of extremes such as drought and heatwaves. Observational evidence indicates that dry soil moisture conditions favour heatwaves, in particular in regions where evapotranspiration is limited by moisture availability (Mueller and Seneviratne 2012; Quesada et al. 2012; Miralles et al. 2018; Geirinhas et al. 2018; Miralles et al. 2014; Chiang et al. 2018; Dong and Crow 2019; Hirschi et al. 2014).

In future climate projections, soil moisture plays an important role in the projected amplification of extreme heatwaves and drought in many regions of the world (*medium confidence*) (Seneviratne et al. 2013; Vogel et al. 2017; Donat et al. 2018; Miralles et al. 2018). In addition, the areas where soil moisture affects heat extremes will not be located exactly where they are today. Changes in rainfall, temperature, and thus in evapotranspiration, will induce changes in soil moisture and therefore where temperature and latent heat flux will be negatively coupled (Seneviratne et al. 2006; Fischer et al. 2012). Quantitative estimates of the actual role of soil moisture feedbacks are, however, very uncertain due to the *low confidence* in projected soil moisture changes (IPCC 2013a), to weaknesses in the representation of soil moisture–atmosphere interactions in climate models (Sippel et al. 2017; Ukkola et al. 2018; Donat et al. 2018; Miralles et al. 2018) and to methodological uncertainties associated with the soil moisture prescription framework commonly used to disentangle the effect of soil moisture on changes in temperature extremes (Hauser et al. 2017).

Where soil moisture is predicted to decrease in response to climate change in the subtropics and temperate latitudes, this drying could be enhanced by the existence of soil moisture feedbacks (*low confidence*) (Berg et al. 2016). The initial decrease in precipitation and increase in potential evapotranspiration and latent heat flux, in response to global climate change, leads to decreased soil moisture at those latitudes and can potentially amplify both. Such a feature is consistent with evidence that, in a warmer climate, land and atmosphere will be more strongly coupled via both the water and energy cycles (Dirmeyer et al. 2014; Guo et al. 2006). This increased sensitivity of atmospheric response to land perturbations implies that changes in land uses and cover are expected to have more impact on climate in the future than they do today.

Beyond temperature, it has been suggested that soil moisture feedbacks influence precipitation occurrence and intensity. But the importance, and even the sign of this feedback, is still largely uncertain and debated (Tuttle and Salvucci 2016; Yang et al. 2018; Froidevaux et al. 2014; Guillod et al. 2015).

2.5.4 Non-local and downwind effects resulting from changes in land cover

Changes in land cover or land management do not just have local consequences but also affect adjacent or more remote areas. Those non-local impacts may occur in three different ways.

1. Any action on land that affects photosynthesis and respiration has an impact on the atmospheric CO_2 content as this GHG is well mixed in the atmosphere. In turn, this change affects the downwelling longwave radiation everywhere on the planet and contributes to global climate change. This is more thoroughly discussed in Section 2.6 where various land-based mitigation solutions are examined. Local land use changes thus have the potential to affect the global climate via changes in atmospheric CO_2 .
2. Any change in land cover or land management may impact on local surface air temperature and moisture, and thus sea-level pressure. Thermal, moisture and surface pressure gradients

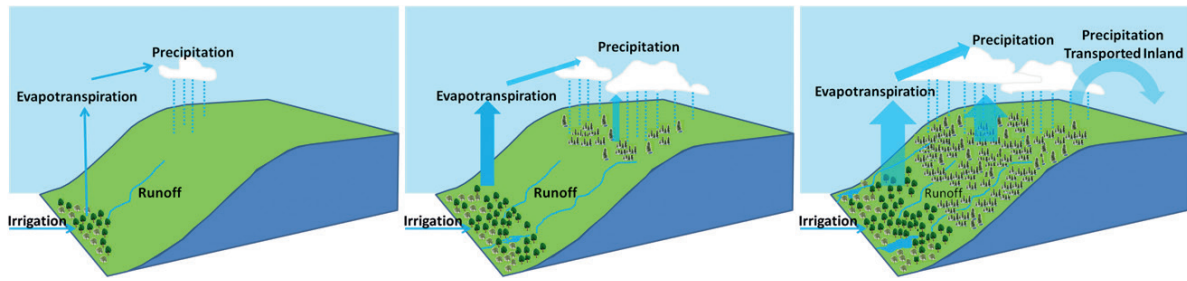


Figure 2.22 | Schematic illustration of how combined forestation and irrigation can influence downwind precipitation on mountainous areas, favour vegetation growth and feed back to the forested area via increased runoff. Showing Los Angeles, California (Layton and Ellison 2016). Areas of forest plantations and irrigation are located on the left panel, whereas consequent downwind effects and feedbacks are illustrated in the middle and right panels.

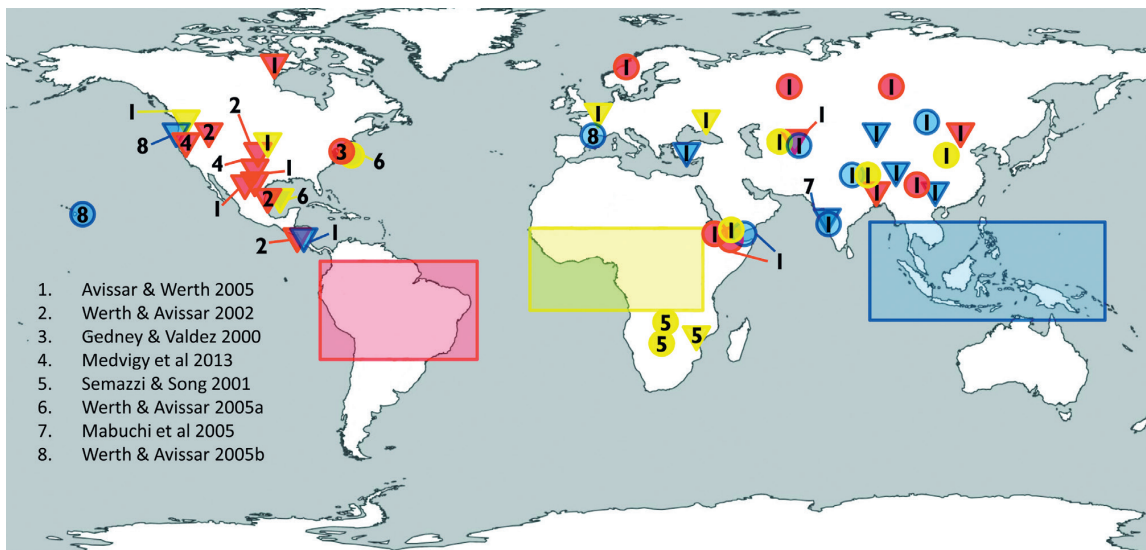


Figure 2.23 | Extra-tropical effects on precipitation due to deforestation in each of the three major tropical regions. Increasing (circles) and decreasing (triangles) precipitation result from complete deforestation of either Amazonia (red), Africa (yellow) or Southeast Asia (blue) as reviewed by Lawrence and Vandcar (2015). Boxes indicate the area where tropical forest was removed in each region. Numbers refer to the study the data were derived from (Avissar and Werth 2005; Gedney and Valdes 2000; Semazzi and Song 2001; Werth 2002; Mabuchi et al. 2005; Werth 2005).

between the area of change and neighbouring areas are then modified and affect the amount of heat, water vapour and pollutants flowing out (downwind) of the area (e.g., Ma et al. (2013b), McLeod et al. (2017), Abiodun et al. (2012), Keys (2012)). Forests, for example, provide water vapour to the atmosphere which supports terrestrial precipitation downwind (Ellison et al. 2017; Layton and Ellison 2016; Spracklen et al. 2012, 2018). Within a few days, water vapour can travel several hundred kilometres before being condensed into rain and potentially being transpired again (Makarieva et al. 2009). This cascading moisture recycling (succession of evapotranspiration, water vapour transport and condensation-rainfall) has been observed in South America (Spracklen et al. 2018; Zemp et al. 2014; Staal et al. 2018; Spracklen et al. 2012). Deforestation can thus potentially decrease rainfall downwind, while combining 'small-scale' forestation and irrigation, which in the semi-arid region is susceptible to boost the precipitation-recycling mechanism with

better vegetation growth downwind (Ellison et al. 2017; Layton and Ellison, 2016) (Figure 2.22).

3. Many studies using global climate models have reported that the climatic changes resulting from changes in land are not limited to the lower part of the atmosphere, but can reach the upper levels via changes in large-scale ascent (convection) or descent (subsidence) of air. This coupling to the upper atmosphere triggers perturbations in large-scale atmospheric transport (of heat, energy and water) and subsequent changes in temperature and rainfall in regions located quite far away from the original perturbation (Laguë and Swann 2016; Feddema et al. 2005, Badger and Dirmeyer 2016; Garcia 2016; Stark 2015; Devaraju 2018; Quesada et al. 2017a) (Figure 2.23).

De Vreese et al. (2016) for example, using a global climate model, found that irrigation in India could affect regions as remote as eastern

Africa through changes in the atmospheric transport of water vapour. At the onset of boreal spring (February to March) evapotranspiration is already large over irrigated crops and the resulting excess moisture in the atmosphere is transported southwestward by low-level winds. This results in increases in precipitation as large as 1 mm d^{-1} in the Horn of Africa. Such a finding implies that, if irrigation is to decrease in India, rainfall can decrease in eastern Africa where the consequences of drought are already disastrous.

Changes in sea-surface temperature have also been simulated in response to large-scale vegetation changes (Cowling et al. 2009; Davin and de Noblet-Ducoudré 2010; Wang et al. 2014b; Notaro Liu 2007). Most of those modelling studies have been carried out with land

cover changes that are extremely large and often exaggerated with respect to reality. The existence of such teleconnections can thus be biased, as discussed in Lorenz et al. (2016).

In conclusion, there is *high confidence* that any action on land (for example, to dampen global warming effects), wherever they occur, will not only have effects on local climate but also generate atmospheric changes in neighbouring regions, and potentially as far as hundreds of kilometres downwind. More remote teleconnections, thousands of kilometres away from the initial perturbation, are impossible to observe and have only been reported by modelling studies using extreme land cover changes. There is *very low confidence* that detectable changes due to such long-range processes can occur.

Cross-Chapter Box 4 | Climate change and urbanisation

Nathalie de Noblet-Ducoudré (France), Peng Cai (China), Sarah Connors (France/United Kingdom), Martin Dallimer (United Kingdom), Jason Evans (Australia), Rafiq Hamdi (Belgium), Gensuo Jia (China), Kaoru Kitajima (Japan), Christopher Lennard (South Africa), Shuaib Lwasa (Uganda), Carlos Fernando Mena (Ecuador), Soojeong Myeong (Republic of Korea), Lennart Olsson (Sweden), Prajal Pradhan (Nepal/Germany), Lindsay Stringer (United Kingdom)

Cities extent, population, and expected growth

Despite only covering 0.4–0.9% of the global land surface (Esch et al. 2017; Zhou et al. 2015), over half the world's population live in towns and cities (United Nations, 2017) generating around three-quarters of the global total carbon emissions from energy use (Creutzig et al. 2015b; Seto et al. 2014). Urban food consumption is a large source of these anthropogenic GHG emissions (Goldstein et al. 2017). In developed countries, per capita emissions are larger in small cities than bigger ones, while the opposite is found in developing countries (Gudipudi et al. 2019). Climate change is expected to increase the energy demand of people living in urban areas (Santamouris et al. 2015; Wenz et al. 2017).

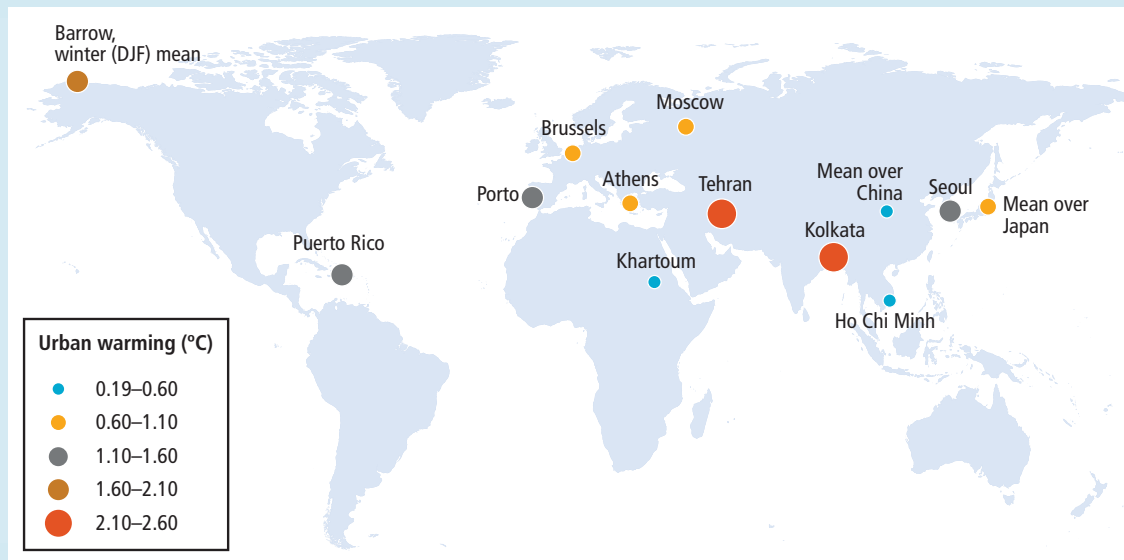
In addition to being a driver of emissions, urbanisation contributes to forest degradation, converts neighbouring agricultural, forested or otherwise undeveloped land to urban use, altering natural or semi-natural ecosystems both within and outside of urban areas (Du and Huang 2017). It has been identified as a major driver of land degradation, as illustrated in Chapters 3, 4 and 5. Highly productive lands are experiencing the highest rate of conversion to urbanised landscapes (Nizeyimana et al. 2001; Pandey et al. 2018), affecting food security. Loss of agricultural land and increased pollution and waste are some of key challenges arising from urbanisation and urban growth (Chen 2007). The proportion of urban population is predicted to reach about 70% by the middle of the century (United Nations 2017) with growth especially taking place in the developing world (Angel et al. 2011; Dahiya 2012). Urban sprawl is projected to consume 1.8–2.4% and 5% of the current cultivated land by 2030 and 2050, respectively (Pradhan et al. 2014; Bren d'Amour et al. 2016), driven by both general population increase and immigration from rural areas (Adger et al. 2015; Seto et al. 2011; Geddes et al. 2012). New city dwellers in developing countries will require land for housing to be converted from non-urban to urban land (Barbero-Sierra et al. 2013), indicating future degradation. These growing urban areas will experience direct and indirect climate change impacts, such as sea level rise and storm surges (Boettle et al. 2016; Revi et al. 2014), increasing soil salinity and landslides from precipitation extremes. Furthermore, poorly planned urbanisation can increase people's risk to climate hazards as informal settlements and poorly built infrastructure are often the most exposed to hazards from fire, flooding and landslides (Adger et al. 2015; Geddes et al. 2012; Revi et al. 2014). Currently, avoiding land degradation and maintaining/enhancing ecosystem services are rarely considered in planning processes (Kuang et al. 2017).

Climate change, urban heat island and threats specific to urban populations

Cities alter the local atmospheric conditions as well as those of the surrounding areas (Wang et al. 2016b; Zhong et al. 2017). There is *high confidence* that urbanisation increases mean annual surface air temperature in cities and in their surroundings, with increases ranging from $0.19\text{--}2.60^\circ\text{C}$ (Torres-Valcárcel et al. 2015; Li et al. 2018a; Doan et al. 2016) (Cross-Chapter Box 4; Figure 1). This phenomenon is referred to as the urban heat island (UHI) effect (Oke et al. 2017; Bader et al. 2018). The magnitude and diurnal amplitude of the UHI varies from one city to another and depends on the local background climate (Wienert and Kuttler 2005; Zhao et al. 2014; Ward et al. 2016). There is nevertheless *high confidence* that urbanisation affects night-time temperatures more substantially than daytime ones (Argüeso et al. 2014; Alghamdi and Moore 2015; Alizadeh-Choobari et al. 2016; Fujibe, 2009; Hausfather et al. 2013; Liao et al. 2017; Sachindra et al. 2016; Camilloni and Barrucand 2012; Wang et al. 2017a; Hamdi, 2010;

Cross-Chapter Box 4 (continued)

Arsiso et al. 2018; Elagib 2011; Lokoshchenko 2017; Robaa 2013). In addition, there is *high confidence* that the UHI effect makes heatwaves more intense in cities by 1.22–4°C, particularly at night (Li and Bou-Zeid 2013; Li et al. 2017b; Hamdi et al. 2016; Founda and Santamouris 2017; Wang et al. 2017a). As there is a well-established relationship between extremely high temperatures and morbidity, mortality (Watts et al. 2015) and labour productivity (Costa et al. 2016), an expected increase in extreme heat events with future climate change will worsen the conditions in cities.



Cross-Chapter Box 4, Figure 1 | Change in annual mean surface air temperature resulting from urbanisation (°C). The colour and size of the circles refer to the magnitude of the change. (This map has been compiled using the following studies: Kim et al. (2016), Sun et al. (2016), Chen et al. (2016a), Founda et al. (2015), Rafael et al. (2017), Hinkel and Nelson (2007), Chrysanthou et al. (2014), Dou et al. (2014), Zhou et al. (2016), (2017), Polydoros et al. (2018), Li et al. (2018a), Bader et al. (2018), Alizadeh-Choobari et al. (2016), Fujibe (2009), Lokoshchenko (2017), Torres-Valcárcel et al. (2015), Doan et al. (2016), Elagib (2011), Liao et al. (2017)).

Individual city case studies show that precipitation mean and extremes are increased over and downwind of urban areas, especially in the afternoon and early evening when convective rise of the atmosphere is the strongest (*medium confidence*). The case studies covered: different inland and coastal US cities (Haberlie et al. 2014; McLeod et al. 2017; Ganeshan and Murtugudde 2015), Dutch coastal cities (Daniels et al. 2016), Hamburg (Schlünen et al. 2010), Shanghai (Liang and Ding 2017), Beijing (Dou et al. 2014), and Jakarta and Kuala Lumpur (Lorenz et al. 2016). Increased aerosol concentrations, however, can interrupt the precipitation formation process and thereby reduce heavy rainfall (Daniels et al. 2016; Zhong et al. 2017). Urban areas also experience altered water cycle in other aspects: the evaporative demand for plants in cities are increased by as much as 10% (Zipper et al. 2017), while the high proportion of paving in cities means that surface runoff of water is high (Hamdi et al. 2011; Pataki et al. 2011). In addition, water retention is lower in degraded, sealed soils beneath urban surfaces compared to intact soils. Increased surface water runoff, especially when and where the rainfall intensity is likely to intensify (IPCC 2013a), leads to a greater likelihood of flooding in urban areas without implementation of adaptation measures (Shade and Kremer 2019; Wang et al. 2013; EPA 2015).

Urbanisation alters the stock size of soil organic carbon (SOC) and its stability. The conversion of vegetated land to urban land results in a loss of carbon stored in plants, while stresses associated with the urban environment (e.g., heat, limited water availability, pollution) reduce plant growth and survival in cities (Xu et al. 2016b). Overall, carbon densities or stocks decrease from natural land areas to the urban core along the rural-urban gradient (Tao et al. 2015; Zhang et al. 2015). For example, the Seoul Forest Park, an urban park, shows a tenfold difference in SOC stocks across its land cover types (Bae and Ryu 2015). In Changchun in Northeast China, however, SOC density is higher in recreational forests within urban areas compared to a production forest (Zhang et al. 2015).

Urban air pollution as an environmental risk increases with climate change. Increased air temperatures can lead to reduced air quality by enhancing the formation of photochemical oxidants and increasing the concentration of air pollutants such as ozone, with corresponding threats to human health (Sharma et al. 2013). The occurrence of bronchial asthma and allergic respiratory diseases is increasing worldwide, and urban residents are experiencing poor air quality conditions more frequently than rural residents

Cross-Chapter Box 4 (continued)

(D'Amato et al. 2010). Excess morbidity and mortality related to extremely poor air quality are found in many cities worldwide (Harlan and Ruddell 2011). Some emissions that lead to reduced air quality are also contributors to climate change (Shindell et al. 2018; de Coninck et al. 2018).

Urban response options for climate change, desertification, land degradation and food security

Urban green infrastructure (UGI) has been proposed as a solution to mitigate climate change directly through carbon sequestration (Davies et al. 2011; Edmondson et al. 2014). However, compared to overall carbon emissions from cities, its mitigation effects are likely to be small (*medium confidence*). UGI nevertheless has an important role in adapting cities to climate change (Demuzere et al. 2014; Sussams et al. 2015; Elmqvist et al. 2016; Gill et al. 2007; Revi et al. 2014). Adaptation through UGIs is achieved through, for example, (i) reduction in air temperature (Cavan et al. 2014; Di Leo et al. 2016; Feyisa et al. 2014; Zöllch et al. 2016; Li et al. 2019) which can help improve human health and comfort (e.g., Brown and Nicholls 2015; Klemm et al. 2015), (ii) reduction in the energy demands of buildings through the use of green roofs and walls (e.g., Coma et al. 2017), and (iii) reduction in surface water runoff and flood risk (Zeleňáková et al. 2017). Given that UGI necessarily involves the retention and management of non-sealed surfaces, co-benefits for land degradation will also be apparent (*limited evidence, high agreement*) (Murata and Kawai 2018; Scalenghe and Marsan 2009).

Urban agriculture is one aspect of UGI that has the potential to both meet some of the food needs of cities and reduce land degradation pressures in rural areas (*low confidence*) (e.g., Wilhelm and Smith (2018)). Urban agriculture has many forms, such as backyard gardening, allotments, plants on rooftops or balconies, urban-fringe/peri-urban agriculture, hydroponics, aquaponics, livestock grazing in open spaces and vertical farming (Gerster-Bentaya 2013) (Section 5.6.5).

Consuming locally produced food and enhancing the efficiency of food processing and transportation can minimise food losses, contribute to food security and, in some circumstances, reduce GHG emissions (Brodt et al. 2013; Michalský and Hooda 2015; Tobarra et al. 2018) (Section 5.5.2.3). Furthermore, urban agriculture has the potential to counteract the separation of urban populations from food production. This separation is one driver of the transition towards more homogeneous, high-protein diets, which are associated with increased GHG emissions (Goldstein et al. 2017; Moragues-Faus and Marceau 2018; Magarini and Calori 2015). Barriers to the uptake of urban agriculture as a climate change mitigation option include the need for efficient distribution systems to ensure lowered carbon emissions (Newman et al. 2012) and the concern that urban agriculture may harbour pathogenic diseases, or that its products be contaminated by soil or air pollution (Hamilton et al. 2014; Ercilla-Montserrat et al. 2018).

In summary

Climate change is already affecting the health and energy demand of large numbers of people living in urban areas (*high confidence*) (Section 2.2). Future changes to both climate and urbanisation will enhance warming in cities and their surroundings, especially during heatwaves (*high confidence*). Urban and peri-urban agriculture and, more generally, the implementation of urban green infrastructure, can contribute to climate change mitigation (*medium confidence*) as well as to adaptation (*high confidence*), including co-benefits for food security and reduced soil-water-air pollution.

2.6 Climate consequences of response options

Response options can affect climate mitigation and adaptation simultaneously, therefore this Special Report on Climate Change and Land (SRCCL) discusses land-based response options in an integrated way (Chapter 1). In this chapter, we assess response options that have an effect on climate. A description of the full set of response options across the SRCCL can be found in Chapter 6, including the interplay between mitigation, adaptation, desertification, land degradation, food security and other co-benefits and trade-offs. Response options specific to desertification, degradation and food security are described in more detail in Chapters 3, 4 and 5.

Some response options lead to land use change and can compete with other land uses, including other response options, while others may free-up land that can be used for further mitigation/adaptation by reducing demand for land or products (e.g., agricultural intensification, diet shifts and reduction of waste) (*high confidence*).

Some response options result in a net removal of GHGs from the atmosphere and storage in living or dead organic material, or in geological stores (IPCC SR15). Such options are frequently referred to in the literature as CO₂ removal (CDR), greenhouse gas removal (GGR) or negative emissions technologies (NETs). CDR options are assessed alongside emissions reduction options. Although they have a land footprint, solar and wind farms are not assessed here as they affect GHG flux in the energy industrial sectors with minimal effect in the land sector, but the impact of solar farms on agricultural land competition is dealt with in Chapter 7.

A number of different types of scenario approach exist for estimating climate contribution of land-based response options (Cross-Chapter Box 1 and Chapter 1). Mitigation potentials have been estimated for single and sometimes multiple response options using stylised ‘bottom-up’ scenarios. Response options are not mutually exclusive (e.g., management of soil carbon and cropland management). Different options interact with each other; they may have additive effects or compete with each other for land or other resources and thus these potentials cannot necessarily be added up. The interplay between different land-based mitigation options, as well as with mitigation options in other sectors (such as energy or transport), in contributing to specific mitigation pathways has been assessed using IAMs (Section 2.7.2). These include interactions with wider socioeconomic conditions (Cross-Chapter Box 1 and Chapter 1) and other sustainability goals (Chapter 6).

2.6.1 Climate impacts of individual response options

Since AR5, there have been many new estimates of the climate impacts of single or multiple response options, summarised in Figure 2.24 and discussed in sub-sections below. Recently published syntheses of mitigation potential of land-based response options (e.g., Hawken (2017a), Smith et al. (2016b), Griscom et al. (2017), Minx et al. (2018), Fuss et al. (2018b), Nemet et al. (2018)) are also included in Figure 2.24. The wide range in mitigation estimates reflects differences in methodologies that may not be directly comparable, and estimates cannot be necessarily be added if they were calculated independently as they may be competing for land and other resources.

Some studies assess a ‘technical mitigation potential’ – the amount possible with current technologies. Some include resource constraints (e.g., limits to yields, limits to natural forest conversion) to assess a ‘sustainable potential’. Some assess an ‘economic potential’ mitigation at different carbon prices. Few include social and political constraints (e.g., behaviour change, enabling conditions) (Chapter 7), the biophysical climate effects (Section 2.5) or the impacts of future climate change (Section 2.3). Carbon stored in biomass and soils may be at risk of future climate change (Section 2.2), natural disturbances such as wildfire (Cross-Chapter Box 3 in this chapter) and future changes in land use or management changes that result in a net loss of carbon (Gren and Aklilu 2016).

2.6.1.1 Land management in agriculture

Reducing non-CO₂ emissions from agriculture through cropland nutrient management, enteric fermentation, manure management, rice cultivation and fertiliser production has a total mitigation potential of 0.30–3.38 GtCO₂-eq yr⁻¹ (*medium confidence*) (combined sub-category measures in Figure 2.24, details below) with a further 0.25–6.78 GtCO₂-eq yr⁻¹ from soil carbon management (Section 2.6.1.3). Other literature that looks at broader categories finds mitigation potential of 1.4–2.3 GtCO₂-eq yr⁻¹ from improved cropland management (Smith et al. 2008, 2014; Pradhan et al., 2013); 1.4–1.8 GtCO₂-eq yr⁻¹ from improved grazing land management (Conant et al. 2017; Herrero et al. 2016; Smith et al. 2008, 2014) and 0.2–2.4 GtCO₂-eq yr⁻¹ from improved livestock management

(Smith et al. 2008, 2014; Herrero et al. 2016; FAO 2007). Detailed discussions of the mitigation potential of agricultural response options and their co-benefits are provided in Chapter 5 and Sections 5.5 and 5.6.

The three main measures to reduce enteric fermentation include improved animal diets (higher quality, more digestible livestock feed), supplements and additives (reduce methane by changing the microbiology of the rumen), and animal management and breeding (improve husbandry practices and genetics). Applying these measures can mitigate 0.12–1.18 GtCO₂-eq yr⁻¹ (*medium confidence*) (Hristov et al. 2013; Dickie et al. 2014; Herrero et al. 2016; Griscom et al. 2017). However, these measures may have limitations such as need of crop-based feed (Pradhan et al. 2013) and associated ecological costs, toxicity and animal welfare issues related to food additives (Llonch et al. 2017). Measures to manage manure include anaerobic digestion for energy use, composting as a nutrient source, reducing storage time and changing livestock diets, and have a potential of 0.01–0.26 GtCO₂-eq yr⁻¹ (Herrero et al. 2016; Dickie et al. 2014).

On croplands, there is a mitigation potential of 0.03–0.71 GtCO₂-eq yr⁻¹ for cropland nutrient management (fertiliser application) (*medium confidence*) (Griscom et al. 2017; Hawken 2017; Paustian et al. 2016; Dickie et al. 2014; Beach et al. 2015). Reducing emissions from rice production through improved water management (periodic draining of flooded fields to reduce methane emissions from anaerobic decomposition) and straw residue management (applying in dry conditions instead of on flooded fields and avoiding burning to reduce methane and N₂O emissions) has the potential to mitigate up to 60% of emissions (Hussain et al. 2015), or 0.08–0.87 GtCO₂-eq yr⁻¹ (*medium confidence*) (Griscom et al. 2017; Hawken 2017; Paustian et al. 2016; Hussain et al. 2015; Dickie et al. 2014; Beach et al. 2015). Furthermore, sustainable intensification through the integration of crop and livestock systems can increase productivity, decrease emission intensity and act as a climate adaptation option (Section 5.5.1.4).

Agroforestry is a land management system that combines woody biomass (e.g., trees or shrubs) with crops and/or livestock. The mitigation potential from agroforestry ranges between 0.08–5.7 GtCO₂ yr⁻¹, (*medium confidence*) (Griscom et al. 2017; Dickie et al. 2014; Zomer et al. 2016; Hawken 2017). The high estimate is from an optimum scenario combining four agroforestry solutions (silvopasture, tree intercropping, multistrata agroforestry and tropical staple trees) of Hawken (2017a). Zomer et al. (2016) reported that the trees in agroforestry landscapes had increased carbon stock by 7.33 GtCO₂ between 2000 and 2010, or 0.7 GtCO₂ yr⁻¹ (Section 5.5.1.3).

2.6.1.2 Land management in forests

The mitigation potential for reducing and/or halting deforestation and degradation ranges from 0.4–5.8 GtCO₂ yr⁻¹ (*high confidence*) (Griscom et al. 2017; Hawken 2017; Busch and Engelmann 2017; Baccini et al. 2017; Zarlin et al. 2016; Federici et al. 2015; Carter et al. 2015; Houghton et al. 2015; Smith et al. 2013a; Houghton and Nassikas 2018). The higher figure represents a complete halting of land use conversion in forests and peatlands (i.e., assuming recent

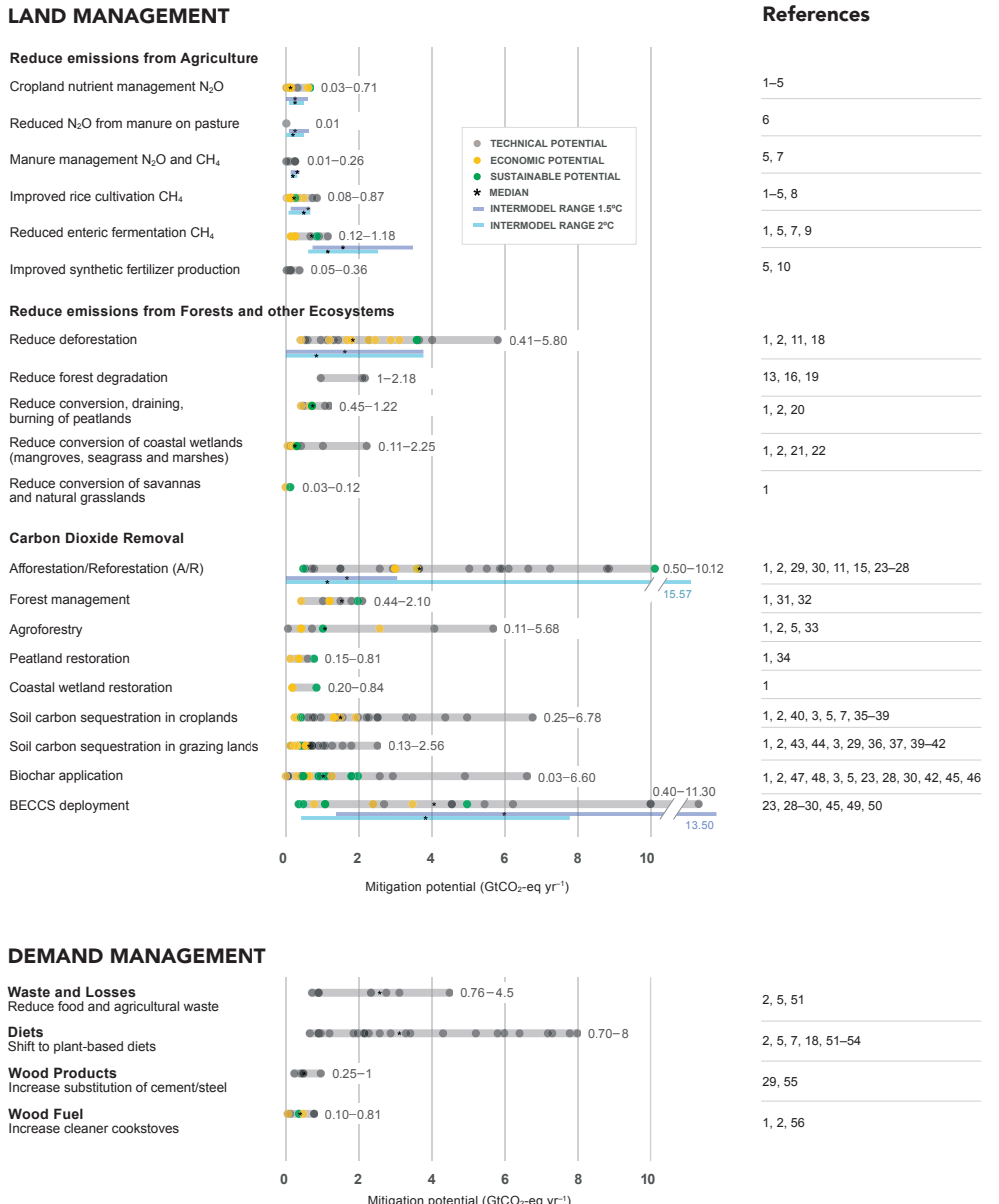


Figure 2.24 | Mitigation potential of response options in 2020–2050, measured in GtCO₂-eq yr⁻¹, adapted from Roe et al. (2017). Mitigation potentials reflect the full range of low to high estimates from studies published after 2010, differentiated according to technical (possible with current technologies), economic (possible given economic constraints) and sustainable potential (technical or economic potential constrained by sustainability considerations). Medians are calculated across all potentials in categories with more than four data points. We only include references that explicitly provide mitigation potential estimates in CO₂-eq yr⁻¹ (or a similar derivative) by 2050. Not all options for land management potentials are additive, as some may compete for land. Estimates reflect a range of methodologies (including definitions, global warming potentials and time horizons) that may not be directly comparable or additive. Results from IAMs are shown to compare with single option ‘bottom-up’ estimates, in available categories from the 2°C and 1.5°C scenarios in the SSP Database (version 2.0). The models reflect land management changes, yet in some instances, can also reflect demand-side effects from carbon prices, so may not be defined exclusively as ‘supply-side’. References: 1) Griscom et al. (2017), 2) Hawken (2017), 3) Paustian et al. (2016), 4) Beach et al. (2016), 5) Dickie et al. (2014), 6) Herrero et al. (2013), 7) Herrero et al. (2016), 8) Hussain et al. (2015), 9) Hristov, et al. (2013), 10) Zhang et al. (2013), 11) Houghton and Nassikas (2018), 12) Busch and Engelmann (2017), 13) Vaccini et al. (2017), 14) Zarlin et al. (2016), 15) Houghton, et al. (2015), 16) Federici et al. (2015), 17) Carter et al. (2015), 18) Smith et al. (2013), 19) Pearson et al. (2017), 20) Hooijer et al. (2010), 21) Howard (2017), 22) Pendleton et al. (2012), 23) Fuss et al. (2018), 24) Dooley and Kartha (2018), 25) Kreidenweis et al. (2016), 26) Yan et al. (2017), 27) Sonntag et al. (2016), 28) Lenton (2014), 29) McLaren (2012), 30) Lenton (2010), 31) Sasaki et al. (2016), 32) Sasaki et al. (2012), 33) Zomer et al. (2016), 34) Couwenberg et al. (2010), 35) Conant et al. (2017), 36) Sanderman et al. (2017), 37) Frank et al. (2017), 38) Henderson et al. (2015), 39) Sommer and Bossio (2014), 40) Lal (2010), 41) Zomer et al. (2017), 42) Smith et al. (2016), 43) Poeplau and Don (2015), 44) Powlson et al. (2014), 45) Powell and Lenton (2012), 46) Woolf et al. (2010), 47) Roberts et al. (2010), 48) Pratt and Moran (2010), 49) Turner et al. (2018), 50) Koornneef et al. (2012), 51) Bajzelj et al. (2014), 52) Springmann et al. (2016), 53) Tilman and Clark (2014), 54) Hedenus et al. (2014), 55) Miner (2010), 56) Bailis et al. (2015).

rates of carbon loss are saved each year). Separate estimates of degradation only range from 1.0–2.18 GtCO₂ yr⁻¹. Reduced deforestation and forest degradation include conservation of existing carbon pools in vegetation and soil through protection in reserves, controlling disturbances such as fire and pest outbreaks, and changing management practices. Differences in estimates stem from varying land cover definitions, the time periods assessed and the carbon pools included (most higher estimates include belowground, dead wood, litter, soil and peat carbon). When deforestation and degradation are halted, it may take many decades to fully recover the biomass initially present in native ecosystems (Meli et al. 2017) (Section 4.8.3).

Afforestation/reforestation (A/R) and forest restoration can increase carbon sequestration in both vegetation and soils by 0.5–10.1 GtCO₂ yr⁻¹ (*medium confidence*) (Fuss et al. 2018; Griscom et al. 2017; Hawken 2017; Kreidenweis et al. 2016; Li et al. 2016; Huang et al. 2017; Sonntag et al. 2016; Lenton 2014; McLaren 2012; Lenton 2010; Erb et al. 2018; Dooley and Kartha 2018; Yan et al. 2017; Houghton et al. 2015; Houghton and Nassikas 2018). Afforestation is the conversion to forest of land that historically has not contained forests. Reforestation is the conversion to forest of land that has previously contained forests but that has been converted to some other use. Forest restoration refers to practices aimed at regaining ecological integrity in a deforested or degraded forest landscape. The lower estimate represents the lowest range from an ESM (Yan et al. 2017) and of sustainable global negative emissions potential (Fuss et al. 2018), and the higher estimate reforests all areas where forests are the native cover type, constrained by food security and biodiversity considerations (Griscom et al. 2017). It takes time for full carbon removal to be achieved as the forest grows. Removal occurs at faster rates in young- to medium-aged forests and declines thereafter such that older forest stands have smaller carbon removals but larger stocks, with net uptake of carbon slowing as forests reach maturity (Yao et al. 2018; Poorter et al. 2016; Tang et al. 2014). The land intensity of afforestation and reforestation has been estimated at 0.0029 km² tC⁻¹ yr⁻¹ (Smith et al. 2016a). Boysen et al. (2017) estimated that to sequester about 100 GtC by 2100 would require 13 Mkm² of abandoned cropland and pastures (Section 4.8.3).

Forest management has the potential to mitigate 0.4–2.1 GtCO₂-eq yr⁻¹ (*medium confidence*) (Sasaki et al. 2016; Griscom et al. 2017; Sasaki et al. 2012). Forest management can alter productivity, turnover rates, harvest rates carbon in soil and carbon in wood products (Erb et al. 2017; Campioli et al. 2015; Birdsey and Pan 2015; Erb et al. 2016; Noormets et al. 2015; Wäldchen et al. 2013; Malhi et al. 2015; Quesada et al. 2018; Nabuurs et al. 2017; Bosello et al. 2009) (Section 4.8.4). Fertilisation may enhance productivity but would increase N₂O emissions. Preserving and enhancing carbon stocks in forests has immediate climate benefits but the sink can saturate and is vulnerable to future climate change (Seidl et al. 2017). Wood can be harvested and used for bioenergy substituting for fossil fuels (with or without carbon capture and storage) (Section 2.6.1.5), for long-lived products such as timber (see below), to be buried as biochar (Section 2.6.1.1) or for use in the wider bioeconomy, enabling areas of land to be used continuously for mitigation. This leads to initial carbon loss and lower carbon stocks but with each harvest cycle, the

carbon loss (debt) can be paid back and after a parity time, result in net savings (Laganière et al. 2017; Bernier and Paré 2013; Mitchell et al. 2012; Haberl et al. 2012; Haberl 2013; Ter-Mikaelian et al. 2015; Macintosh et al. 2015). The trade-off between maximising forest carbon stocks and maximising substitution is highly dependent on the counterfactual assumption (no-use vs extrapolation of current management), initial forest conditions and site-specific contexts (such as regrowth rates and the displacement factors and efficiency of substitution), and relative differences in emissions released during extraction, transport and processing of the biomass- or fossil-based resources, as well as assumptions about emission associated with the product or energy source that is substituted (Grassi et al. 2018b; Nabuurs et al. 2017; Pingoud et al. 2018; Smyth et al. 2017a; Luyssaert et al. 2018; Valade et al. 2017; York 2012; Ter-Mikaelian et al. 2014; Naudts et al. 2016b; Mitchell et al. 2012; Haberl et al. 2012; Macintosh et al. 2015; Laganière et al. 2017; Haberl 2013). This leads to uncertainty about optimum mitigation strategies in managed forests, while high carbon ecosystems such as primary forests would have large initial carbon losses and long pay-back times, and thus protection of stocks would be more optimal (Lemprière et al. 2013; Kurz et al. 2016; Keith et al. 2014) (Section 4.8.4).

Global mitigation potential from increasing the demand of wood products to replace construction materials range from 0.25–1 GtCO₂-eq yr⁻¹ (*medium confidence*) (McLaren 2012; Miner 2010), the uncertainty is determined in part by consideration of the factors described above, and is sensitive to the displacement factor, or the substitution benefit in CO₂, when wood is used instead of another material, which may vary in the future as other sectors reduce emissions (and may also vary due to market factors) (Sathre and O'Connor 2010; Nabuurs et al. 2018; Iordan et al. 2018; Braun et al. 2016; Gustavsson et al. 2017; Peñaloza et al. 2018; Soimakallio et al. 2016; Grassi et al. 2018b). Using harvested carbon in long-lived products (e.g., for construction) can represent a store that can sometimes be from decades to over a century, while the wood can also substitute for intensive building materials, avoiding emissions from the production of concrete and steel (Sathre and O'Connor 2010; Smyth et al. 2017b; Nabuurs et al. 2007; Lemprière et al. 2013). The harvest of carbon and storage in products affects the net carbon balance of the forest sector, with the aim of sustainable forest management strategies being to optimise carbon stocks and use harvested products to generate sustained mitigation benefits (Nabuurs et al. 2007).

Biophysical effects of forest response options are variable depending on the location and scale of activity (Section 2.6). Reduced deforestation or afforestation in the tropics contributes to climate mitigation through both biogeochemical and biophysical effects. It also maintains rainfall recycling to some extent. In contrast, in higher latitude boreal areas, observational and modelling studies show that afforestation and reforestation lead to local and global warming effects, particularly in snow covered regions in the winter as the albedo is lower for forests than bare snow (Bathiany et al. 2010; Dass et al. 2013; Devaraju et al. 2018; Ganopolski et al. 2001; Snyder et al. 2004; West et al. 2011; Arora and Montenegro 2011) (Section 2.6). Management, for example, thinning practices in forestry, could increase the albedo in regions where albedo

decreases with age. The length of rotation cycles in forestry affects tree height and thus roughness, and through the removal of leaf mass harvest reduces evapotranspiration (Erb et al. 2017), which could lead to increased fire susceptibility in the tropics. In temperate and boreal sites, biophysical forest management effects on surface temperature were shown to be of similar magnitude than changes in land cover (Luyssaert et al. 2014). These biophysical effects could be of a magnitude to overcompensate biogeochemical effects, for example, the sink strength of regrowing forests after past depletions (Luyssaert et al. 2018; Naudts et al. 2016b), but many parameters and assumptions on counterfactual influence the account (Anderson et al. 2011; Li et al. 2015b; Bright et al. 2015).

Forest cover also affects climate through reactive gases and aerosols, with *limited evidence* and *medium agreement* that the decrease in the emissions of BVOC resulting from the historical conversion of forests to cropland has resulted in a positive radiative forcing through direct and indirect aerosol effects. A negative radiative forcing through reduction in the atmospheric lifetime of CH₄ has increased and decreased ozone concentrations in different regions (Section 2.4).

2.6.1.3 Land management of soils

The global mitigation potential for increasing soil organic matter stocks in mineral soils is estimated to be in the range of 0.4–8.64 GtCO₂ yr⁻¹ (*high confidence*), though the full literature range is wider with high uncertainty related to some practices (Fuss et al. 2018; Sommer and Bossio 2014; Lal 2010; Lal et al. 2004; Conant et al. 2017; Dickie et al. 2014; Frank et al. 2017a; Griscom et al. 2017; Herrero et al. 2015, 2016; McLaren 2012; Paustian et al. 2016; Poeplau and Don 2015; Powlson et al. 2014; Smith et al. 2016c; Zomer et al. 2017). Some studies have separate potentials for soil carbon sequestration in croplands (0.25–6.78 GtCO₂ yr⁻¹) (Griscom et al. 2017; Hawken 2017; Frank et al. 2017a; Paustian et al. 2016; Herrero et al. 2016; Henderson et al. 2015; Dickie et al. 2014; Conant et al. 2017; Lal 2010) and soil carbon sequestration in grazing lands (0.13–2.56 GtCO₂ yr⁻¹) (Griscom et al. 2017; Hawken 2017; Frank et al. 2017a; Paustian et al. 2016; Powlson et al. 2014; McLaren 2012; Zomer et al. 2017; Smith et al. 2015; Sommer and Bossio 2014; Lal 2010). The potential for soil carbon sequestration and storage varies considerably depending on prior and current land management approaches, soil type, resource availability, environmental conditions, microbial composition and nutrient availability among other factors (Hassink and Whitmore 1997; Smith and Dukes 2013; Palm et al. 2014; Lal 2013; Six et al. 2002; Feng et al. 2013). Soils are a finite carbon sink and sequestration rates may decline to negligible levels over as little as a couple of decades as soils reach carbon saturation (West et al. 2004; Smith and Dukes 2013). The sink is at risk of reversibility, in particular due to increased soil respiration under higher temperatures (Section 2.3).

Land management practices to increase carbon interact with agricultural and fire management practices (Cross-chapter Box 3 and Chapter 5) and include improved rotations with deeper rooting cultivars, addition of organic materials and agroforestry (Lal 2011; Smith et al. 2008; Lorenz and Pitman 2014; Lal 2013; Vermeulen et al.

2012; de Rouw et al. 2010). Adoption of green manure cover crops, while increasing cropping frequency or diversity, helps sequester SOC (Poeplau and Don 2015; Mazzoncini et al. 2011; Luo et al. 2010). Studies of the long-term SOC sequestration potential of conservation agriculture (i.e., the simultaneous adoption of minimum tillage, (cover) crop residue retention and associated soil surface coverage, and crop rotations) include results that are both positive (Powlson et al. 2016; Zhang et al. 2014) and inconclusive (Cheesman et al. 2016; Palm et al. 2014; Govaerts et al. 2009).

The efficacy of reduced and zero-till practices is highly context-specific; many studies demonstrate increased carbon storage (e.g., Paustian et al. (2000), Six et al. (2004), van Kessel et al. (2013)), while others show the opposite effect (Sisti et al. 2004; Álvaro-Fuentes et al. 2008; Christopher et al. 2009). On the other hand, deep ploughing can contribute to SOC sequestration by burying soil organic matter in the subsoil where it decomposes slowly (Alcántara et al. 2016). Meta-analyses (Haddaway et al. 2017; Luo et al. 2010; Meurer et al. 2018) also show a mix of positive and negative responses, and the lack of robust comparisons of soils on an equivalent mass basis continues to be a problem for credible estimates (Wendt and Hauser 2013; Powlson et al. 2011; Powlson et al. 2014).

Soil carbon management interacts with N₂O (Paustian et al. 2016). For example, Li et al. (2005) estimate that the management strategies required to increase carbon sequestration (reduced tillage, crop residue and manure recycling) would increase N₂O emissions significantly, offsetting 75–310% of the carbon sequestered in terms of CO₂ equivalence, while other practices such as cover crops can reduce N₂O emissions (Kaye and Quemada 2017).

The management of soil erosion could avoid a net emissions of 1.36–3.67 GtCO₂ yr⁻¹ and create a sink of 0.44–3.67 GtCO₂ yr⁻¹ (*low confidence*) (Jacinthe and Lal 2001; Lal et al. 2004; Stallard 1998; Smith et al. 2001; Van Oost et al. 2007). The overall impact of erosion control on mitigation is context-specific and uncertain at the global level and the final fate of eroded material is still debated (Hoffmann et al. 2013).

Biochar is produced by thermal decomposition of biomass in the absence of oxygen (pyrolysis) into a stable, long-lived product like charcoal that is relatively resistant to decomposition (Lehmann et al. 2015) and which can stabilise organic matter when added to soil (Weng et al. 2017). Although charcoal has been used traditionally by many cultures as a soil amendment, ‘modern biochar’, produced in facilities that control emissions, is not widely used. The range of global potential of biochar is 0.03–6.6 GtCO₂-eq yr⁻¹ by 2050, including energy substitution, with 0.03–4.9 GtCO₂ yr⁻¹ for CDR only (*medium confidence*) (Griscom et al. 2017; Hawken 2017; Paustian et al. 2016; Fuss et al. 2018; Lenton 2014, 2010; Powell and Lenton 2012; Woolf et al. 2010; Pratt and Moran 2010; Smith 2016; Roberts et al. 2010). An analysis in which biomass supply constraints were applied to protect against food insecurity, loss of habitat and land degradation, estimated *technical potential* abatement of 3.7–6.6 GtCO₂-eq yr⁻¹ (including 2.6–4.6 GtCO₂ yr⁻¹ carbon stabilisation) (Woolf et al. 2010). Fuss et al. (2018) propose a range of 0.5–2 GtCO₂-eq yr⁻¹ as the *sustainable potential* for negative

emissions through biochar. Griscom et al. (2017) suggest a potential of 1.0 GtCO₂ yr⁻¹ based on available residues. Biochar can provide additional climate change mitigation benefits by decreasing N₂O emissions from soil and reducing nitrogen fertiliser requirements in agricultural soils (Borchard et al. 2019). Application of biochar to cultivated soils can darken the surface and reduce its mitigation potential via decreases in surface albedo, but the magnitude of this effect depends on soil moisture content, biochar application method and type of land use (*low confidence*) (Verheijen et al. 2013; Bozzi et al. 2015) (Section 4.9.5).

2.6.1.4 Land management in other ecosystems

Protection and restoration of wetlands, peatlands and coastal habitats reduces net carbon loss (primarily from sediment/soils) and provides continued or enhanced natural CO₂ removal (Section 4.9.4). Reducing annual emissions from peatland conversion, draining and burning could mitigate 0.45–1.22 GtCO₂-eq yr⁻¹ up to 2050 (*medium confidence*) (Hooijer et al. 2010; Griscom et al. 2017; Hawken 2017) and peatland restoration 0.15–0.81 (*low confidence*) (Couwenberg et al. 2010; Griscom et al. 2017). The upper end from Griscom et al. (2017) represents a maximum sustainable potential (accounting for biodiversity and food security safeguards) for rewetting and biomass enhancement. Wetland drainage and rewetting was included as a flux category under the second commitment period of the Kyoto Protocol, with significant management knowledge gained over the last decade (IPCC 2013b). However, there are high uncertainties as to carbon storage and flux rates, in particular the balance between CH₄ sources and CO₂ sinks (Spencer et al. 2016). Peatlands are sensitive to climate change which may increase carbon uptake by vegetation and carbon emissions due to respiration, with the balance being regionally dependent (*high confidence*). There is *low confidence* about the future peatland sink globally. Some peatlands have been found to be resilient to climate change (Minayeva and Sirin 2012), but the combination of land use change and climate change may make them vulnerable to fire (Sirin et al. 2011). While models show mixed results for the future sink (Spahni et al. 2013; Chaudhary et al. 2017; Ise et al. 2008), a study that used extensive historical data sets to project change under future warming scenarios found that the current global peatland sink could increase slightly until 2100 and decline thereafter (Gallego-Sala et al. 2018).

Reducing the conversion of coastal wetlands (mangroves, seagrass and marshes) could reduce emissions by 0.11–2.25 GtCO₂-eq yr⁻¹ by 2050 (*medium confidence*) (Pendleton et al. 2012; Griscom et al. 2017; Howard et al. 2017; Hawken 2017). Mangrove restoration can mitigate the release of 0.07 GtCO₂ yr⁻¹ through rewetting (Crooks et al. 2011) and take up 0.02–0.84 GtCO₂ yr⁻¹ from biomass and soil enhancement (*medium confidence*) (Griscom et al. 2017). The ongoing benefits provided by mangroves as a natural carbon sink can be nationally-important for small island developing states (SIDS) and other countries with extensive coastlines, based on estimates of high carbon sequestration rates per unit area (McLeod et al. 2011; Duarte et al. 2013; Duarte 2017; Taillardat et al. 2018). There is only *medium confidence* in the effectiveness of enhanced carbon uptake using mangroves, due to the many uncertainties regarding the response of mangroves to future climate change (Jennerjahn

et al. 2017), dynamic changes in distributions (Kelleway et al. 2017) and other local-scale factors affecting long-term sequestration and climatic benefits (e.g., methane release) (Dutta et al. 2017). The climate mitigation potential of coastal vegetated habitats (mangrove forests, tidal marshes and seagrasses) is considered in Chapter 5 of the IPCC Special Report on the Ocean, Cryosphere and Climate Change (SROCC), in a wider ‘blue carbon’ context.

2.6.1.5 Bioenergy and bioenergy with carbon capture and storage

An introduction and overview of bioenergy and bioenergy with carbon capture and storage (BECCS) can be found in Cross-Chapter Boxes 7 and 12, and Chapters 6 and 7. CCS technologies are discussed in SR15. The discussion below refers to modern bioenergy only (e.g., liquid biofuels for transport and the use of solid biofuels in combined heat and power plants).

The mitigation potential of bioenergy coupled with CCS (i.e., BECCS), is estimated to be between 0.4 and 11.3 GtCO₂ yr⁻¹ (*medium confidence*) based on studies that directly estimate mitigation for BECCS (not bioenergy) in units of CO₂ (not EJ) (McLaren 2012; Lenton 2014; Fuss et al. 2018; Turner et al. 2018b; Lenton 2010; Koornneef et al. 2012; Powell and Lenton 2012). SR15 reported a potential of 1–85 GtCO₂ yr⁻¹ which they noted could be narrowed to a range of 0.5–5 GtCO₂ yr⁻¹ when taking account of sustainability aims (Fuss et al. 2018). The upper end of the SR15 range is considered as a theoretical potential. Previously, the IPCC Special Report on Renewable Energy Sources concluded the technical potential of biomass supply for energy (without BECCS) could reach 100–300 EJ yr⁻¹ by 2050, which would be 2–15 GtCO₂ yr⁻¹ (using conversion factors 1 EJ = 0.02–0.05 GtCO₂ yr⁻¹ emission reduction, SR15). A range of recent studies including sustainability or economic constraints estimate that 50–244 EJ (1–12 GtCO₂ yr⁻¹ using the conversion factors above) of bioenergy could be produced on 0.1–13 Mkm² of land (Fuss et al. 2018; Chan and Wu 2015; Schueler et al. 2016; Wu et al. 2013; Searle and Malins 2015; Wu et al. 2019; Heck et al. 2018; Fritz et al. 2013).

There is *high confidence* that the most important factors determining future biomass supply for energy are land availability and land productivity (Berndes et al. 2013; Creutzig et al. 2015a; Woods et al. 2015; Daioglou et al. 2019). Estimates of marginal/degraded lands currently considered available for bioenergy range from 3.2–14.0 Mkm², depending on the adopted sustainability criteria, land class definitions, soil conditions, land mapping method and environmental and economic considerations (Campbell et al. 2008; Cai et al. 2011; Lewis and Kelly 2014).

Bioenergy production systems can lead to net emissions in the short term that can be ‘paid-back’ over time, with multiple harvest cycles and fossil fuel substitution, unlike fossil carbon emissions (Campbell et al. 2008; Cai et al. 2011; Lewis and Kelly 2014; De Oliveira Bordonal et al. 2015). Stabilising bioenergy crops in previous high carbon forestland or peatland results in high emissions of carbon that may take from decades to more than a century to be re-paid in terms of net CO₂ emission savings from replacing fossil fuels,

depending on previous forest carbon stock, bioenergy yields and displacement efficiency (Elshout et al. 2015; Harper et al. 2018; Daioglou et al. 2017). In the case of bioenergy from managed forests, the magnitude and timing of the net mitigation benefits is controversial as it varies with differences due to local climate conditions, forest management practice, fossil fuel displacement efficiency and methodological approaches (Hudiburg et al. 2011; Berndes et al. 2013; Guest et al. 2013; Lamers and Junginger 2013; Cherubini et al. 2016; Cintas et al. 2017; Laurance et al. 2018; Valade et al. 2018; Baker et al. 2019). Suitable bioenergy crops can be integrated in agricultural landscapes to reverse ecosystem carbon depletion (Creutzig et al. 2015a; Robertson et al. 2017; Vaughan et al. 2018; Daioglou et al. 2017). Cultivation of short rotation woody crops and perennial grasses on degraded land or cropland previously used for annual crops typically accumulate carbon in soils due to their deep root systems (Don et al. 2012; Robertson et al. 2017). The use of residues and organic waste as bioenergy feedstock can mitigate land use change pressures associated with bioenergy deployment, but residues are limited and the removal of residues that would otherwise be left on the soil could lead soil degradation (Chum et al. 2011; Liska et al. 2014; Monforti et al. 2015; Zhao et al. 2015; Daioglou et al. 2016).

The steps required to cultivate, harvest, transport, process and use biomass for energy generate emissions of GHGs and other climate pollutants (Chum et al. 2011; Creutzig et al. 2015b; Staples et al. 2017; Daioglou et al. 2019). Life-cycle GHG emissions of modern bioenergy alternatives are usually lower than those for fossil fuels (*robust evidence, medium agreement*) (Chum et al. 2011; Creutzig et al. 2015b). The magnitude of these emissions largely depends on location (e.g., soil quality, climate), prior land use, feedstock used (e.g., residues, dedicated crops, algae), land use practice (e.g., soil management, fertiliser use), biomass transport (e.g., distances and transport modes) and the bioenergy conversion pathway and product (e.g., wood pellets, ethanol). Use of conventional food and feed crops as a feedstock generally provides the highest bioenergy yields per hectare, but also causes more GHG emissions per unit energy compared to agriculture residues, biomass from managed forests and lignocellulosic crops such as short-rotation coppice and perennial grasses (Chum et al. 2011; Gerbrandt et al. 2016) due to the application of fertilisers and other inputs (Oates et al. 2016; Rowe et al. 2016; Lai et al. 2017; Robertson et al. 2017).

Bioenergy from dedicated crops are in some cases held responsible for GHG emissions resulting from indirect land use change (iLUC), that is the bioenergy activity may lead to displacement of agricultural or forest activities into other locations, driven by market-mediated effects. Other mitigation options may also cause iLUC. At a global level of analysis, indirect effects are not relevant because all land-use emissions are direct. iLUC emissions are potentially more significant for crop-based feedstocks such as corn, wheat and soybean, than for advanced biofuels from lignocellulosic materials (Chum et al. 2011; Wicke et al. 2012; Valin et al. 2015; Ahlgren and Di Lucia 2014). Estimates of emissions from iLUC are inherently uncertain, widely debated in the scientific community and are highly dependent on modelling assumptions, such as supply/demand elasticities, productivity estimates, incorporation or exclusion of emission credits for coproducts and scale of biofuel

deployment (Rajagopal and Plevin 2013; Finkbeiner 2014; Kim et al. 2014; Zilberman 2017). In some cases, iLUC effects are estimated to result in emission reductions. For example, market-mediated effects of bioenergy in North America showed potential for increased carbon stocks by inducing conversion of pasture or marginal land to forestland (Cintas et al. 2017; Duden et al. 2017; Dale et al. 2017; Baker et al. 2019). There is a wide range of variability in iLUC values for different types of biofuels, from $-75\text{--}55 \text{ gCO}_2 \text{ MJ}^{-1}$ (Ahlgren and Di Lucia 2014; Valin et al. 2015; Plevin et al. 2015; Taheripour and Tyner 2013; Bento and Klotz 2014). There is low confidence in attribution of emissions from iLUC to bioenergy.

Bioenergy deployment can have large biophysical effects on regional climate, with the direction and magnitude of the impact depending on the type of bioenergy crop, previous land use and seasonality (*limited evidence, medium agreement*). A study of two alternative future bioenergy scenarios using 15 Mkm^2 of intensively used managed land or conversion of natural areas showed a nearly neutral effect on surface temperature at global levels (considering biophysical effects and CO_2 and N_2O fluxes from land but not substitution effects), although there were significant seasonal and regional differences (Kicklighter et al. 2013). Modelling studies on biofuels in the US found the switch from annual crops to perennial bioenergy plantations like Miscanthus could lead to regional cooling due to increases in evapotranspiration and albedo (Georgescu et al. 2011; Harding et al. 2016), with perennial bioenergy crop expansion over suitable abandoned and degraded farmlands causing near-surface cooling up to 5°C during the growing season (Wang et al. 2017b). Similarly, growing sugarcane on existing cropland in Brazil cools down the local surface during daytime conditions up to -1°C , but warmer conditions occur if sugar cane is deployed at the expense of natural vegetation (Brazilian Cerrado) (Loarie et al. 2011). In general, bioenergy crops (as for all crops) induce a cooling of ambient air during the growing season, but after harvest the decrease in evapotranspiration can induce warming (Harding et al. 2016; Georgescu et al. 2013; Wang et al. 2017b). Bioenergy crops were found to cause increased isoprene emissions in a scenario where 0.69 Mkm^2 of oil palm for biodiesel in the tropics and 0.92 Mkm^2 of short rotation coppice (SRC) in the mid-latitudes were planted, but effects on global climate were negligible (Ashworth et al. 2012).

2.6.1.6 Enhanced weathering

Weathering is the natural process of rock decomposition via chemical and physical processes in which CO_2 is removed from the atmosphere and converted to bicarbonates and/or carbonates (IPCC 2005). Formation of calcium carbonates in the soil provides a permanent sink for mineralised organic carbon (Manning 2008; Beerling et al. 2018). Mineral weathering can be enhanced through grinding up rock material to increase the surface area, and distributing it over land to provide carbon removals of $0.5\text{--}4.0 \text{ GtCO}_2 \text{ yr}^{-1}$ (*medium confidence*) (Beerling et al. 2018; Lenton 2010; Smith et al. 2016a; Taylor et al. 2016). While the geochemical potential is quite large, agreement on the technical potential is low due to a variety of unknown parameters and limits, such as rates of mineral extraction, grinding, delivery and challenges with scaling and deployment.

2.6.1.7 Demand management in the food sector (diet change, waste reduction)

Demand-side management has the potential for climate change mitigation via reducing emissions from production, switching to consumption of less emission intensive commodities and making land available for CO₂ removal (Section 5.5.2). Reducing food losses and waste increases the overall efficiency of food value chains (with less land and inputs needed) along the entire supply chain and has the potential to mitigate 0.8–4.5 GtCO₂-eq yr⁻¹ (*high confidence*) (Bajželj et al. 2014; Dickie et al. 2014; Hawken 2017; Hiç et al. 2016) (Section 5.5.2.5).

Shifting to diets that are lower in emissions-intensive foods like beef delivers a mitigation potential of 0.7–8.0 GtCO₂-eq yr⁻¹ (*high confidence*) (Bajželj et al. 2014; Dickie et al. 2014; Herrero et al. 2016; Hawken 2017; Springmann et al. 2016; Tilman and Clark 2014; Hedenus et al. 2014; Stehfest et al. 2009) with most of the higher end estimates (>6 GtCO₂-eq yr⁻¹) based on veganism, vegetarianism or very low ruminant meat consumption (Section 5.5.2). In addition to direct mitigation gains, decreasing meat consumption, primarily of ruminants, and reducing wastes further reduces water use, soil degradation, pressure on forests and land used for feed potentially freeing up land for mitigation (Tilman and Clark 2014) (Chapters 5 and 6). Additionally, consumption of locally produced food, shortening the supply chain, can in some cases minimise food loss, contribute to food security and reduce GHG emissions associated with energy consumption and food loss (Section 5.5.2.6).

2.6.2 Integrated pathways for climate change mitigation

Land-based response options have the potential to interact, resulting in additive effects (e.g., climate co-benefits) or negating each other (e.g., through competition for land). They also interact with mitigation options in other sectors (such as energy or transport) and thus they need to be assessed collectively under different climate mitigation targets and in combination with other sustainability goals (Popp et al. 2017; Obersteiner et al. 2016; Humpenöder et al. 2018). IAMs with distinctive land-use modules are the basis for the assessment of mitigation pathways as they combine insights from various disciplines in a single framework and cover the largest sources of anthropogenic GHG emissions from different sectors (see also SR15 Chapter 2 and Technical Annex for more details). IAMs consider a limited, but expanding, portfolio of land-based mitigation options. Furthermore, the inclusion and detail of a specific mitigation measure differs across IAMs and studies (see also SR15 and Chapter 6). For example, the IAM scenarios based on the shared socio-economic pathways (SSPs) (Riahi et al. 2017) (Cross-Chapter Box 1 and Chapter 1) include possible trends in agriculture and land use for five different socioeconomic futures, but cover a limited set of land-based mitigation options: dietary changes, higher efficiency in food processing (especially in livestock production systems), reduction of food waste, increasing agricultural productivity, methane reductions in rice paddies, livestock and grazing management for reduced methane emissions from enteric

fermentation, manure management, improvement of N-efficiency, 1st generation biofuels, reduced deforestation, afforestation, 2nd generation bioenergy crops and BECCS (Popp et al. 2017). However, many ‘natural climate solutions’ (Griscom et al. 2017), such as forest management, rangeland management, soil carbon management or wetland management, are not included in most of these scenarios. In addition, most IAMs neglect the biophysical effects of land-use such as changes in albedo or evapotranspiration with few exceptions (Kreidenweis et al. 2016).

Mitigation pathways, based on IAMs, are typically designed to find the least cost pathway to achieve a pre-defined climate target (Riahi et al. 2017). Such cost-optimal mitigation pathways, especially in RCP2.6 (broadly a 2°C target) and 1.9 scenarios (broadly a 1.5°C target), project GHG emissions to peak early in the 21st century, strict GHG emission reduction afterwards and, depending on the climate target, net CDR from the atmosphere in the second half of the century (Chapter 2 of SR15; Tavoni et al. 2015; Riahi et al. 2017). In most of these pathways, land use is of great importance because of its mitigation potential as discussed in Section 2.7.1: these pathways are based on the assumptions that (i) large-scale afforestation and reforestation removes substantial amounts of CO₂ from the atmosphere, (ii) biomass grown on cropland or from forestry residues can be used for energy generation or BECCS substituting fossil fuel emissions and generating CDR, and (iii) non-CO₂ emissions from agricultural production can be reduced, even under improved agricultural management (Popp et al. 2017; Rogelj et al. 2018a; Van Vuuren et al. 2018; Frank et al. 2018).

From the IAM scenarios available to this assessment, a set of feasible mitigation pathways has been identified which is illustrative of the range of possible consequences on land use and GHG emissions (presented in this chapter) and sustainable development (Chapter 6). Thus, the IAM scenarios selected here vary due to underlying socio-economic and policy assumptions, the mitigation options considered, long-term climate goals, the level of inclusion of other sustainability goals (such as land and water restrictions for biodiversity conservation or food production) and the models by which they are generated.

In the baseline case without climate change mitigation, global CO₂ emissions from land-use change decrease over time in most scenarios due to agricultural intensification and decreases in demand for agricultural commodities – some even turning negative by the end of the century due to abandonment of agricultural land and associated carbon uptake through vegetation regrowth. Median global CO₂ emissions from land-use change across 5 SSPs and 5 IAMs decrease throughout the 21st century: 3, 1.9 and –0.7 GtCO₂ yr⁻¹ in 2030, 2050 and 2100 respectively (Figure 2.25). In contrast, CH₄ and N₂O emissions from agricultural production remain rather constant throughout the 21st century (CH₄: 214, 231.7 and 209.1 MtCH₄ yr⁻¹ in 2030, 2050 and 2100 respectively; N₂O: 9.1, 10.1 and 10.3 MtN₂O yr⁻¹ in 2030, 2050 and 2100 respectively).

In the mitigation cases (RCP4.5, RCP2.6 and RCP1.9), most of the scenarios indicate strong reductions in CO₂ emissions due to (i) reduced deforestation and (ii) carbon uptake due to afforestation. However, CO₂ emissions from land use can occur in some mitigation

scenarios as a result of weak land-use change regulation (Fujimori et al. 2017; Calvin et al. 2017) or displacement effects into pasture land caused by high bioenergy production combined with forest protection only (Popp et al. 2014). The level of CO₂ removal globally (median value across SSPs and IAMs) increases with the stringency of the climate target (RCP4.5, RCP2.6 and RCP1.9) for both afforestation (-1.3 , -1.7 and -2.4 GtCO₂ yr⁻¹ in 2100) and BECCS (-6.5 , -11 and -14.9 GtCO₂ yr⁻¹ in 2100) (Cross-Chapter Box 7 and Chapter 6). In the mitigation cases (RCP4.5, RCP2.6 and RCP1.9), CH₄ and N₂O emissions are remarkably lower compared to the baseline case (CH₄: 133.2, 108.4 and 73.5 MtCH₄ yr⁻¹ in 2100; N₂O: 7.4, 6.1 and 4.5 MtN₂O yr⁻¹ in 2100; see previous paragraph for CH₄ and N₂O emissions in the baseline case). The reductions in the mitigation cases are mainly due to improved agricultural management such as improved nitrogen fertiliser management, improved water management in rice production, improved manure management (by, for example, covering of storages or adoption

of biogas plants), better herd management and better quality of livestock through breeding and improved feeding practices. In addition, dietary shifts away from emission-intensive livestock products also lead to decreased CH₄ and N₂O emissions especially in RCP2.6 and RCP1.9 scenarios. However, high levels of bioenergy production can result in increased N₂O emissions due to nitrogen fertilisation of dedicated bioenergy crops.

Such high levels of CO₂ removal through mitigation options that require land conversion (BECCS and afforestation) shape the land system dramatically (Figure 2.26). Across the different RCPs, SSPs and IAMs, median change of global forest area throughout the 21st century ranges from about -0.2 to $+7.2$ Mkm² between 2010 and 2100, and agricultural land used for 2nd generation bioenergy crop production ranges from about 3.2–6.6 Mkm² in 2100 (Popp et al. 2017; Rogelj et al. 2018). Land requirements for bioenergy and afforestation for a RCP1.9 scenario are higher than for a RCP2.6 scenario and

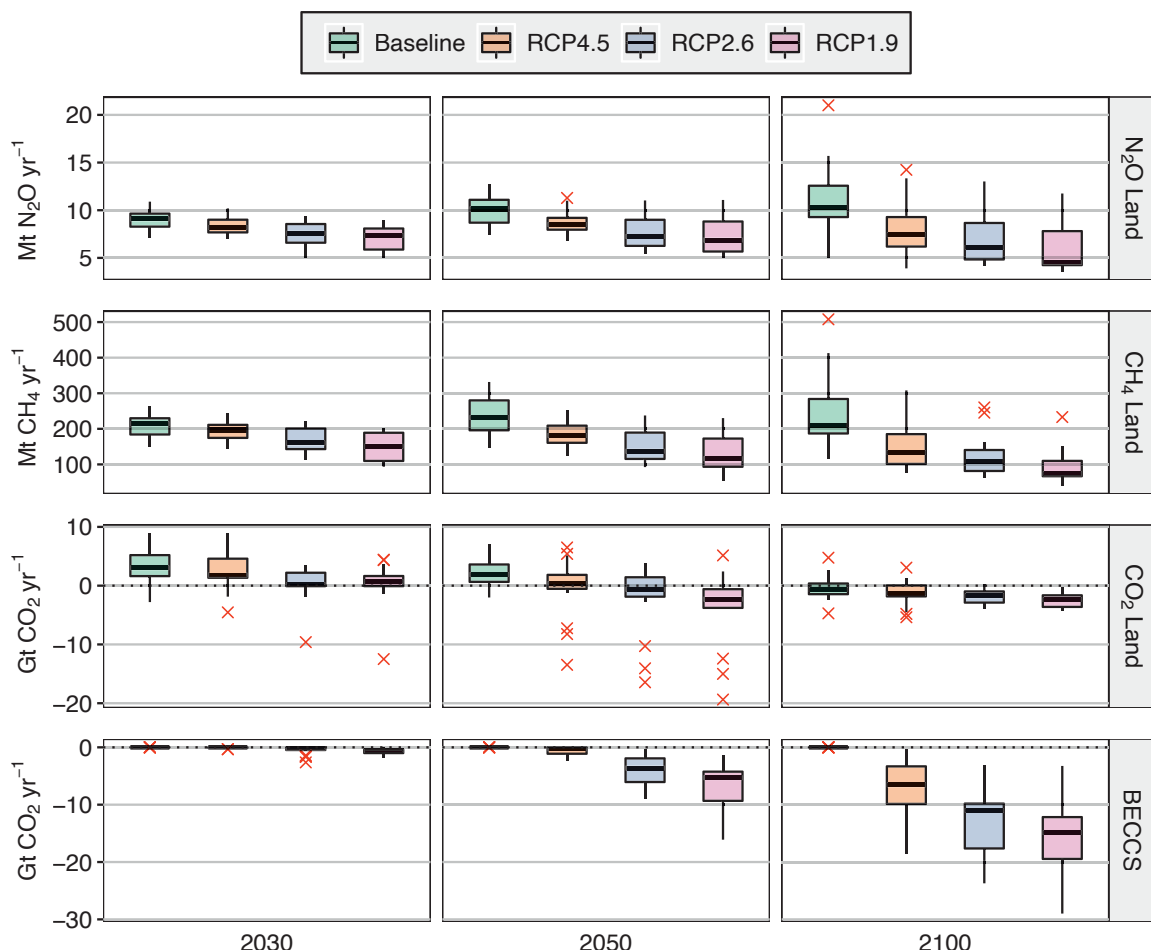


Figure 2.25 | Land-based global GHG emissions and removals in 2030, 2050 and 2100 for baseline, RCP4.5, RCP2.6 and RCP1.9 based on the SSP. Source: Popp et al. (2017), Rogelj et al. (2018), Riahi et al. (2017). Data is from an update of the IAMC Scenario Explorer developed for the SR15 (Huppmann et al. 2018; Rogelj et al. 2018). Boxplots (Tukey style) show median (horizontal line), interquartile range (IQR box) and the range of values within $1.5 \times \text{IQR}$ at either end of the box (vertical lines) across 5 SSPs and across 5 IAMs. Outliers (red crosses) are values greater than $1.5 \times \text{IQR}$ at either end of the box. The categories CO₂ Land, CH₄ Land and N₂O Land include GHG emissions from land-use change and agricultural land use (including emissions related to bioenergy production). In addition, the category CO₂ Land includes negative emissions due to afforestation. BECCS reflects the CO₂ emissions captured from bioenergy use and stored in geological deposits.

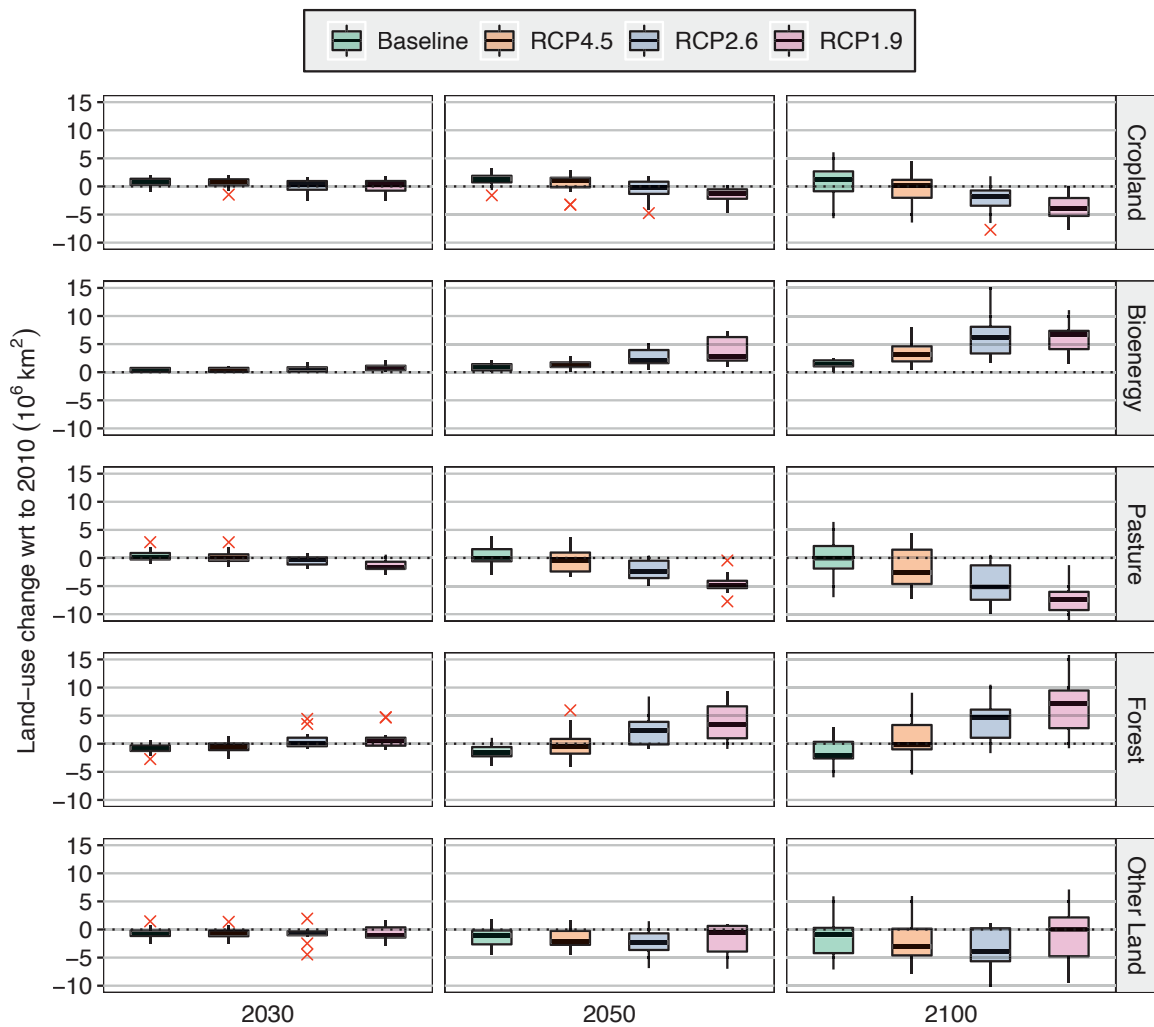


Figure 2.26 | Global change of major land cover types by 2030, 2050 and 2100 relative to 2010 for baseline, RCP4.5, RCP2.6 and RCP1.9 based on the SSP. Source: Popp et al. (2017), Rogelj et al. (2018), Riahi et al. (2017). Data is from an update of the IAMC Scenario Explorer developed for the SR15 (Huppmann et al. 2018; Rogelj et al. 2018). Boxplots (Tukey style) show median (horizontal line), interquartile range IQR (box) and the range of values within $1.5 \times \text{IQR}$ at either end of the box (vertical lines) across 5 SSPs and across 5 IAMs. Outliers (red crosses) are values greater than $1.5 \times \text{IQR}$ at either end of the box. In 2010, total land cover at global scale was estimated $15\text{--}16 \text{ Mkm}^2$ for cropland, $0\text{--}0.14 \text{ Mkm}^2$ for bioenergy, $30\text{--}35 \text{ Mkm}^2$ for pasture and $37\text{--}42 \text{ Mkm}^2$ for forest, across the IAMs that reported SSP pathways (Popp et al. 2017).

especially a RCP4.5 mitigation scenario. As a consequence of the expansion of mainly land-demanding mitigation options, global pasture land is reduced in most mitigation scenarios much more strongly than compared to baseline scenarios (median reduction of 0 , 2.6 , 5.1 and 7.5 Mkm^2 between 2010 and 2100 in baseline, RCP4.5, RCP2.6 and RCP1.9 respectively). In addition, cropland for food and feed production decreases with the stringency of the climate target ($+1.2$, $+0.2$, -1.8 and -4 Mkm^2 in 2100 compared to 2010 in baseline, RCP4.5, RCP2.6 and RCP1.9 respectively). These reductions in agricultural land for food and feed production are facilitated by agricultural intensification on agricultural land and in livestock production systems (Popp et al. 2017), but also by changes in consumption patterns (Fujimori et al. 2017; Frank et al. 2017b).

The pace of projected land-use change over the coming decades in ambitious mitigation scenarios goes well beyond historical changes in some instances (Turner et al. (2018b), see also SR15). This raises issues for societal acceptance, and distinct policy and governance will be required (Humppenöder et al. 2018; Obersteiner et al. 2016; Calvin et al. 2014) (Chapters 6 and 7).

Different mitigation strategies can achieve the net emissions reductions that would be required to follow a pathway that limits global warming to 2°C or 1.5°C , with very different consequences on the land system.

Figure 2.27 shows six alternative pathways (archetypes) for achieving ambitious climate targets (RCP2.6 and RCP1.9), highlighting land-based strategies and GHG emissions. All pathways are assessed by different models but are all based on the SSP2 (Riahi et al. 2017), with all based on an RCP 1.9 mitigation pathway except for Pathway 1, which is RCP2.6. All scenarios show land-based negative emissions, but the amount varies across pathways, as do the relative contributions of different land-based CDR options, such as afforestation/reforestation and BECCS.

Pathway 1 RCP2.6 ‘Portfolio’ (Fricko et al. 2017) shows a strong near-term decrease of CO₂ emissions from land-use change, mainly due to reduced deforestation, as well as slightly decreasing N₂O and CH₄ emissions after 2050 from agricultural production due to improved agricultural management and dietary shifts away from emissions-intensive livestock products. However, in contrast to CO₂ emissions, which turn net-negative around 2050 due to afforestation/reforestation, CH₄ and N₂O emissions persist throughout the century due to difficulties of eliminating these residual emissions based on existing agricultural management methods (Stevanović et al. 2017;

Frank et al. 2017b). In addition to abating land related GHG emissions as well as increasing the terrestrial sink, this example also shows the importance of the land sector in providing biomass for BECCS and hence CDR in the energy sector. In this scenario, annual BECCS-based CDR is about three times higher than afforestation-based CDR in 2100 (-11.4 and $-3.8 \text{ GtCO}_2 \text{ yr}^{-1}$ respectively). Cumulative CDR throughout the century amounts to -395 GtCO_2 for BECCS and -73 GtCO_2 for afforestation. Based on these GHG dynamics, the land sector turns GHG emission neutral in 2100. However, accounting also for BECCS-based CDR taking place in the energy sector, but with biomass provided by the land sector, turns the land sector GHG emission neutral already in 2060, and significantly net-negative by the end of the century.

Pathway 2 RCP1.9 ‘Increased Ambition’ (Rogelj et al. 2018) has dynamics of land-based GHG emissions and removals that are very similar to those in Pathway 1 (RCP2.6) but all GHG emission reductions as well as afforestation/reforestation and BECCS-based CDR start earlier in time at a higher rate of deployment. Cumulative CDR throughout the century amounts to -466 GtCO_2 for BECCS and -117 GtCO_2 for afforestation.

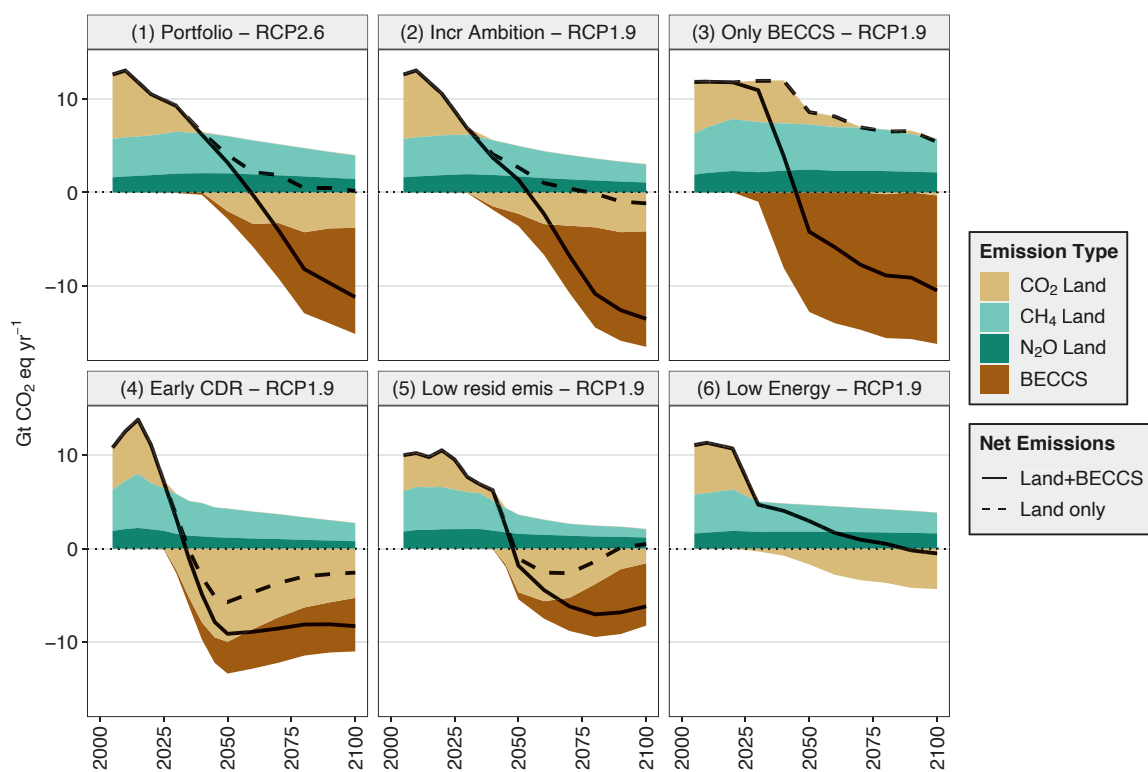


Figure 2.27 | Evolution and breakdown of global land-based GHG emissions and removals under six alternative mitigation pathways. This figure illustrates the differences in timing and magnitude of land-based mitigation approaches including afforestation and BECCS. All pathways are based on different IAM realisations of SSP2. Pathway 1 is based on RCP 2.6, while all other pathways are based on RCP 1.9. Pathway 1: MESSAGE-GLOBIOM (Fricko et al. 2017); Pathway 2: MESSAGE-GLOBIOM (Rogelj et al. 2018); Pathway 3: REMIND-MagPIE (Kriegler et al. 2017); Pathway 4: REMIND-MagPIE (Bertram et al. 2018); Pathway 5: IMAGE (van Vuuren et al. 2018); Pathway 6: MESSAGE-GLOBIOM (Grubler et al. 2018). Data is from an update of the IAMC Scenario Explorer developed for the SR15 (Rogelj et al. 2018). The categories CO₂ Land, CH₄ Land and N₂O Land include GHG emissions from land-use change and agricultural land use (including emissions related to bioenergy production). In addition, the category CO₂ Land includes negative emissions due to afforestation. BECCS reflects the CO₂ emissions captured from bioenergy use and stored in geological deposits. Solid lines show the net effect of all land based GHG emissions and removals (CO₂ Land, CH₄ Land, N₂O Land and BECCS), while dashed lines show the net effect excluding BECCS. CH₄ and N₂O emissions are converted to CO₂-eq using GWP factors of 28 and 265 respectively.

Pathway 3 RCP 1.9 'Only BECCS', in contrast to Pathway 2, includes only BECCS-based CDR (Kriegler et al. 2017). As a consequence, CO₂ emissions are persistent much longer, predominantly from indirect land-use change due to large-scale bioenergy cropland expansion into non-protected natural areas (Popp et al. 2017; Calvin et al. 2014). While annual BECCS CDR rates in 2100 are similar to Pathways 1 and 2 ($-15.9 \text{ GtCO}_2 \text{ yr}^{-1}$), cumulative BECCS-based CDR throughout the century is much larger (-944 GtCO_2).

Pathway 4 RCP1.9 'Early CDR' (Bertram et al. 2018) indicates that a significant reduction in the later century in the BECCS-related CDR as well as CDR in general can be achieved with earlier and mainly terrestrial CDR, starting in 2030. In this scenario, terrestrial CDR is based on afforestation but could also be supported by soil organic carbon sequestration (Paustian et al. 2016) or other natural climate solutions, such as rangeland or forest management (Griscom et al. 2017). This scenario highlights the importance of the timing for CDR-based mitigation pathways (Obersteiner et al. 2016). As a result of near-term and mainly terrestrial CDR deployment, cumulative BECCS-based CDR throughout the century is limited to -300 GtCO_2 , while cumulative afforestation-based CDR amounts to -428 GtCO_2 .

In Pathway 5 RCP1.9 'Low residual emissions' (van Vuuren et al. 2018), land-based mitigation is driven by stringent enforcement of measures and technologies to reduce end-of-pipe non-CO₂ emissions and by introduction of in-vitro (cultured) meat, reducing residual N₂O and CH₄ emissions from agricultural production. In consequence, much lower amounts of CDR from afforestation and BECCS are needed with much later entry points to compensate for residual emissions. Cumulative CDR throughout the century amounts to -252 GtCO_2 for BECCS and -128 GtCO_2 for afforestation. Therefore, total cumulative land-based CDR in Pathway 5 is substantially lower compared to Pathways 2–4 (380 GtCO₂).

Finally, Pathway 6 RCP1.9 'Low Energy' (Grubler et al. 2018), equivalent to Pathway LED in SR15, indicates the importance of other sectoral GHG emission reductions for the land sector. In this example, rapid and early reductions in energy demand and associated drops in energy-related CO₂ emissions limit overshoot and decrease the requirements for negative emissions technologies, especially for land-demanding CDR, such as biomass production for BECCS and afforestation. While BECCS is not used at all in Pathway 6, cumulative CDR throughout the century for afforestation amounts to -124 GtCO_2 .

Besides their consequences on mitigation pathways and land consequences, those archetypes can also affect multiple other sustainable development goals that provide both challenges and opportunities for climate action (Chapter 6).

2.6.3 The contribution of response options to the Paris Agreement

The previous sections indicated how land-based response options have the potential to contribute to the Paris Agreement, not only

though reducing anthropogenic emissions but also for providing anthropogenic sinks that can contribute to "...a balance between anthropogenic emissions by sources and removals by sinks of greenhouse gases in the second half of this century..." (Paris Agreement, Article 4). The balance applies globally, and relates only to GHGs, not aerosols (Section 2.4) or biophysical effects (Section 2.5).

The Paris Agreement includes an enhanced transparency framework to track countries' progress towards achieving their individual targets (i.e., nationally determined contributions (NDCs)), and a global stocktake (every five years starting in 2023), to assess the countries' collective progress towards the long-term goals of the Paris Agreement. The importance of robust and transparent definitions and methods (including the approach to separating anthropogenic from natural fluxes) (Fuglestvedt et al. 2018), and the needs for reconciling country GHG inventories and models (Grassi et al. 2018a), was highlighted in Section 2.3 in relation to estimating emissions. Issues around estimating mitigation is also key to transparency and credibility and is part of the Paris Rulebook.

The land sector is expected to deliver up to 25% of GHG mitigation pledged by countries by 2025–2030 in their NDCs, based on early assessments of 'Intended' NDCs submitted ahead of the Paris Agreement and updates immediately after (*low confidence*) (Grassi et al. 2017; Forsell et al. 2016). While most NDCs submitted to date include commitments related to the land sector, they vary with how much information is given and the type of target, with more ambitious targets for developing countries often being 'conditional' on support and climate finance. Some do not specify the role of AFOLU but include it implicitly as part of economy-wide pledges (e.g., reducing total emission or emission intensity), a few mention multi-sectoral mitigation targets which include AFOLU in a fairly unspecified manner. Many NDCs include specific AFOLU response options, with most focused on the role of forests. A few included soil carbon sequestration or agricultural mitigation and a few explicitly mentioned bioenergy (e.g., Cambodia, Indonesia and Malaysia), but this could be implicitly included with reduced emissions in energy sectors through fuel substitution (see Cross-Chapter Box 7 and Chapter 6 for discussion on cross sector flux reporting). The countries indicating AFOLU mitigation most prominently were Brazil and Indonesia, followed by other countries focusing either on avoiding carbon emissions (e.g., Ethiopia, Gabon, Mexico, DRC, Guyana and Madagascar) or on promoting the sink through large afforestation programmes (e.g., China, India) (Grassi et al. 2017).

Figure 2.28 shows the CO₂ mitigation potential of NDCs compared to historical fluxes from LULUCF.³ It shows future fluxes based on current policies in place and on country-stated Business As Usual (BAU) activities (these are different from current policies as many countries are already implementing policies that they do not include as part of their historical business-as-usual baseline) (Grassi et al. 2017). Under implementation of unconditional pledges, the net LULUCF flux in 2030 has been estimated to be a sink of $-0.41 \pm 0.68 \text{ GtCO}_2 \text{ yr}^{-1}$, which increases to $-1.14 \pm 0.48 \text{ GtCO}_2 \text{ yr}^{-1}$ in 2030 with conditional activities. This compares to net LULUCF in 2010 calculated from

³ CO₂ fluxes due to land use, land-use change and forestry, in essence, not including the part of AFOLU fluxes that are from agriculture.

the GHG Inventories of $0.01 \pm 0.86 \text{ GtCO}_2 \text{ yr}^{-1}$ (Grassi et al. 2017). Forsell et al. (2016) similarly find a reduction in 2030 compared to 2010 of $0.5 \text{ GtCO}_2 \text{ yr}^{-1}$ (range: $0.2\text{--}0.8$) by 2020 and $0.9 \text{ GtCO}_2 \text{ yr}^{-1}$ (range: $0.5\text{--}1.3$) by 2030 for unconditional and conditional cases.

The approach of countries to calculating the LULUCF contribution towards the NDC varies, with implications for comparability and transparency. For example, by following the different approaches used to include LULUCF in country NDCs, Grassi et al. (2017) found a three-fold difference in estimated mitigation: $1.2\text{--}1.9 \text{ GtCO}_2\text{-eq yr}^{-1}$ when 2030 expected emissions are compared to 2005 emissions, $0.7\text{--}1.4 \text{ GtCO}_2\text{-eq yr}^{-1}$ when 2030 emissions are compared to reference scenarios based on current policies or $2.3\text{--}3.0 \text{ GtCO}_2\text{-eq yr}^{-1}$ when compared to BAU, and $3.0\text{--}3.8 \text{ GtCO}_2\text{-eq yr}^{-1}$ when based on using each countries' approach to calculation stated in the NDC

(i.e., when based on a mix of country approaches, using either past years or BAU projections as reference).

In exploring the effectiveness of the NDCs, SR15 concluded “[e]stimates of global average temperature increase are $2.9^\circ\text{--}3.4^\circ\text{C}$ above preindustrial levels with a greater than 66% probability by 2100” (Roberts et al. 2006; Rogelj et al. 2016), under a full implementation of unconditional NDCs and a continuation of climate action similar to that of the NDCs. In order to achieve either the 1.5°C or 2°C pathways, this shortfall would imply the need for submission (and achievement) of more ambitious NDCs, and plan for a more rapid transformation of their national energy, industry, transport and land use sectors (Peters and Geden 2017; Millar et al. 2017; Rogelj et al. 2016).

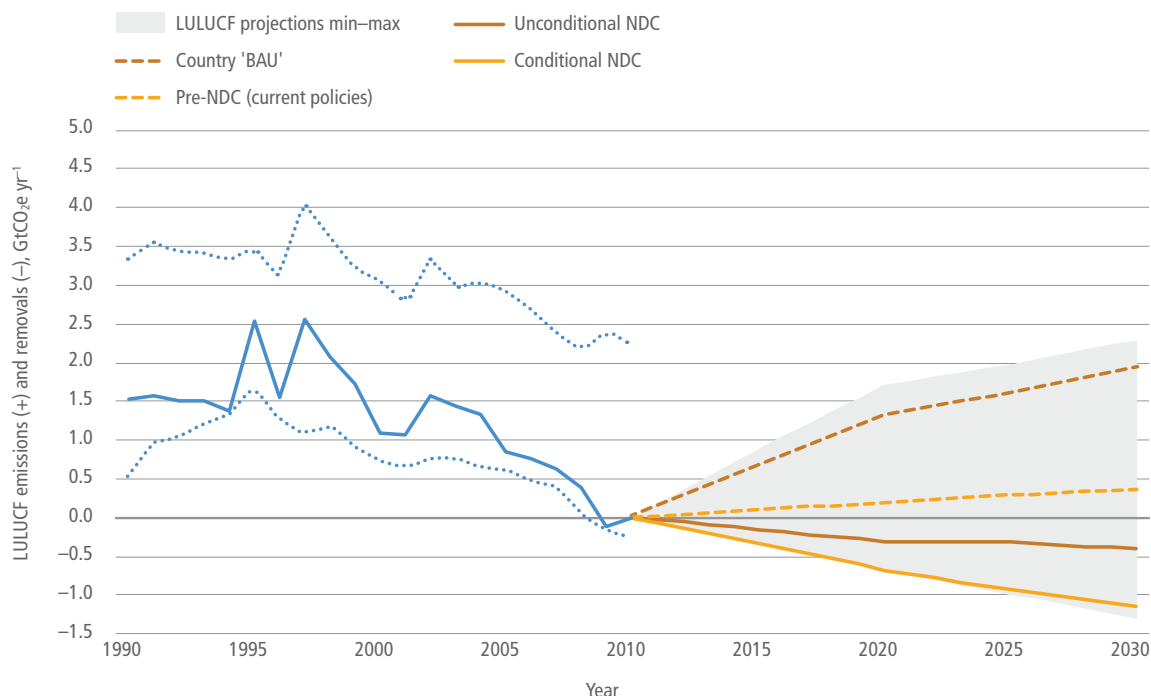


Figure 2.28 | Global LULUCF net GHG flux for the historical period and future scenarios based on analyses of countries' NDCs. The LULUCF historical data (blue solid line) reflect the following countries' documents (in order of priority): (i) data submitted to UNFCCC (NDCs⁴, 2015 GHG Inventories⁵ and recent National Communications^{6,7}), (ii) other official countries' documents, (iii) FAO-based datasets (i.e., FAO-FRA for forest (Tian et al. 2015) as elaborated by (Federici et al. 2015), and (iv) FAOSTAT for non-forest land use emissions (FAO 2015). The four future scenarios reflect official countries' information, mostly intended NDCs or updated NDCs available at the time of the analysis (Feb 2016), complemented by Biennial Update Reports⁸ and National Communications, and show (i) the BAU scenario as defined by the country, (ii) the trend based on pre-NDC levels of activity (current policies in place in countries), and (iii) the unconditional NDC and conditional NDC scenarios. The shaded area indicates the full range of countries' available projections (min-max), expressing the available countries' information on uncertainties beyond the specific scenarios shown. The range of historical country datasets (dotted lines) reflects differences between alternative selections of country sources, in essence, GHG inventories for developed countries complemented by FAO-based datasets (upper range) or by data in National Communications (lower range) for developing countries.

⁴ UNFCCC. INDCs as communicated by Parties, www4.unfccc.int/submissions/indc/Submission%20Pages/submissions.aspx (UNFCCC, 2015).

⁵ UNFCCC. Greenhouse Gas Inventories, unfccc.int/national_reports/annex_i_ghg_inventories/national_inventories_submissions/items/8812.php (UNFCCC, 2015).

⁶ UNFCCC. National Communications Non-Annex 1, unfccc.int/nationalreports/non-annexnatcom/submittednatcom/items/653.php (UNFCCC, 2015).

⁷ UNFCCC. National Communications Annex 1, unfccc.int/nationalreports/annexnatcom/submittednatcom/items/7742.php (UNFCCC, 2015).

⁸ UNFCCC. Biennial Update Reports, unfccc.int/national_reports/non-annex_i_natcom/reporting_on_climate_change/items/8722.php (UNFCCC, 2015).

Response options relying on the use of land could provide around a third of the additional mitigation needed in the near term (2030) to close the gap between current policy trajectories based on NDCs and what is required to achieve a 2°C (>66% chance) or 1.5°C (50–66% chance) pathway according to the UNEP Emissions Gap Report (Roberts et al. 2006). The report estimates annual reduction potentials in 2030 from agriculture at 3.0 (2.3–3.7) GtCO₂-eq yr⁻¹, a combination of ‘uncertain measures’ (biochar, peat-related emission reductions and demand-side management) at 3.7 (2.6–4.8) GtCO₂-eq yr⁻¹; forests at 5.3 (4.1–6.5) GtCO₂-eq yr⁻¹, bioenergy at 0.9 GtCO₂-eq yr⁻¹ and BECCS at 0.3 (0.2–0.4) GtCO₂-eq yr⁻¹ (UNEP 2017) (Table 4.1). These response options account for 35% of potential reduction (or 32% without bioenergy and BECCS) out of a total (all sector) potential of 38 (35–41) GtCO₂-eq yr⁻¹. The potentials estimated in the UNEP Emissions Gap Report are based on the technical potential of individual response options from literature including that presented in Section 2.1. CDR related to land use, while not a substitute for strong action in the energy sector, has the technical potential to balance unavoidable emissions that are difficult to eliminate with current technologies (*high confidence*), with early action avoiding deeper and more rapid action later (*very high confidence*) (Strefler et al. 2018; Elmar et al. 2018; SR15).

2.7 Plant and soil processes underlying land–climate interactions

Projecting future complex interactions between land and climate require ESMs. A growing number of studies suggested that many processes important for interactions between land and climate were missing in the CMIP5-class ESMs and that the DGVMs used tended to elevate CO₂ emission and removals (*high confidence*) (Busch and Sage 2017; Rogers et al. 2017; Anderegg et al. 2016; Tjoelker 2018; Sulman et al. 2014; Wieder et al. 2018; Davidson et al. 2006a).

Ecosystem complexity stemming from the diversity of plants, animals and microbes, as well as their biological responses to gradual climate changes (e.g., adaptive migration) and disturbance events (e.g., extreme weather events, fire, pest outbreaks) (Section 2.2), are of potential importance. Of these processes, this section focuses on plant and soil processes as recent empirical work, including those explained in the following subsections, offers potential for improved model projections under warmer and CO₂-rich futures.

The magnitude of future uptake and release of CO₂ and other GHGs by vegetation are among the greatest uncertainties (Ciais et al. 2013b). One reason for this uncertainty stems from the lack of understanding of the mechanisms responsible for plant responses to increasing temperatures. The short- and long-term projections of gross photosynthesis responses to changes in temperature, CO₂ and nutrient availability vary greatly among the models (Busch and Sage 2017; Rogers et al. 2017). Net CO₂ exchange requires estimation of autotrophic respiration, which is another source of uncertainty in ESM projections (Malhi et al. 2011). The importance of plant acclimation of photosynthesis and respiration in understanding vegetation response to climate change is now widely recognised (*high confidence*) (Rogers et al., 2017; Tan et al., 2017; Tjoelker, 2018;

Vanderwel et al. 2015) (Section 2.7.1). Acclimation is broadly defined as the biochemical, physiological, morphological or developmental adjustments within the lifetime of organisms that result in improved performance under the new condition. Acclimation often operates over a time span of days to weeks, and can mitigate the negative effects of climate change on organismal growth and ecosystem functions (Tjoelker 2018).

Soil carbon and microbial processes, which interact with plant responses to climate, represent another large source of uncertainty in model projections (*medium confidence*) (Sections 2.7.2, 2.7.3 and 2.7.4). Given the wide range of uncertainty associated with SOC size estimates, CMIP5 models use a wide range of starting SOC stocks from 510–3040 GtC (Todd-Brown et al. 2013). Soil microbial respiration is estimated to release 40–70 GtC annually from the soil to the atmosphere globally (Hawkes et al. 2017). Projections of changes in global SOC stocks during the 21st century by CMIP5 models also ranged widely, from a loss of 37 Gt to a gain of 146 Gt, with differences largely explained by initial SOC stocks, differing carbon input rates and different decomposition rates and temperature sensitivities (Todd-Brown et al. 2013). With respect to land–climate interactions, the key processes affecting SOC stocks are warming (which is expected to accelerate SOC losses through microbial respiration) and acceleration of plant growth (which increases inputs of carbon to soils). However, complex mechanisms underlying SOC responses to moisture regimes, carbon addition, and warming drive considerable uncertainty in projections of future changes in SOC stocks (Sulman et al. 2014; Singh et al. 2010; Wieder et al. 2018).

2.7.1 Temperature responses of plant and ecosystem production

Climate-change responses of net ecosystem production cannot be modelled by simple instantaneous response functions because of thermal acclimation responses of plants and soil microbes, as well as delayed responses arising from interactions between plants and the soil (*high confidence*) (Slot et al. 2014; Rogers et al. 2017; Tan et al. 2017; Tjoelker 2018). Photosynthesis and respiration of component plant species exhibit different functional shapes among species (Slot et al. 2014), and carbon balance at the stand level is influenced by respiration of ecosystem biomass other than plants. Large uncertainty remains for thermal responses of bacteria and other soil organisms (Section 2.7.5). Bayesian statistical estimates of global photosynthesis and total ecosystem respirations suggest that they exhibit different responses to thermal anomalies during the last 35 years (Li et al. 2018b).

Thermal responses of plant respiration, which consumes approximately one half of GPP, have not been appropriately incorporated in most ESMs (Davidson et al., 2006; Tjoelker, 2018). Assumptions associated with respiration have been a major source of uncertainty for ESMs at the time of AR5. In most existing models, a simple assumption that respiration doubles with each 10°C increase of temperature (i.e., Q10 = 2) is adopted, ignoring acclimation. Even a small error stemming from this assumption can strongly influence estimated net carbon balance at large spatial scales of ecosystems and biomes

over the time period of multiple decades (Smith and Dukes 2013; Smith et al. 2016b). In order to estimate more appropriate thermal response curves of respiration, a global database including data from 899 plant species has been compiled (Atkin et al. 2015), and respiration data from 231 plants species across seven biomes have been analysed (Heskel et al. 2016). These empirical data on thermal responses of respiration demonstrate a globally convergent pattern (Huntingford et al. 2017). According to a sensitivity analysis of a relatively small number of ESMs, a newly derived function of instantaneous responses of plant respiration to temperature (instead of a traditional exponential function of $Q10 = 2$) makes a significant difference in estimated autotrophic respiration especially in cold biomes (Heskel et al. 2016).

Acclimation results in reduced sensitivity of plant respiration with rising temperature, in essence, down regulation of warming-related increase in respiratory carbon emission (*high confidence*) (Atkin et al. 2015; Slot and Kitajima 2015; Tjoelker 2018). For example, experimental data from a tropical forest canopy show that temperature acclimation ameliorates the negative effects of rising temperature to leaf and plant carbon balance (Slot et al. 2014). Analysis of CO_2 flux data to quantify optimal temperature of net primary production of tropical forests also suggest acclimation potential for many tropical forests (Tan et al. 2017). Comparisons of models with and without thermal acclimation of respiration show that acclimation can halve the increase of plant respiration with projected temperature increase by the end of 21st century (Vanderwel et al. 2015).

It is typical that acclimation response to warming results in increases of the optimum temperature for photosynthesis and growth (Slot and Winter 2017; Yamori et al. 2014; Rogers et al. 2017). Although such shift is a result of a complex interactions of biochemical, respiratory and stomatal regulation (Lloyd and Farquhar 2008), it can be approximated by a simple algorithm to address acclimation (Kattge et al. 2007). Mercado et al. (2018), using this approach, found that inclusion of biogeographical variation in photosynthetic temperature response was critically important for estimating future land surface carbon uptake. In the tropics, CO_2 fertilisation effect (Box 2.3) is suggested to be more important for observed increases in carbon sink strength than increased leaf area index or a longer growing season (Zhu et al. 2016). Acclimation responses of photosynthesis and growth to simultaneous changes of temperature and CO_2 , as well as stress responses above the optimal temperature for photosynthesis, remain a major knowledge gap in modelling responses of plant productivity under future climate change (Rogers et al. 2017).

2.7.2 Water transport through soil-plant-atmosphere continuum and drought mortality

How climate change, especially changes of precipitation patterns, influence water transport through the soil-plant-atmosphere continuum, is a key element in projecting the future of water vapour flux from land and cooling via latent heat flux (*high confidence*) (Sellers et al. 1996; Bonan 2008; Brodribb 2009; Choat et al. 2012; Sperry and Love 2015; Novick et al. 2016; Sulman et al. 2016). Even without changes in leaf area per unit area of land, when plants

close stomata in response to water shortage, dry atmosphere or soil moisture deficit, the stand-level fluxes of water (and associated latent heat flux) decrease (Seneviratne et al. 2018). Closing stomata enhances drought survival at the cost of reduced photosynthetic production, while not closing stomata avoids loss of photosynthetic production at the cost of increased drought mortality (Sperry and Love 2015). Hence, species-specific responses to drought, in terms of whether they close stomata or not, have short- and long-term consequences (Anderegg et al. 2018a; Buotte et al. 2019). Increased drought-induced mortality of forest trees, often exacerbated by insect outbreak and fire (e.g., Breshears et al. (2005), Kurz et al. (2008), Allen et al. (2010)) (Section 2.2.4), have long-term impact on hydrological interactions between land and atmosphere (Anderegg et al. 2018b).

New models linking plant water transport with canopy gas exchange and energy fluxes are expected to improve projections of climate change impacts on forests and land-atmosphere interactions (*medium confidence*) (Bohrer et al., 2005; Anderegg et al., 2016; Sperry and Love, 2015; Wolf et al., 2016). Yet, there is much uncertainty in the ability of current vegetation and land surface models to adequately capture tree mortality and the response of forests to climate extremes like drought (Rogers et al. 2017; Hartmann et al. 2018). Most vegetation models use climate stress envelopes or vegetation carbon balance estimations to project climate-driven mortality and loss of forests (McDowell et al. 2011); these may not adequately project biome shifts and impacts of disturbance in future climates. For example, a suite of vegetation models was compared to a field drought experiment in the Amazon on mature rainforest trees and all models performed poorly in projecting the timing and magnitude of biomass loss due to drought (Powell et al. 2013). More recently, the loss of water transport due to embolism (disruption of xylem water continuity) (Sperry and Love 2015), rather than carbon starvation (Rowland et al. 2015), is receiving attention as a key physiological process relevant for drought-induced tree mortality (Hartmann et al. 2018). A key challenge to modelling efforts is to consider differences among plant species and vegetation types in their drought responses. One approach is to classify plant species to ‘functional types’ that exhibit similar responses to environmental variations (Anderegg et al. 2016). Certain traits of species, such as tree height, is shown to be predictive of growth decline and mortality in response to drought (Xu et al. 2016a). Similarly, tree rooting depth is positively related to mortality, contrary to expectation, during prolonged droughts in tropical dry forest (Chitra-Tarak et al. 2017).

2.7.3 Soil microbial effects on soil nutrient dynamics and plant responses to elevated CO_2

Soil microbial processes influencing nutrient and carbon dynamics represent a large source of uncertainty in projecting land–climate interactions. For example, ESMs incorporating nitrogen and phosphorus limitations (but without considering the effects of mycorrhizae and rhizosphere priming) indicate that the simulated future carbon-uptake on land is reduced significantly when both nitrogen and phosphorus are limited as compared to only carbon-stimulation, by 63% (of 197 Pg C) under RCP2.6 and by 67% (of 425 Pg C) under RCP8.5 (Zhang et al. 2013c). Mineral nutrient

limitation progressively reduces the CO₂ fertilisation effects on plant growth and productivity over time (*robust evidence, medium agreement*) (Norby et al. 2010; Sardans et al. 2012; Reich and Hobbie 2013; Feng et al. 2015; Terrer et al. 2017). The rates at which nutrient limitation develops differ among studies and sites. A recent meta-analysis shows that experimental CO₂ enrichment generally results in lower nitrogen and phosphorus concentrations in plant tissues (Du et al. 2019), and isotopic analysis also suggest a global trend of decreases in leaf nutrient concentration (Craine et al. 2018; Jonard et al. 2015). However, reduced responses to elevated CO₂ (eCO₂) may not be a simple function of nitrogen dilution per se, as they result from complex interactions of ecosystem factors that influence nitrogen acquisition by plants (Liang et al. 2016; Rutting 2017; Du et al. 2019).

Increasing numbers of case studies suggest that soil microbial processes, such as nitrogen mineralisation rates and symbiosis with plants, influence nutrient limitation on eCO₂ effects on plant growth (*medium confidence*) (Drake et al. 2011; Zak et al. 2011; Hungate et al. 2013; Talhelm et al. 2014; Du et al. 2019). Rhizosphere priming effects (i.e., release of organic matters by roots to stimulate microbial activities) and mycorrhizal associations are proposed to explain why some sites are becoming nitrogen limited after a few years and others are sustaining growth through accelerated nitrogen uptake (*limited evidence, medium agreement*) (Phillips et al. 2011; Terrer et al. 2017).

Model assessments that including rhizosphere priming effects and ectomycorrhizal symbiosis suggest that soil organic matter (SOM) cycling is accelerated through microbial symbiosis (*medium confidence*) (Elbert et al. 2012; Sulman et al. 2017; Orwin et al. 2011; Baskaran et al. 2017). Uncertainty exists in differences among ectomycorrhizal fungal species in their ability to decompose SOM (Pellitier and Zak 2018) and the capacity of ecosystems to sustain long-term growth with these positive symbiotic feedbacks is still under debate (Terrer et al. 2017). ESMs include only biological nitrogen cycles, even though a recent study suggests that bedrock weathering can be a significant source of nitrogen to plants (Houlton et al. 2018). In contrast, rock weathering is widely considered to be key for phosphorus availability, and tropical forests with highly weathered soils are considered to be limited by phosphorus availability rather than nitrogen availability (Reed et al. 2015). Yet evidence from phosphorus fertilisation experiments is lacking (Schulte-Uebbing and de Vries 2018) and phosphorus limitation of tropical tree growth may be strongly species-specific (Ellsworth et al. 2017; Turner et al. 2018a). Limitation by availability of soil nutrients other than nitrogen and phosphorus has not been studied in the context of land–climate interactions, except potassium as a potentially limiting factor for terrestrial plant productivity in interaction with nitrogen, phosphorus and hydrology (Sardans and Peñuelas 2015; Zhao et al. 2017; Wright et al. 2018).

Anthropogenic alteration of global and regional nitrogen and phosphorus cycles, largely through use of chemical fertilisers and pollution, has major implications for future ecosystem attributes, including carbon storage, in natural and managed ecosystems (*high confidence*) (Peñuelas et al. 2013, 2017; Wang et al. 2017c; Schulte-Uebbing and de Vries 2018; Yuan et al. 2018). During 1997–2013, the contribution of nitrogen deposition to the global carbon sink

has been estimated at 0.27 ± 0.13 GtC yr⁻¹, and the contribution of phosphorus deposition as 0.054 ± 0.10 GtC yr⁻¹; these constitute about 9% and 2% of the total land carbon sink, respectively (Wang et al. 2017c). Anthropogenic deposition of nitrogen enhances carbon sequestration by vegetation (Schulte-Uebbing and de Vries 2018), but this effect of nitrogen deposition on carbon sequestration may be offset by increased emission of GHGs such as N₂O and CH₄ (Liu and Greaver 2009). Furthermore, nitrogen deposition may lead to imbalance of nitrogen vs phosphorus availability (Peñuelas et al. 2013), soil microbial activity and SOM decomposition (Janssens et al. 2010) and reduced ecosystem stability (Chen et al. 2016b).

2.7.4 Vertical distribution of soil organic carbon

It has long been recognised that dynamics of soil organic carbon (SOC) represent a large source of uncertainties on biogeochemical interactions of land with atmosphere and climate as detailed below. Since AR5, there have been new understandings on SOC size, as well as on the microbial processes that influence SOM dynamics under climate change and LULCC. Three existing databases (SoilGrids, the Harmonized World Soil Data Base and Northern Circumpolar Soil Database) substantially differ in the estimated size of global SOC stock down to 1 m depth, varying between 2500 Pg to 3400 Pg with differences among databases largely attributable to carbon stored in permafrost (Joosten 2015; Köchy et al. 2015; Tifafi et al. 2018). These values are four to eight times larger than the carbon stock associated with the terrestrial vegetation (Bond-Lamberty et al. 2018). New estimates since AR5 show that much larger areas in the Amazon and Congo basins are peatlands (Gumbricht et al. 2017; Dargie et al. 2019).

Deep soil layers can contain much more carbon than previously assumed (*limited evidence, medium agreement*) (e.g., González-Jaramillo et al. (2016)). Based on radiocarbon measurements, deep SOC can be very old, with residence times up to several thousand years (Rumpel and Kögel-Knabner 2011) or even several tens of thousands of years (Okuno and Nakamura 2003). Dynamics associated with such deeply buried carbon remain poorly studied and ignored by the models, and are not addressed in most of the studies assessed in this subsection. Deep soil carbon is thought to be stabilised by mineral interactions, but recent experiments suggest that CO₂ release from deep soils can also be increased by warming, with a 4°C warming enhancing annual soil respiration by 34–37% (Hicks Pries et al. 2017), or with the addition of fresh carbon (Fontaine et al. 2007). While erosion is not typically modelled as a carbon flux in ESMs, erosion and burial of carbon-containing sediments is likely a significant carbon transfer from land to ocean (*medium confidence*) (Berhe et al. 2007; Asefaw et al. 2008; Wang et al. 2017e).

2.7.5 Soil carbon responses to warming and changes in soil moisture

Annually, 119 GtC is estimated to be emitted from the terrestrial ecosystem to the atmosphere, of which about 50% is attributed to soil microbial respiration (Auffret et al. 2016; Shao et al. 2013). It is

yet not possible to make mechanistic and quantitative projections about how multiple environmental factors influence soil microbial respiration (Davidson et al. 2006a; Dungait et al. 2012). Soil warming experiments show significant variability in temperature and moisture responses across biomes and climates; Crowther et al. (2016) found that warming-induced SOC loss is greater in regions with high initial carbon stocks, while an analysis of an expanded version of the same dataset did not support this conclusion (Gestel et al. 2018). Studies of SOC responses to warming over time have also shown complex responses. In a multi-decadal warming experiment, Melillo et al. (2017) found that soil respiration response to warming went through multiple phases of increasing and decreasing strength, which were related to changes in microbial communities and available substrates over time. Conant et al. (2011) and Knorr et al. (2005) suggested that transient decomposition responses to warming could be explained by depletion of labile substrates, but that long-term SOC losses could be amplified by high temperature sensitivity of slowly decomposing SOC components. Overall, long-term SOC responses to warming remain uncertain (Davidson et al. 2006a; Dungait et al. 2012; Nishina et al. 2014; Tian et al. 2015).

It is widely known that soil moisture plays an important role in SOM decomposition by influencing microbial processes (e.g., Monard et al. (2012), Moyano et al. (2013), Yan et al. (2018)), as confirmed by a recent global meta-analysis (*high confidence*) (Hawkes et al. 2017). A likely mechanism is that increased soil moisture lowers carbon mineralisation rates under anaerobic conditions, resulting in enhanced carbon stocks, but experimental analyses have shown that this effect may last for only 3–4 weeks after which iron reduction can actually accelerate the loss of previously protected OC by facilitating microbial access (Huang and Hall 2017).

Experimental studies of responses of microbial respiration to warming have found variable results (Luo et al. 2001; Bradford et al. 2008; Zhou et al. 2011; Carey et al. 2016; Teramoto et al. 2016). No acclimation was observed in carbon-rich calcareous temperate forest soils (Schindlbacher et al. 2015) and arctic soils (Hartley et al. 2008), and a variety of ecosystems from the Arctic to the Amazon indicated that microbes appear to enhance the temperature sensitivity of soil respiration in Arctic and boreal soils, thereby releasing even more carbon than currently projected (Karhu et al. 2014). In tropical forests, phosphorus limitation of microbial processes is a key factor influencing soil respiration (Camenzind et al. 2018). Temperature responses of symbiotic mycorrhizae differ widely among host plant species, without a clear pattern that may allow generalisation across plant species and vegetation types (Fahey et al. 2016).

Some new insights have been obtained since AR5 from investigations of improved mechanistic understanding of factors that regulate temperature responses of soil microbial respiration. Carbon use efficiency and soil nitrogen dynamics have large influence on SOC responses to warming (*high confidence*) (Allison et al. 2010; Frey et al. 2013; Wieder, William R., Bonan, Gordon B., Allison 2013; García-Palacios et al. 2015). More complex community interactions including competitive and trophic interactions could drive unexpected responses to SOC cycling to changes in temperature, moisture and carbon inputs (Crowther et al. 2015; Buchkowski et al. 2017).

Competition for nitrogen among bacteria and fungi could also suppress decomposition (Averill et al. 2014). Overall, the roles of soil microbial community and trophic dynamics in global SOC cycling remain very uncertain.

2.7.6 Soil carbon responses to changes in organic matter inputs by plants

While current ESM structures mean that increasing carbon inputs to soils drive corresponding increases in SOC stocks, long-term carbon addition experiments have found contradictory SOC responses. Some litter addition experiments have observed increased SOC accumulation (Lajtha et al. 2014b; Liu et al. 2009), while others suggest insignificant SOC responses (Lajtha et al. 2014a; van Groenigen et al. 2014). Microbial dynamics are believed to have an important role in driving complex responses to carbon additions. The addition of fresh organic material can accelerate microbial growth and SOM decomposition via priming effects (Kuzyakov et al. 2014; Cheng et al. 2017). SOM cycling is dominated by ‘hot spots’ including the rhizosphere as well as areas surrounding fresh detritus (*medium evidence, high agreement*) (Finzi et al. 2015; Kuzyakov and Blagodatskaya 2015). This complicates projections of SOC responses to increasing plant productivity as increasing carbon inputs could promote higher SOC storage, but these fresh carbon inputs could also deplete SOC stocks by promoting faster decomposition (Hopkins et al. 2014; Guenet et al. 2018; Sulman et al. 2014). A meta-analysis by van Groenigen et al. (2014) suggested that elevated CO₂ accelerated SOC turnover rates across several biomes. These effects could be especially important in high-latitude regions where soils have high organic matter content and plant productivity is increasing (Hartley et al. 2012), but have also been observed in the tropics (Sayer et al. 2011).

Along with biological decomposition, another source of uncertainty in projecting responses of SOC to climate change is stabilisation via interactions with mineral particles (*high confidence*) (Kögel-Knabner et al. 2008; Kleber et al. 2011; Marschner et al. 2008; Schmidt 2011). Historically, conceptual models of SOC cycling have centred on the role of chemical recalcitrance: the hypothesis that long-lived components of SOC are formed from organic compounds that are inherently resistant to decomposition. Under the emerging new paradigm, stable SOC is primarily formed by the bonding of microbially-processed organic material to mineral particles, which limits the accessibility of organic material to microbial decomposers (Lützow et al. 2006; Keiluweit et al. 2015; Kallenbach et al. 2016; Kleber et al. 2011; Hopkins et al. 2014). SOC in soil aggregates can be protected from microbial decomposition by being trapped in soil pores too small for microbes to access (Blanco-Canqui and Lal 2004; Six et al. 2004) or by oxygen limitation (Keiluweit et al. 2016). Some new models are integrating these mineral protection processes into SOC cycling projections (Wang et al. 2017a; Sulman et al. 2014; Riley et al. 2014; Wieder et al. 2015), although the sensitivity of mineral-associated organic matter to changes in temperature, moisture, fire (Box 2.1) and carbon inputs is highly uncertain. Improved quantitative understanding of soil ecosystem processes will be critically important for projection of future land–climate feedback interactions.

Frequently Asked Questions

FAQ 2.1 | How does climate change affect land use and land cover?

Contemporary land cover and land use is adapted to current climate variability within particular temperature and/or rainfall ranges (referred to as climate envelopes). Anthropogenic GHG emissions impact land through changes in the weather and climate and also through modifications in atmospheric composition through increased GHGs, especially CO₂. A warming climate alters the current regional climate variability and results in a shift of regional climate envelopes poleward and to higher elevations. The shift of warmer climate envelopes into high latitude areas has potential benefits for agriculture here through extended growing seasons, warmer seasonal temperatures and increased atmospheric CO₂ concentrations which enhance photosynthetic activity. However, this warming will also lead to enhanced snowmelt and reduced albedo, permafrost melting and the further release of CH₄ and CO₂ into the atmosphere as the permafrost begins to decompose. Concurrent with these climate envelope shifts will be the emergence of new, hot climates in the tropics and increases in the frequency, intensity and duration of extreme events (e.g., heatwaves, very heavy rainfall, drought). These emergent hot climates will negatively affect land use (through changes in crop productivity, irrigation needs and management practices) and land cover through loss of vegetation productivity in many parts of the world, and would overwhelm any benefits to land use and land cover derived from increased atmospheric CO₂ concentrations.

FAQ 2.2 | How do the land and land use contribute to climate change?

Any changes to the land and how it is used can effect exchanges of water, energy, GHGs (e.g., CO₂, CH₄, N₂O), non-GHGs (e.g., BVOCs) and aerosols (mineral, e.g., dust, or carbonaceous, e.g., BC) between the land and the atmosphere. Land and land use change therefore alter the state (e.g., chemical composition and air quality, temperature and humidity) and the dynamics (e.g., strength of horizontal and vertical winds) of the atmosphere, which, in turn, can dampen or amplify local climate change. Land-induced changes in energy, moisture and wind can affect neighbouring, and sometimes more distant, areas. For example, deforestation in Brazil warms the surface, in addition to global warming, and enhances convection which increases the relative temperature difference between the land and the ocean, boosting moisture advection from the ocean and thus rainfall further inland. Vegetation absorbs CO₂ to use for growth and maintenance. Forests contain more carbon in their biomass and soils than croplands and so a conversion of forest to cropland, for example, results in emissions of CO₂ to the atmosphere, thereby enhancing the GHG-induced global warming. Terrestrial ecosystems are both sources and sinks of chemical compounds such as nitrogen and ozone. BVOCs contribute to forming tropospheric ozone and secondary aerosols, which respectively effect surface warming and cloud formation. Semi-arid and arid regions release dust, as do cropland areas after harvest. Increasing the amount of aerosols in the atmosphere impacts temperature in both positive and negative ways depending on the particle size, altitude and nature (carbonaceous or mineral, for example). Although global warming will impact the functioning and state of the land (FAQ 2.1), this is not a one-way interaction as changes in land and land use can also affect climate and thus modulate climate change. Understanding this two-way interaction can help improve adaptation and mitigation strategies, as well as manage landscapes.

FAQ 2.3 | How does climate change affect water resources?

Renewable freshwater resources are essential for the survival of terrestrial and aquatic ecosystems and for human use in agriculture, industry and in domestic contexts. As increased water vapour concentrations are expected in a warmer atmosphere, climate change will alter the hydrological cycle and therefore regional freshwater resources. In general, wet regions are projected to get wetter and dry regions drier, although there are regional exceptions to this. The consequent impacts vary regionally; where rainfall is projected to be lower in the future (many arid subtropical regions and those with a Mediterranean climate), a reduction of water resources is expected. Here increased temperatures and decreased rainfall will reduce surface and groundwater resources, increase plant evapotranspiration and increase evaporation rates from open water (rivers, lakes, wetlands) and water supply infrastructure (canals, reservoirs). In regions where rainfall is projected to be higher in the future (many high latitude regions and the wet tropics), an increase in water resources can be expected to benefit terrestrial and freshwater ecosystems, agriculture and domestic use, however, these benefits may be limited due to increased temperatures. An increase in extreme rainfall events is also expected which will lead to increases in surface runoff, regional flooding and nutrient removal as well as a reduction in soil water and groundwater recharge in many places. Anthropogenic land use change may amplify or moderate the climate change effect on water resources, therefore informed land management strategies need to be developed. A warming climate will exacerbate the existing pressures on renewable freshwater resources in water-stressed regions of the Earth and result in increased competition for water between human and natural systems.